ASPHALT INSTITUTE

RHEOLOGICAL PROPERTIES OF BINDERS AND THE RELATION TO THE PERFORMANCE OF ASPHALT SHINGLES

A REPORT PREPARED FOR:
THE ROOFING TECHNICAL ADVISORY COMMITTEE
OF THE ASPHALT INSTITUTE

IS-245
DECEMBER 2025

RHEOLOGICAL PROPERTIES OF BINDERS AND THE RELATION TO THE PERFORMANCE OF ASPHALT SHINGLES

- Contents -

- Acknowledgements -

This report has been developed by the Rheology Task Force working for the Asphalt Institute Roofing Technical Advisory Committee (RTAC) and authored by Geoffrey M. Rowe, Alison R. Schultz, Wesley G. Cooper, Lorena Garcia Cucalon, & Gaylon Baumgardner. The task force (at the time of writing) comprises members as follows:

Sara Akbarian-Tefaghi, Owens Corning
Mike Anderson, Asphalt Institute
Amir Bahadori, CertainTeed / Saint-Gobain
Gaylon Baumgardner, Ergon
Richard Blackwell, Kraton
Judge Brown, Hunt Refining
Wes Cooper, Asphalt Institute
Eileen Dutton, Malarkey Roofing
Lorena Garcia Cucalon, Kraton
Ann Hamer, Wright Asphalt
Luke Henderson, Malarkey Roofing
Dwayne Johnson, Paragon Technical Services
Laurand Lewandowski, Owens Corning
Andy Parker, Tamko
Alison Schultz, Owens Corning
Punit Singhvi, Crafco
Saleh Yousefi, Crafco

The contributions of the task force have been invaluable in the development of this report and their work is acknowledged by the Asphalt Institute in the development of technology relating to the performance of asphalt binders for roofing applications. Additionally, the task force would also like to acknowledge the financial contributions of **Owens Corning** and **Paragon Technical Services** that supported the commissioning of the broad scope of laboratory testing and analysis that forms the foundation of this report.

This report was approved for publication by the RTAC as an Asphalt Institute Information Series document on December 9, 2025 at the Asphalt Institute Annual Meeting.

Executive Summary

Hail damage is a leading cause of roof replacements in geographic regions where severe storms are prevalent, annually costing insurance companies substantial amounts in claims. The asphalt coating on shingles ages over time, causing embrittlement and a reduced ability to relax mechanical stress, potentially leaving the shingle more susceptible to damage from hail impact. In Asphalt Institute Foundation (AIF) Project 22-03, it was shown from a limited dataset that impact damage could be correlated to specific rheological characteristics of the asphalt extracted from affected shingles.

At the request of the Asphalt Institute Roofing Technical Advisory Committee (RTAC), the Rheology Task Force (RTF) conducted an in-depth evaluation of asphalt shingle coating technologies. This study focused on rheological assessments before and after laboratory-simulated aging, aiming to identify tools that aid in the design and optimization of impact-resistant shingle coatings. Additional high-temperature measurements were performed to assess parameters potentially related to scuffing, though these results have not yet been correlated with field observations. Key findings indicate that low-temperature rheology can be used to analyze asphalt coating behavior in the high-stiffness region, effectively characterizing viscoelastic properties such as embrittlement and energy dissipation thought to relate to impact damage, as demonstrated in AIF Project 22-03.

The study evaluated six materials, representing one (1) conventional and five (5) modified roofing-grade asphalts, using rheological, empirical, and failure-based testing methods. For each material and aging condition, complex modulus, G^*, and phase angle, δ, were measured using temperature-frequency sweeps on the dynamic shear rheometer (DSR), utilizing 4-mm, 8-mm and 25-mm parallel plate geometry across a dynamic stiffness range of 100 Pa to 100 MPa. This data was analyzed using RHEA software to generate master curves. In the modeling analysis and evaluation of other fitting parameters, it was determined that the use of the Christensen-Anderson model for roofing grade binders was generally unsuccessful, and that the use of a cross-over modulus, G_c, typically occurred at a stiffness that was too low to be associated with cracking. Alternatively, analysis showed that the phase angle at a constant modulus (10 MPa) and the properties associated with a phase angle of 27 degrees were more accurate and reliable indicators of the shape of the master curve and the relative hardness of the binder in the high stiffness region, respectively. Each of these parameters can be measured with relative ease and were well correlated with observed impact damage in AIF Project 22-03. As part of this study, the Rheology Task Force drafted and submitted an American Society of Testing Materials (ASTM) test method for use of the DSR to standardize measurement of these and other low-temperature rheological parameters[1]. The Asphalt Institute will incorporate this test method into its annual Roofing Proficiency Sample Program for round-robin testing.

High-temperature rheology work focused on the use of the Multiple Stress Creep Recovery (MSCR) test. Analysis showed considerable differences between materials. Some preliminary work was conducted using the Ostwald-DeWaele power law parameter, which could provide useful information on the structural performance of the materials evaluated.

[1]Draft ASTM method is included as an appendix to this report.

Several ultimate tests were evaluated in this study, building upon the work conducted with project AIF Project 22-03. While AIF Project 22-03 considered the Asphalt Binder Cracking Device (ABCD), Simplified Double-Edge Notched Tension (SDENT) and Monotonic Shear Strength (MOSS) tests, this work concentrated on only those methods that could be tested using the DSR: the Linear Amplitude Sweep (LAS) and MOSS tests. The results from the LAS test showed some general trends but interpreting the data in its applicability to roofing projects and lack of data consistency resulted in this test being problematic. Further LAS testing was curtailed after three initial materials were evaluated. However, the MOSS tests showed some significant promise, with testing temperatures targeted to enable failure to be defined in a stiffness range near 1 MPa, where the transition from ductile to brittle behavior is thought to occur. The modifications and draft method are given in an appendix to this work. The yield energy, E_f, and Fatigue-Fracture Performance Ratio (FFPR) from this test showed good correlation with rheology. These parameters were also shown to correlate with hail damage in AIF Project 22-03.

Useful correlations have been established with empirical measures for Penetration (25°C at standard loading conditions) and Ring-and-ball (R&B) Softening Point. The best correlations were obtained with the Glover-Rowe (G-R) parameter measured at 10 rad/s and with the temperature that corresponded to a non-recoverable creep compliance ($J_{nr3.2}$) of 1.0 kPa^{-1}.

This study expands upon AIF Project 22-03 findings by incorporating new materials and providing insights for formulators and manufacturers on optimizing shingle performance. The correlations with traditional test methods offer a bridge between historical material performance data and modern rheological techniques, facilitating improved material selection and formulation strategies for enhanced impact resistance.

Introduction

The Asphalt Institute Roofing Technical Advisory Committee (RTAC) Rheology Task Force aspires to create industry rheological guidelines for faster, cheaper, and better means of characterizing and producing roofing asphalt shingles. Impact-resistant (IR) shingles offer a unique opportunity to support this mission, providing a variety of high-performance industrial products predominantly ranked by the Insurance Institute for Business & Home Safety (IBHS) annual hail impact simulation ratings (IBHS, 2024). IBHS evaluates IR shingle performance through standard distribution channels using artificial hailstones and ranks commercial products based on three criteria: dents/ridges, tears, and granule loss using a method developed by IBHS (IBHS, 2019). Figure 1 reveals overall commercial rankings from poor to excellent, showing the broadest product differentiation in dents and ridges. Variability in hailstone production and impact simulation continues to challenge the test method and warrants further ASTM method development. Understanding viscoelastic properties of fundamental polymer-modified asphalt binders (PmB) offers an opportunity to generate precise characterization methods and binder modification guidance prior to variable hail impact simulations.

The following report details an RTAC Rheology Task Force learning study involving rheological characterization of fundamental PmB impact-resistant binders. The task force initiative leverages extensive binder characterization at the Asphalt Institute to connect empirical and rheological binder properties to fracture/failure modes. Rheological shape and point analyses of the binders provide an assessment of high stiffness properties and the correlation to impact resistance. Other properties are measured that can indicate safeguards for other distress modes such as scuffing and bundle sticking, which tend to occur at higher temperatures and lower levels of stiffness.

Key learnings from this study are extremely beneficial for the industry in moving towards more performance-based testing. New rheological characterization now permits the first ever industry-shared best practice for assessing impact performance from asphalt shingle coatings. From the results of this work, there is the potential to change asphalt coatings specifications for IR shingles. This would allow for cost-effective engineered solutions and expedited innovation, while also shifting to a more material-based approach to shingle development. These initiatives are considered vital to addressing the many challenges facing the roofing industry today regarding durability and resilience, and ultimately, could create a more durable product that drives both building codes and industry standards.

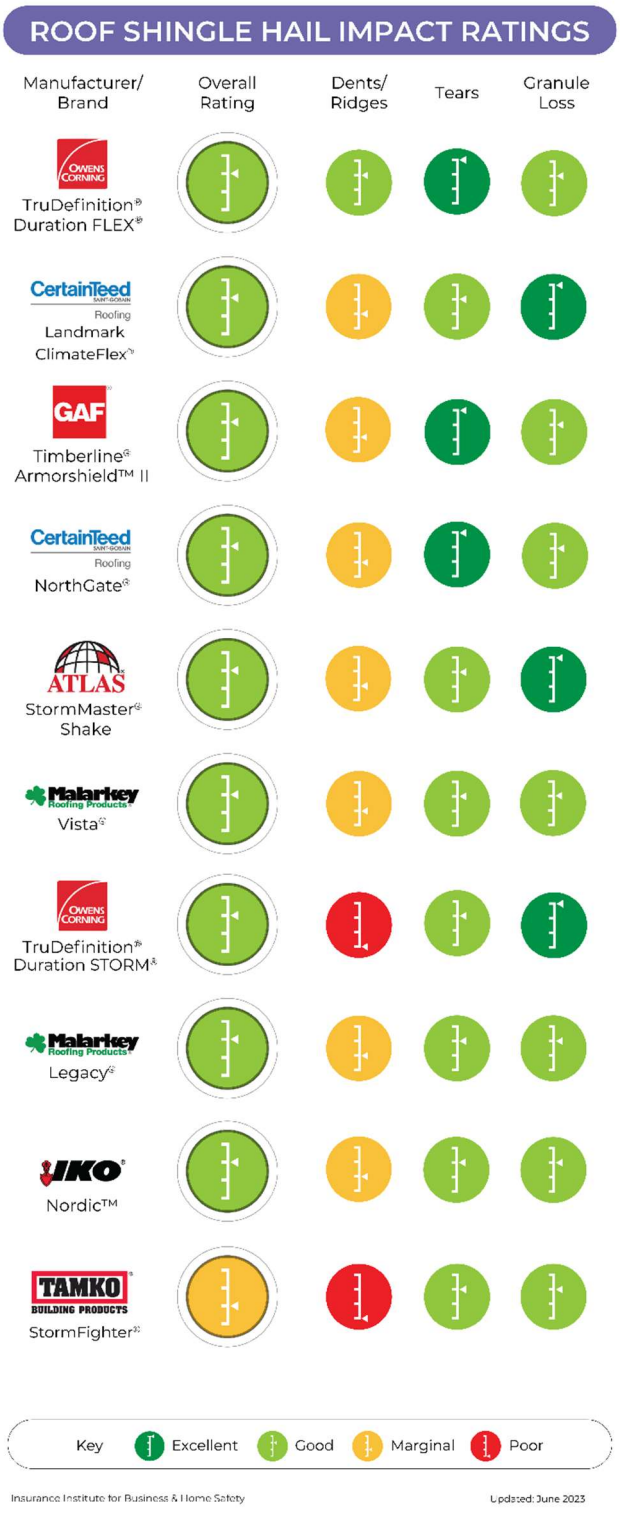

Figure 1. IBHS 2023 roof shingle hail impact ratings (IBHS, 2024)

Components of an Asphalt Shingle and Relationship to Performance

Asphalt shingles consist of the following components (ARMA, 2023):

- Fiberglass mat;
- Coating asphalt;
- Mineral fillers;
- Granules; and
- Back surfacing

The fiberglass mat provides the backbone of the shingle, needed for handling and durability. The coating asphalt serves to provide waterproofing characteristics and holds the granules in place. The granules, in turn, protect the asphalt from degradation that would occur from prolonged exposure to ultraviolet (UV) light. The mineral fillers help increase the asphalt's resistance to fire, and can improve weathering, flexibility and durability, while back surfacing allows shingles to be more easily manufactured and stored (ARMA, 2023).

The durability of an asphalt shingle is most related to the coating asphalt since it comprises a substantial portion of the shingle and is significantly affected by oxidation and UV exposure, unlike the other components – the granules and mineral fillers – which exist to assist the coating asphalt. As such, it is expected that the properties of the coating asphalt will be important to the performance of the shingle.

Research Objective

The research objectives are considered as follows:

1. To test various formulations of IR coating asphalts for both rheology and fracture
2. To provide a link between binder properties and fracture properties
3. To evaluate low stiffness properties that can impact handling and scuffing
4. To assess relationships between rheological parameters and key empirical tests used to characterize roofing grade binders (i.e. Penetration and Softening Point)

Experimental Materials and Testing Plan

Materials

The materials have been supplied by members of the RTAC and have been coded as shown below, along with generic descriptions. The specifics of the formulations are only known to those suppliers and members that have contributed materials to this data set.[2]

Table 1. Material references and generic descriptions

Ref.	Material
A	Commercial oxidized roofing grade
B	PG52-34 + 10% Radial SBS
C	PG58-28 + 10% Radial SBS
D	PG64-22 + 10% Radial SBS
E	PG64-22 + SBS/Post-consumer waste hybrid
F	Same as E – all modification reduced by half

Testing Plan

The test plan for each of the materials consists of performing rheological and empirical tests and includes targeted rheological parameters that enable assessment of both high and low temperature properties. Low temperature rheology has been shown to relate to fracture (Rowe et al., 2023); this work will extend that evaluation with additional products, but without field validation. Recent developments with fracture tests using the DSR have also been included in this work and have been used as a partial validation of the rheological data. High temperature rheology has been assessed in two ways. The first is associated with the low stiffness part of the master curve which was typically measured to 120-150°C. Data can be used to assess dynamic and complex viscosity over an extended temperature range, associated with small strain measurements. The second is the Multiple Stress Creep Recovery test (MSCR), which applies larger stresses and resulting strains. The MSCR test was used to measure non-recoverable creep compliance (J_{nr}) at multiple temperatures.

The linear amplitude sweep (LAS) test was conducted on three of the binders. However, due to inconsistencies in the data, this testing was discontinued and replaced with the Monotonic Shear Strength test (MOSS) for use in measuring ultimate properties and fracture performance.

Empirical testing using Penetration and R&B Softening Point methods was also conducted. Various methods have been proposed to use rheological measurements in place of these parameters. This empirical testing allows relationships between rheological parameters and empirical measurements to be explored as a secondary objective of the workplan.

[2]It is important to note that several of modified blends used in this study do not fully conform to ASTM requirements for roofing asphalts. The blends should be considered as generic materials that might have similar characteristics of roofing asphalts. The generic nature of the blends is intended to protect formulation identity.

For each of the modified binder systems, UV fluorescent images were obtained to ensure satisfactory blending and compatibility[3]. In some cases, additional mixing time was required to produce a fully incorporated polymer network. This is discussed in further detail in later sections of this report.

Test Methods

PmB Material preparation

Materials B, C and D were blended using a Silverson L5M-A high-shear mixer following protocols consistent with manufacturer recommendations. As general rule, this involved:

- Use of a rotary shear head to mill polymer pellets into a heated sample (~180°C) over the course of 2-5 minutes
- Continued mixing using a dispersion head at a rotational speed capable of sufficiently agitating the sample for an additional 4-6 hours

After completion of the blending process, the PmB materials were evaluated using UV fluorescent imaging. These images are shown below for materials B, C and D. The material represented as Blend D shows an example of a material that had extended mixing to ensure a continuous polymer network was achieved. This material had an additional hour of mixing before the final image was taken. Samples E and F were pre-blended by the supplier before being submitted for laboratory analysis.

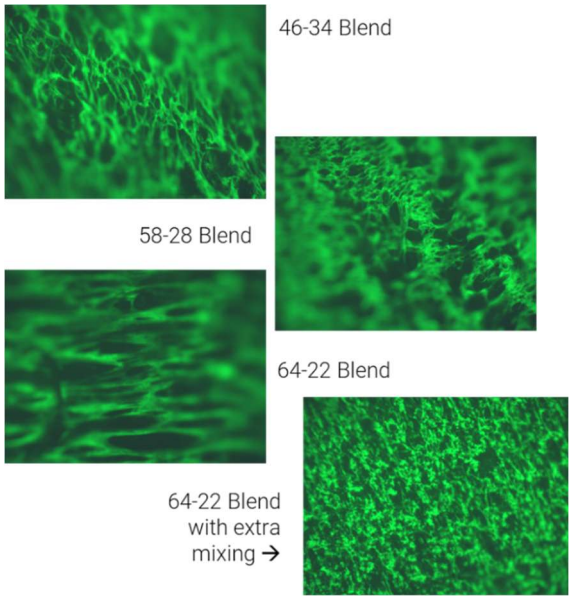

Figure 2. Blend B (PG46-34), Blend C (PG58-28) and Blend D (PG64-22) – examples of UV fluorescent images to examine SBS/ asphalt compatibility

[3]Microscope used was Motic BA4000-600 Upright Microscope.

Each material was tested in three conditions:

- Original / unaged
- 20-hour Pressure Aging Vessel cycle (PAV20) at 100°C per ASTM D6521, *Standard Practice for Accelerated Aging of Asphalt Binder Using a Pressurized Aging Vessel (PAV)*
- 40-hour Pressure Aging Vessel cycle (PAV40) at 100°C per modified ASTM D6521

PAV40 aging was considered to be simulative of 90 days in dark oven aging (DOA) at 80°C (Singhvi and Yousfi, 2023). Work previously conducted by Maynard (1983) suggests that 1 month of dark oven aging at 80°C would approximate 5 years of in-service aging. Thus, 90 days and/or PAV40 would in some instances would approximate 15 years of in-service aging, assuming a relatively linear aging rate.

Material	Original / Unaged	PAV20	PAV40
A			
B			
C			
D			
E			
F			

Figure 3. Photographs of PAV pans before and after aging

After aging in the PAV, the materials were homogenized through gentle stirring prior to testing. However, with some of the more complex materials it is possible that complete homogeneity was not possible. No vacuum degassing was performed on the PAV-aged materials.

Rheology

Rheological testing utilized the DSR, which is used in characterizing paving grade asphalt binders. Analysis was conducted using the RHEA software (Rowe and Raposo, 2021). RHEA develops the master curves used in the analysis without any assumptions regarding the model format, with the free-shifting method developed by Gordon and Shaw (1994). Additional details regarding the methods and analysis are described later in this section.

Dynamic Shear Rheometer

DSR testing, shown in Figure 4, was conducted using an Anton Paar MCR 302e rheometer employing 4-mm, 8-mm and 25-mm parallel plate geometry, generally following the procedures in ASTM D7175, *Determining the Rheological Properties of Asphalt Binder Using a Dynamic Shear Rheometer*. Test temperatures generally ranged from -35°C to 150°C, with slight variations depending on the stiffness of the material. A frequency sweep was conducted at each temperature using eleven frequencies from 0.1 to 10 rad/s, inclusive, spaced logarithmically at 5 points per decade.

Prior to temperature-frequency sweep testing, strain sweeps were performed from -20°C to 120°C to assess linear viscoelasticity in the test temperature range. Based on this data, the applied shear strain varied depending on the test temperatures and geometry. At very low temperatures using the 4-mm parallel plate geometry, the applied shear strain was 0.05%. An applied shear strain in the range of 0.1% to 0.2% was used at intermediate test temperatures tested with the 8-mm geometry, and an applied shear strain in the range of 0.3% to 0.5% was used for testing conducted at high temperatures with the 25-mm parallel plate geometry. A typical example of the data collected is presented in Figure 5.

Using RHEA software, the data from each of these experiments were then combined to form master curves over a complex modulus, G^*, range from 100 Pa to 100 MPa. Example master curves for G* and phase angle, δ, are shown in Figure 6, with a reference temperature (T_{ref}) of 20°C.

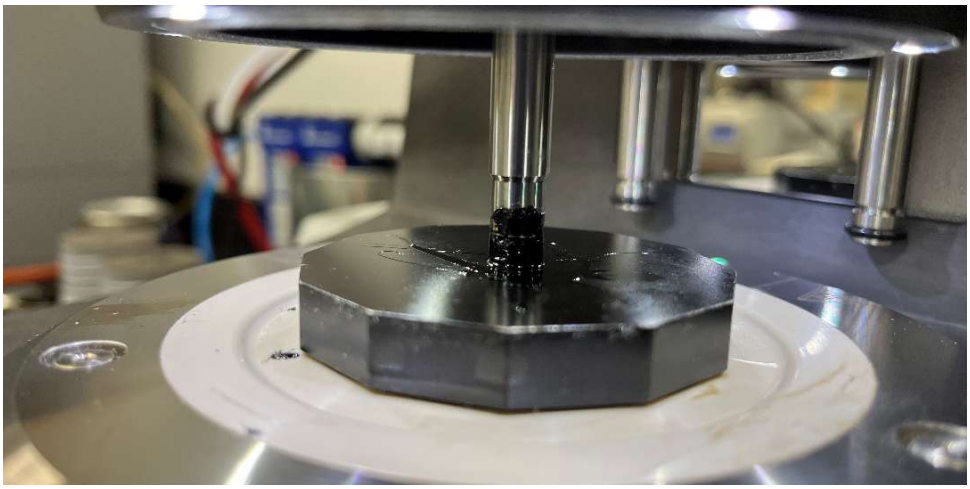

Figure 4. DSR testing using the 8-mm parallel plate measurement geometry

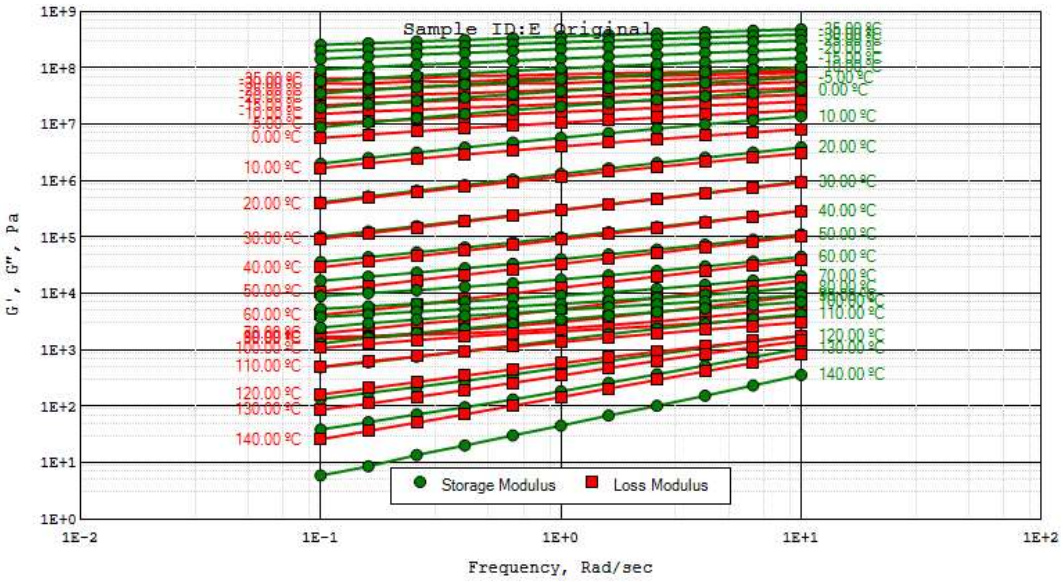

Figure 5. Isotherms of stiffness for Sample E (Original) collected from DSR testing

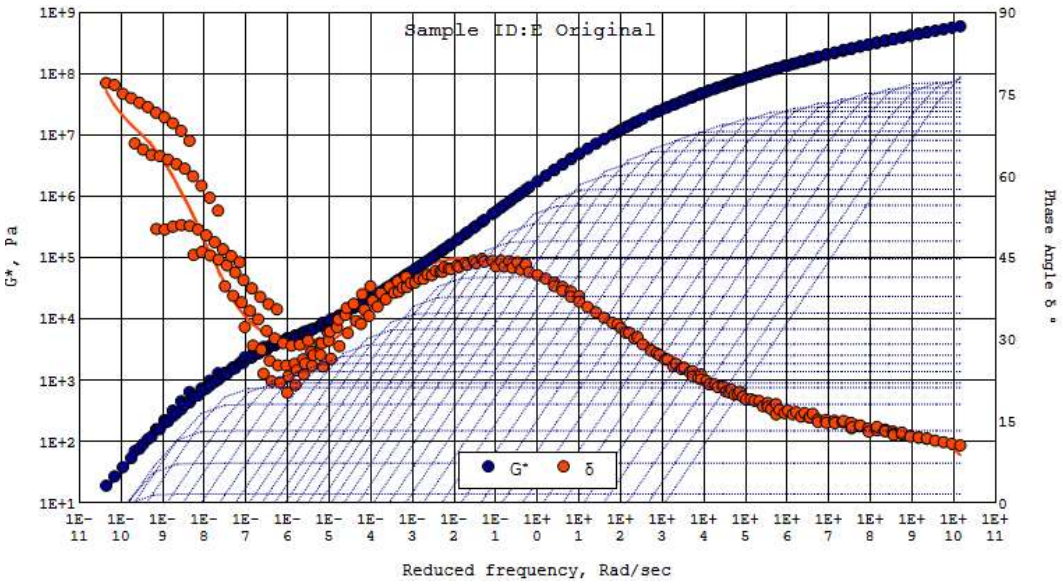

Figure 6. Master curve of modulus, *G, and phase angle, *δ*, for Sample E (Original), T_{ref} = 20°C**

High Temperature Rheology

High temperature measurements were conducted using the MSCR test from which the non-recoverable creep compliance, J_{nr}, and recovery percentage, R, were determined. The test was conducted at two stress levels (100 Pa and 3,200 Pa) per ASTM D7405, *Standard Test Method for Multiple Stress Creep and Recovery (MSCR) of Asphalt Binder Using a Dynamic Shear Rheometer*. To ensure a reasonable resolution of stress and strain it was decided to vary the temperature so that the J_{nr} at 3,200 Pa ($J_{nr3.2}$) would be approximately in the range 1 to 2 kPa^{-1}. The variation in temperatures did result in different temperatures being used for the various aging conditions. The targeted range of 1 to 2 kPa^{-1} was generally achieved, with the exception of material "E" at the PAV20 condition.

Ultimate Test - Monotonic Shear Strength (MOSS) Test

The Monotonic Shear Strength (MOSS) test measures the required energy needed to cause an asphalt binder to yield when subjected to a monotonically applied shear stress. It is performed on the DSR by applying a constant shear strain, γ, to the binder at rotational rate of 0.05 RPM until a peak stress, τ_f, is observed at the yield strain, γ_f. Binder yield energy, E_f, is determined by finding the area under the stress-strain curve to the point of maximum stress (Figure 7). Details on the procedure are given in a draft ASTM method, appended to this report.

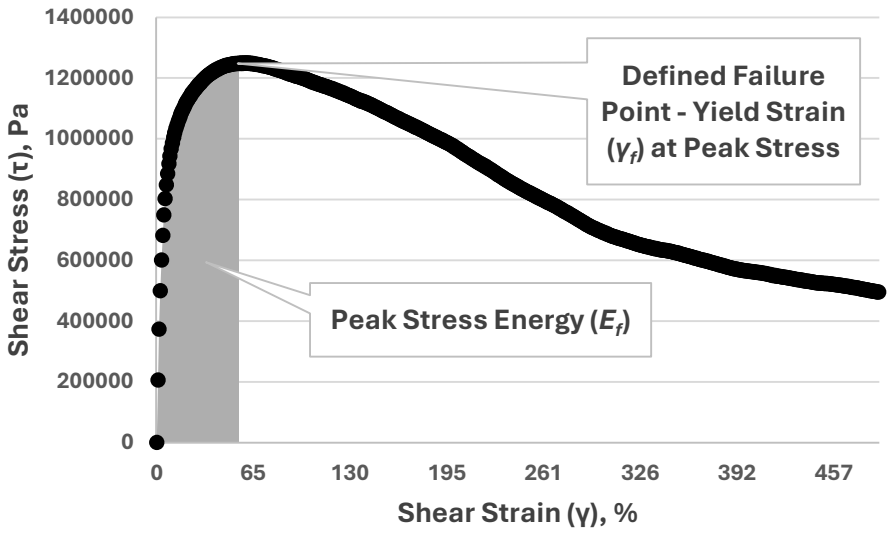

Figure 7. Typical stress-strain curve for MOSS

Materials were tested using the MOSS procedure at temperatures such that peak stress occurred in a stiffness range of approximately 1 to 10 MPa. Previous work has shown that the transition from ductile to brittle failure occurs near this range of stiffness; thus, analysis in this region captures true fatigue and cohesive failure rather than instability flow or adhesive failure. The temperature range used was -10°C to +37.3°C and varied depending upon the binder. The test temperatures are included in the data reports.

Traditional Tests

Penetration was measured per ASTM D5, *Standard Test Method for Penetration of Bituminous Materials*, at 25°C using the standard loading mass of 100g and loading time of 5 seconds. Other tests conducted were Ring-and-Ball Softening Point (*ASTM D36, Standard Test Method for Softening Point of Bitumen*) and Rotational Viscosity (ASTM D4402, *Standard Test Method for Viscosity Determination of Asphalt at Elevated Temperatures Using a Rotational Viscometer*) at 350°F (176.7°C). These tests typify current industry practice for classifying the empirical properties of asphalt coatings.

Data summary

The data collected is summarized in Appendix A and discussed in detail in the following sections of this report.

Rheological Analysis

Master curves

Master curves were constructed using the RHEA software. A constant reference temperature of 20°C was used in all the analysis conducted. To allow comparisons of materials, all the data has been presented in two formats; 1) plots of G* versus reduced frequency at T_{ref} = 20°C, and 2) a Black

Space plot (G* vs. δ). The first plot shows the relative hardness of the material and the changes associated with aging can be clearly viewed. The second plot provides an assessment of the rheological type of the binder. In some cases, this plot shows transitions from thermo-rheological simple behavior to more complex material behavior which does not conform to the assumption of thermo-rheological simplicity. The comparisons shown, with brief summary discussion, are as follows:

- **Material A -** This material is typical of an oxidized roofing grade asphalt binder. The samples all increase in stiffness with aging (Figure 8). In the Black Space plot (Figure 9), the resulting lines are fairly straight, which is typical with oxidized grades.
- **Material B** - The modification effect on the shape of the master curve is clear from the two plots in Figure 10 and Figure 11. It should be noted that stiffness increases as the material progressively ages. However, the differences in the shapes in the Black Space plot are similar for 20 and 40 hours of PAV aging. At these two aging conditions the cross-over modulus, G_c, lies below the stiffness range normally associated with cracking behavior.
- **Material C –** The modification effect on the shape of the master curve is clear from the two plots in Figure 12 and Figure 13. These plots have similar behavior to that seen for Material B. The stiffness increases as the material progressively ages and the differences in the shapes in the Black Space plot are similar for 20 and 40 hours of PAV aging. At these two aging conditions the cross-over modulus lies below the stiffness range normally associated with cracking behavior.
- **Material D –** The complex modulus increases with aging (Figure 14) , but unlike the two previous PmB examples, some changes are observed in Black Space for each aging condition (Figure 15) This indicates change in rheological type, which is more significant when viewing the two PAV conditions.
- **Material E** – The initial testing of this material (Figure 16 and Figure 17) showed some unexpected behavior with regard to the high stiffnesses region, with the PAV20 having a higher stiffness than the PAV40 in certain regions. This was considered a possible test error, leading to a repeat of the testing (
- Figure 18 and
- Figure 19). When this material was aged, the appearance of the sample was very non-homogeneous (see Figure 3). This may have resulted in some non-representative materials being used in the rheological testing. The two sets of tests are compared in Figure 20 and Figure 21. It can be seen that the data for the Original and PAV40 are very close in both the frequency and temperature domains, whereas the PAV20 results are different. The results for the repeat sample that show increased stiffness with aging are considered more logical; therefore, this data has been adopted for the ongoing analysis.
- **Material F** - Figure 22 shows the hardening as expected. The Black Space plot (Figure 23) shows some changes in the high temperature rheology in a similar manner to the other modified binders, with the rheological type changing with increasing aging.

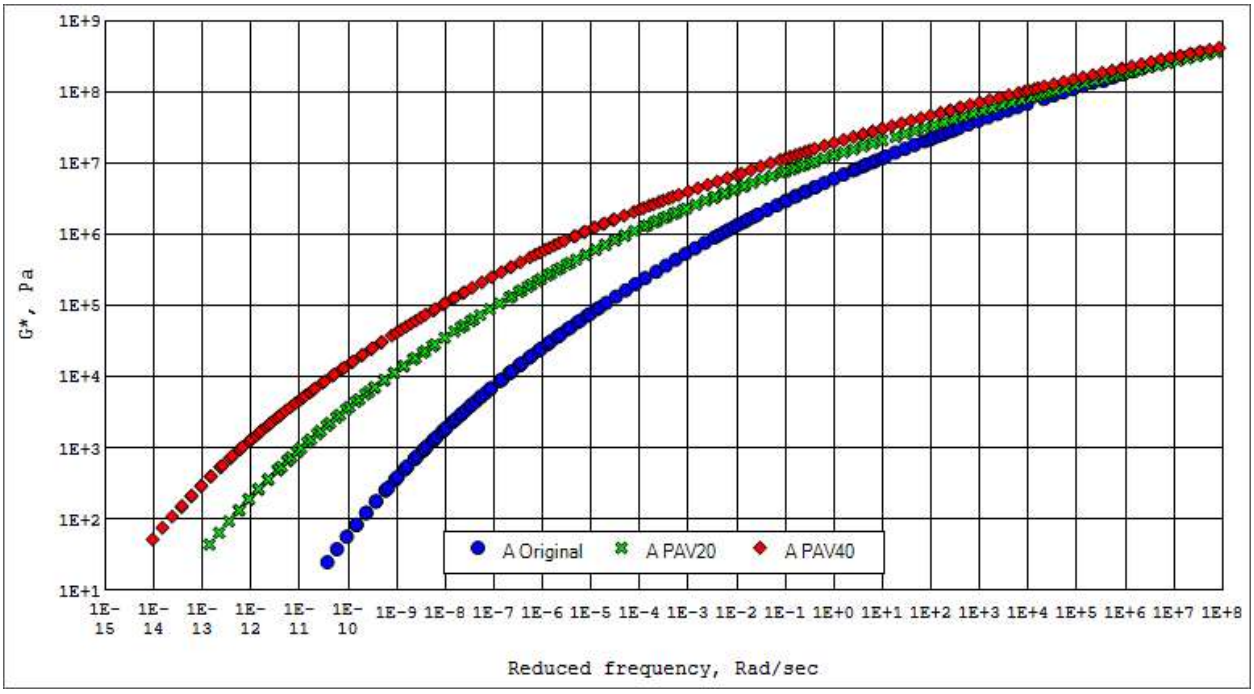

Figure 8. Master curves for Sample A (Original, PAV20 and PAV40 conditioning) - G* versus reduced frequency at a reference temperature (T_{ref}) of 20°C

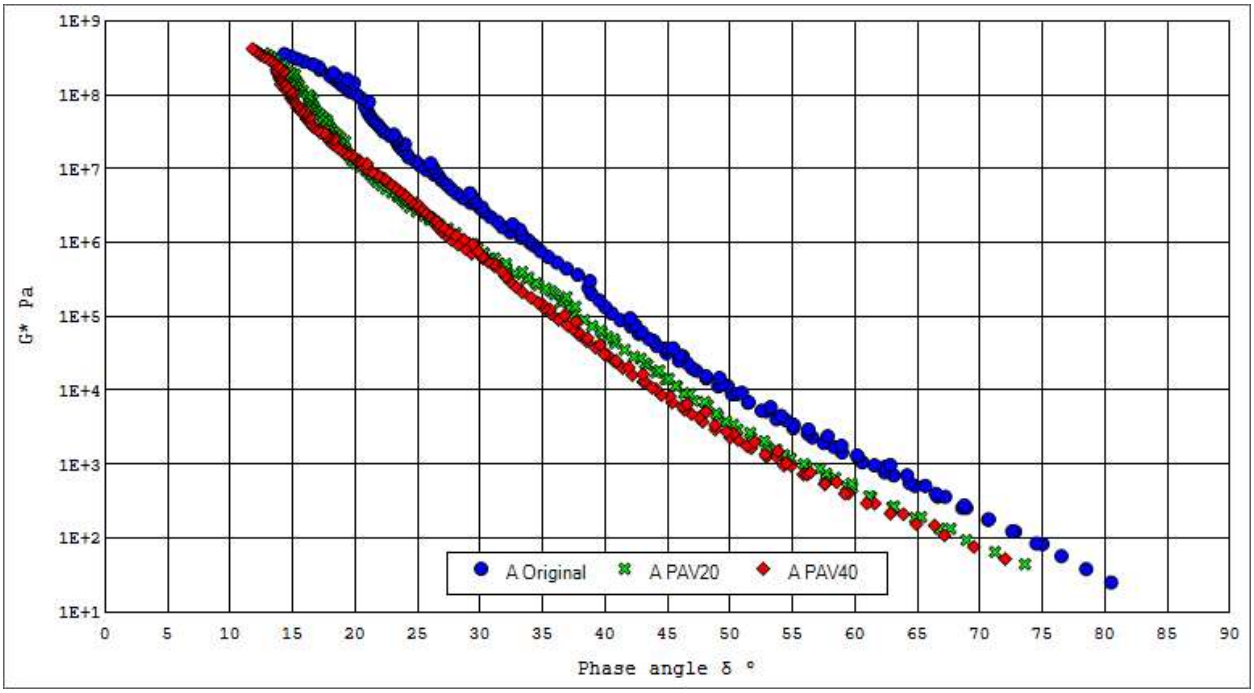

Figure 9. Black Space plot for Sample A (Original, PAV20 and PAV40 conditioning)

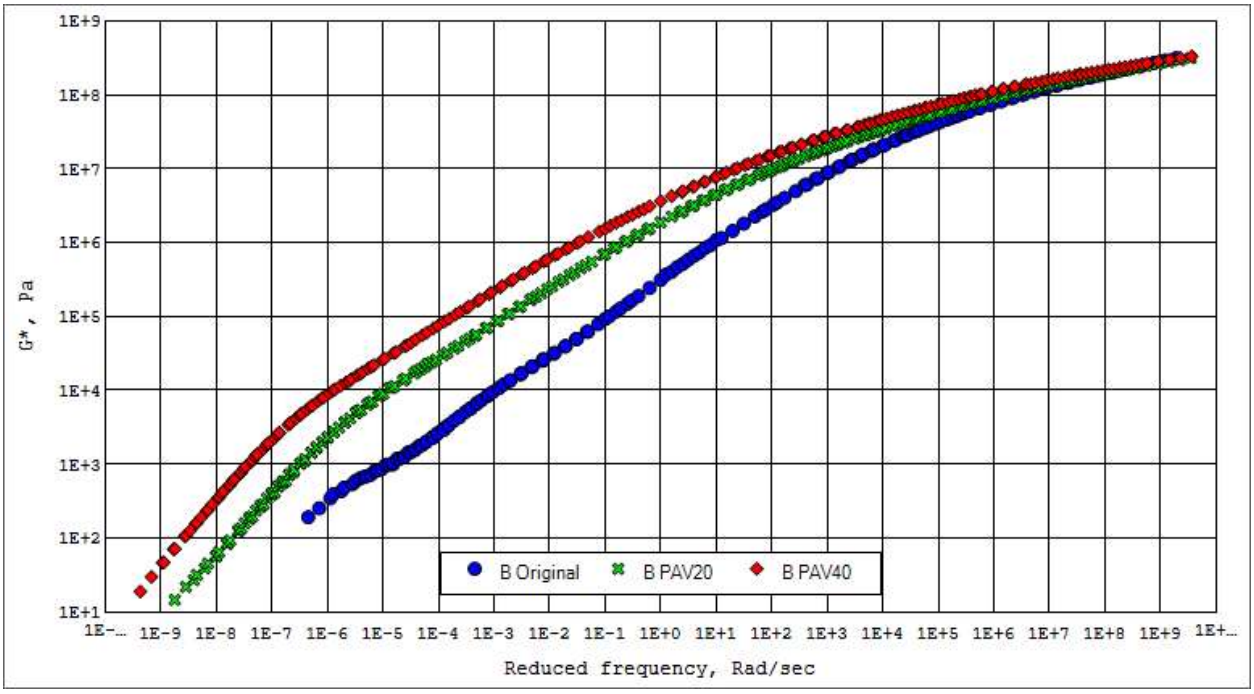

Figure 10. Master curves for Sample B (Original, PAV20 and PAV40 conditioning) - G* versus reduced frequency at a reference temperature (T_{ref}) of 20°C

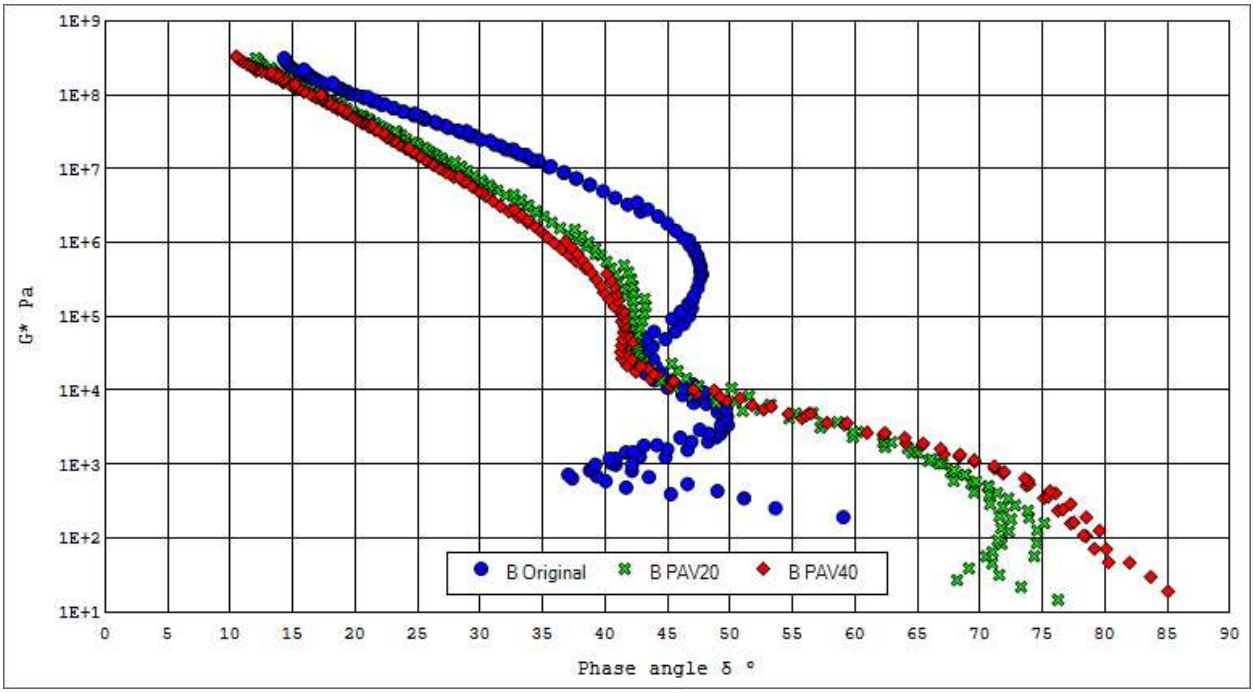

Figure 11. Black Space plot for Sample B (Original, PAV20 and PAV40 conditioning)

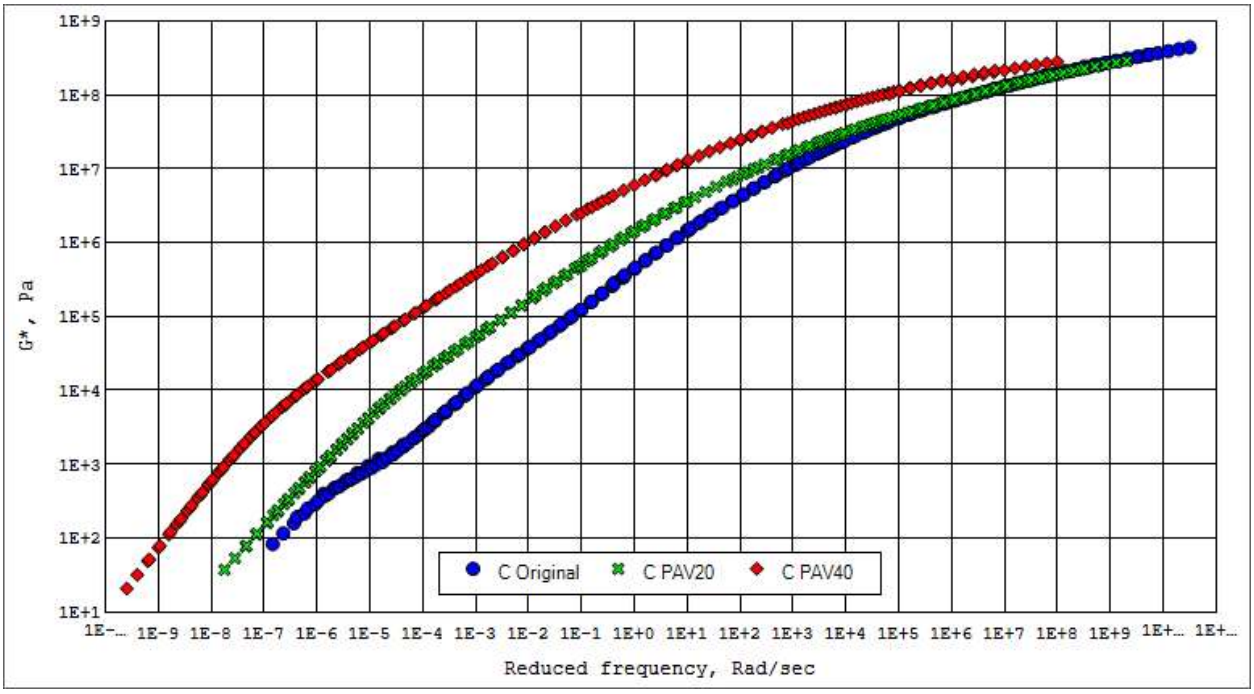

Figure 12. Master curves for Sample C (Original, PAV20 and PAV40 conditioning) - G* versus reduced frequency at a reference temperature (T_{ref}) of 20°C

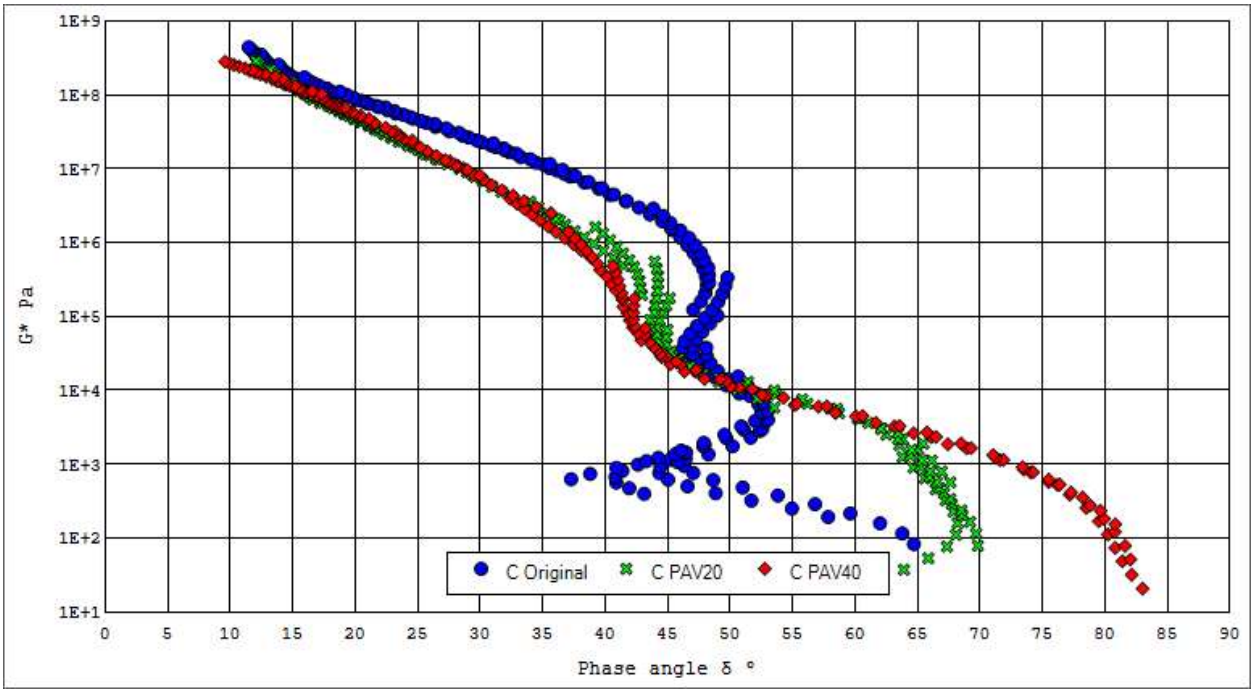

Figure 13. Black Space plot for Sample C (Original, PAV20 and PAV40 conditioning)

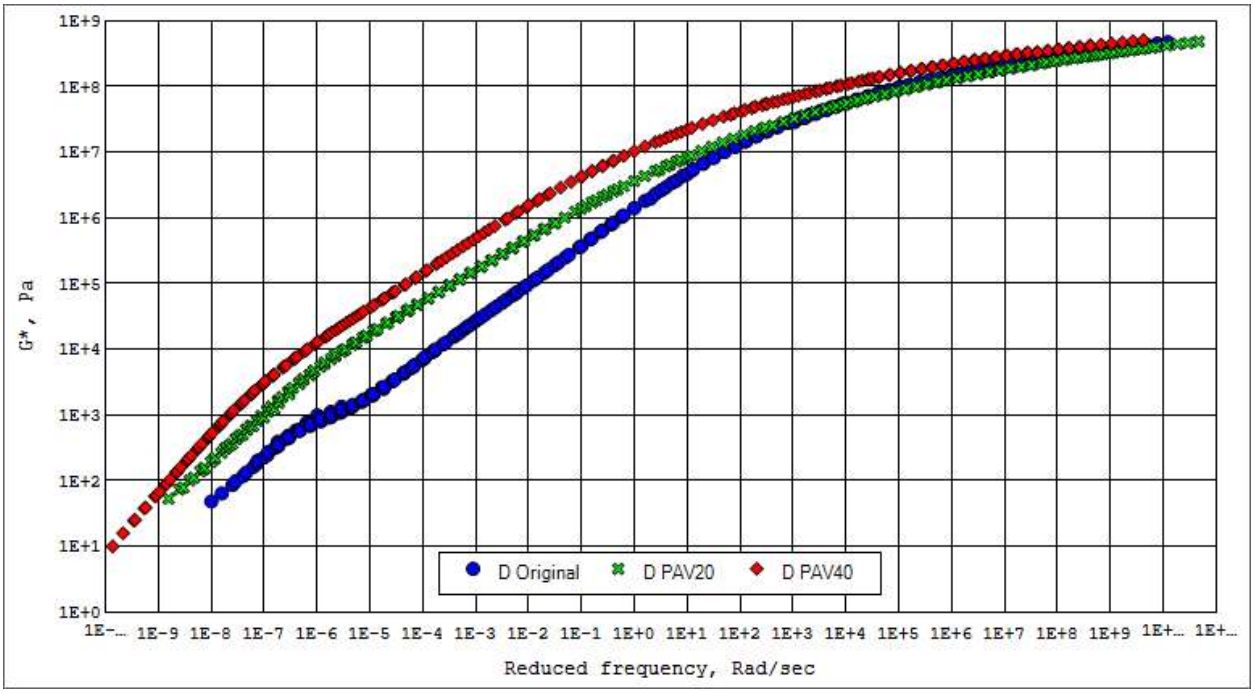

Figure 14. Master curves for Sample D (Original, PAV20 and PAV40 conditioning) - G* versus reduced frequency at a reference temperature (T_{ref}) of 20°C

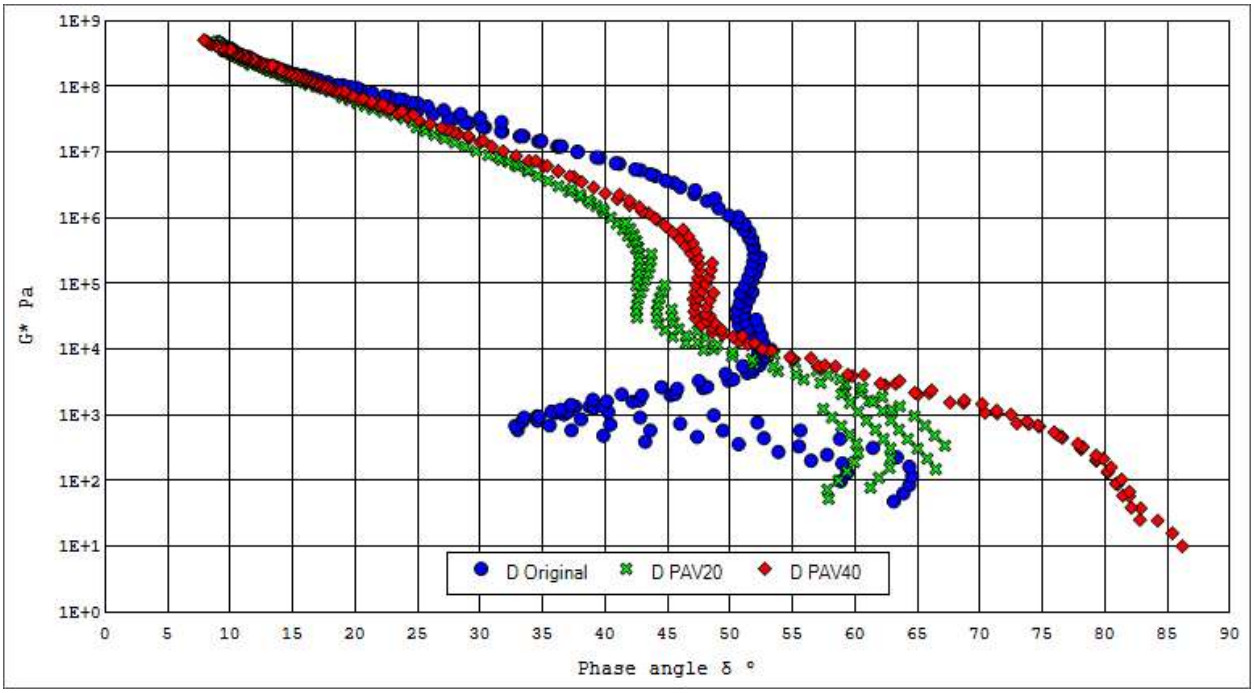

Figure 15. Black Space plot for Sample D (Original, PAV20 and PAV40 conditioning)

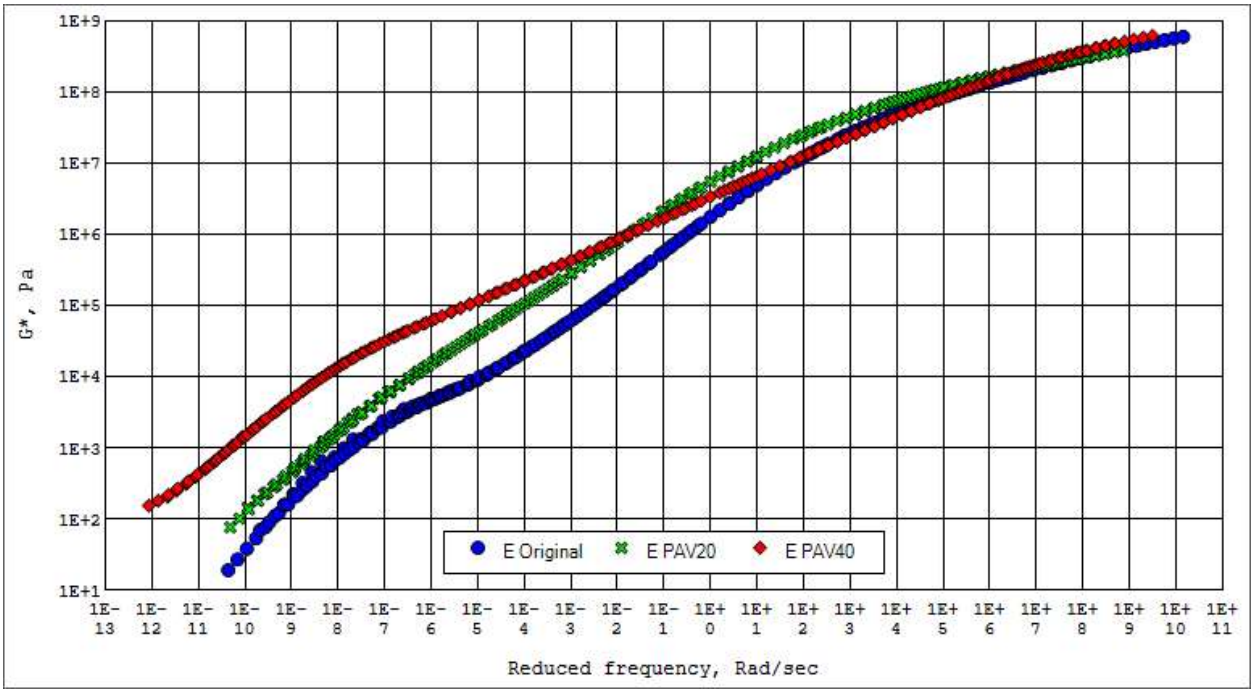

Figure 16. Master curves for Sample E (Original, PAV20 and PAV40 conditioning) - G* versus reduced frequency at a reference temperature (T_{ref}) of 20°C

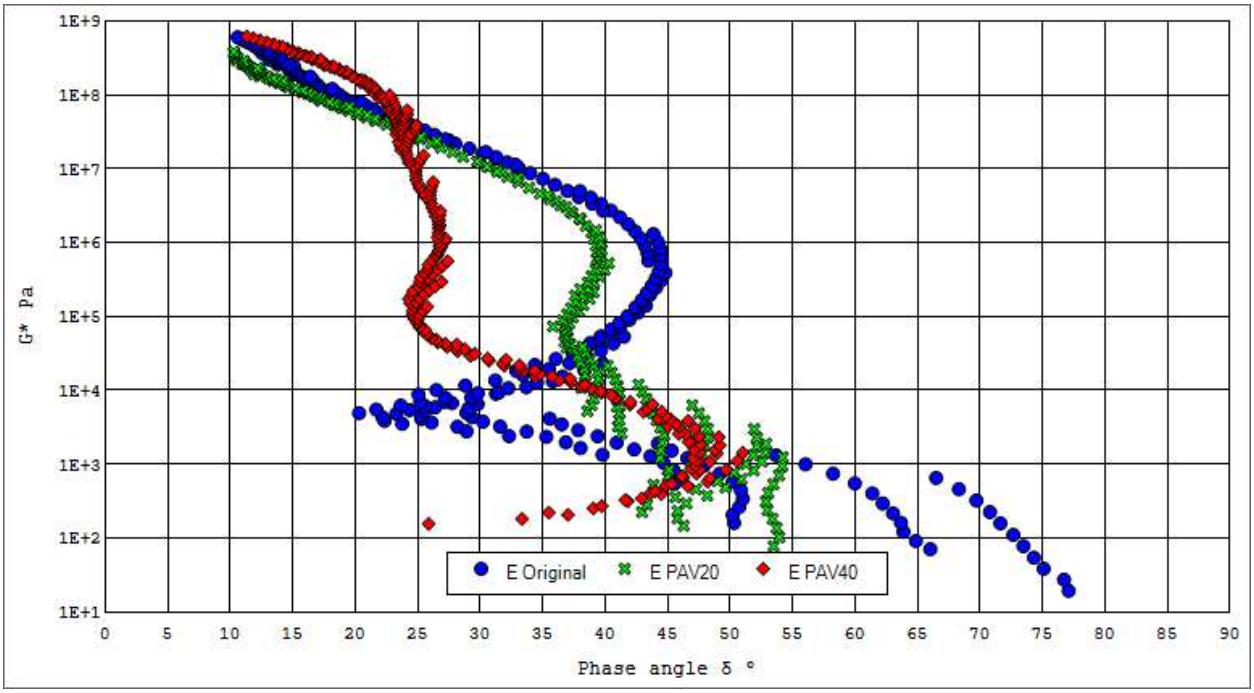

Figure 17. Black Space plot for Sample E (Original, PAV20 and PAV40 conditioning)

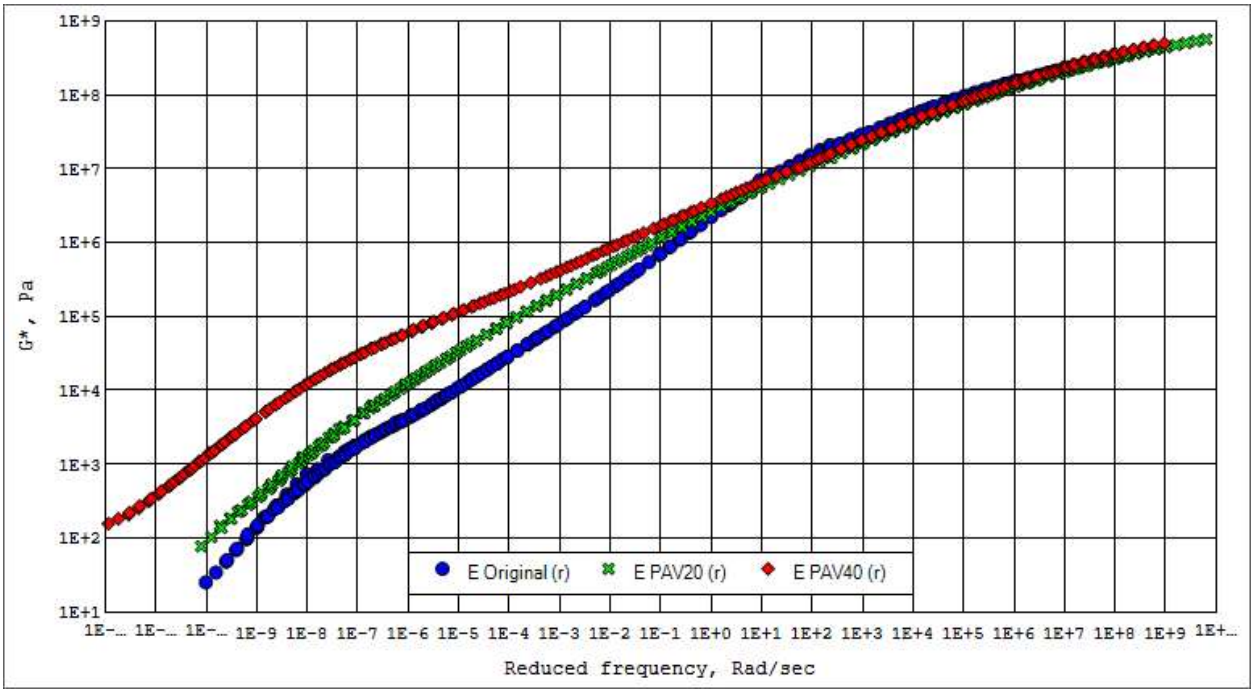

Figure 18. Master curves for Sample E (Original, PAV20 and PAV40 conditioning) with repeated (r) results - G* versus reduced frequency at a reference temperature (T_{ref}) of 20°C

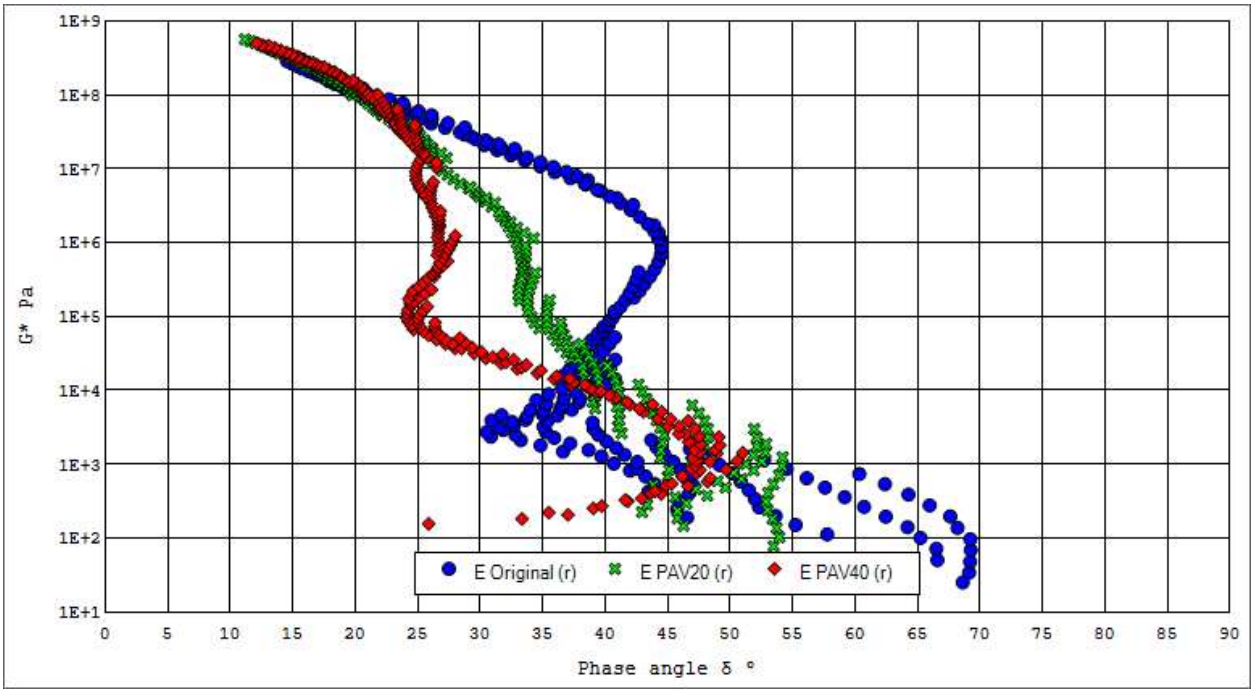

Figure 19. Black Space plot for Sample E (Original, PAV20 and PAV40 conditioning) – repeated (r) results

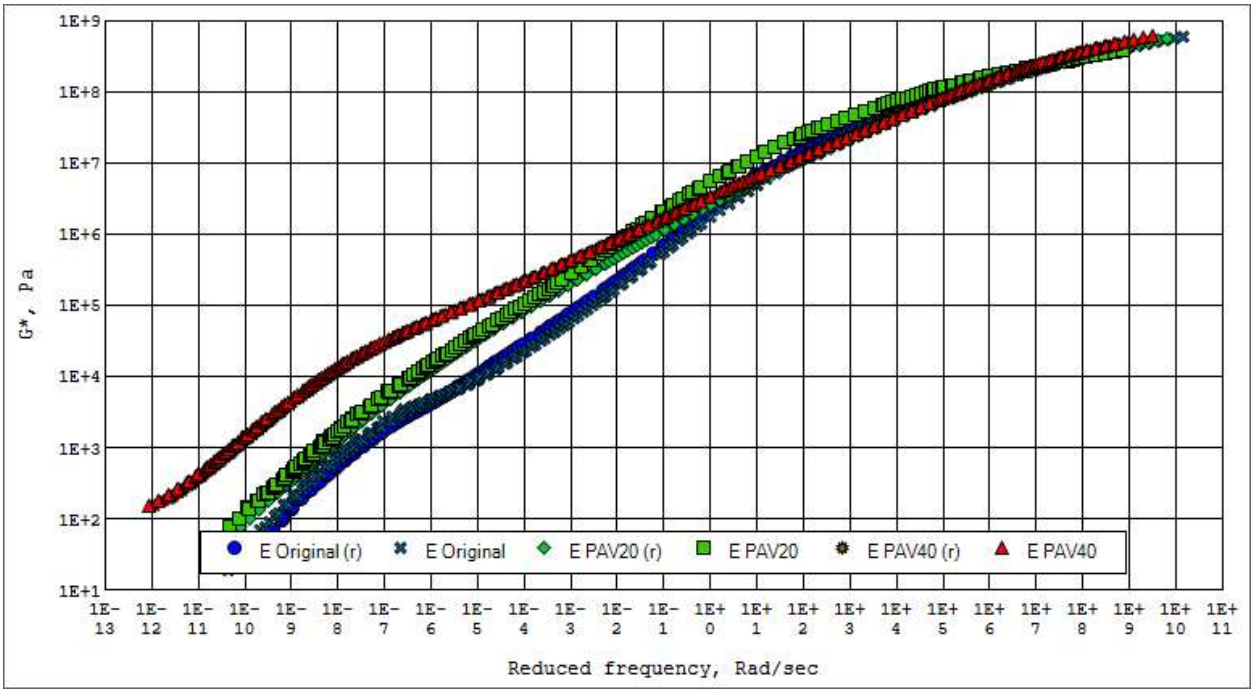

Figure 20. Master curves for Sample E (Original, PAV20 and PAV40 conditioning) with first results and repeated (r) results - G* versus reduced frequency at a reference temperature (T_{ref}) of 20°C

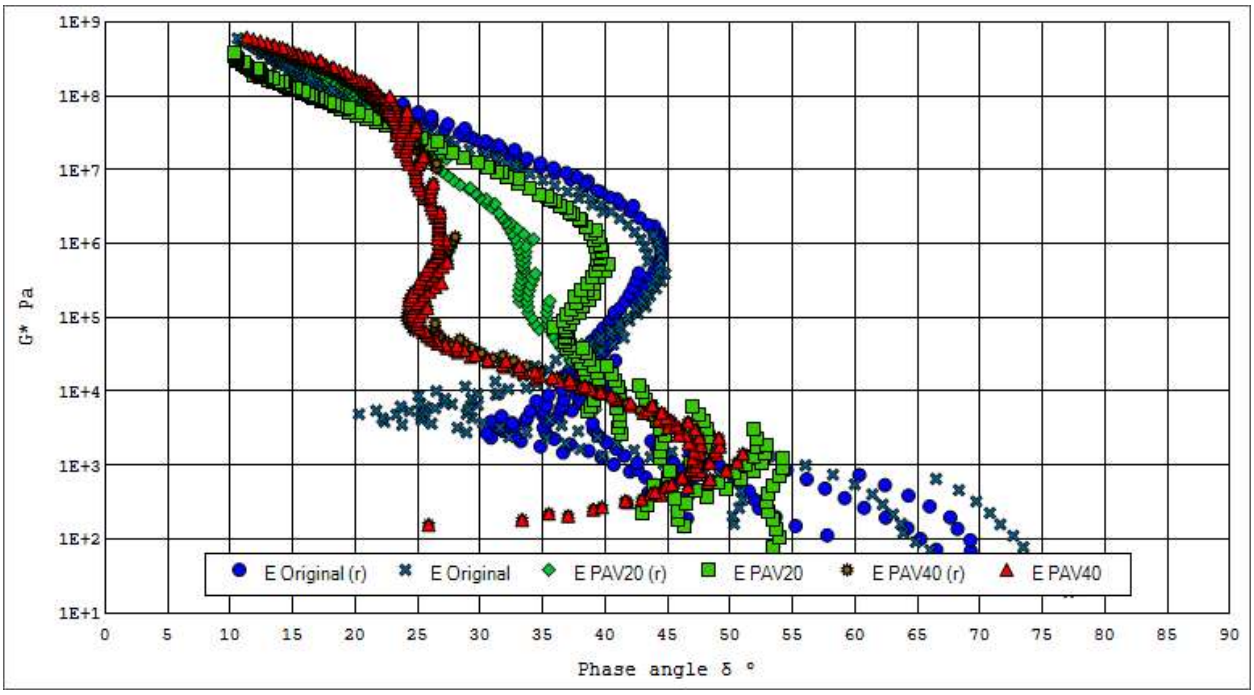

Figure 21. Black Space plot for Sample E (Original, PAV20 and PAV40 conditioning) – first results and repeated (r) results

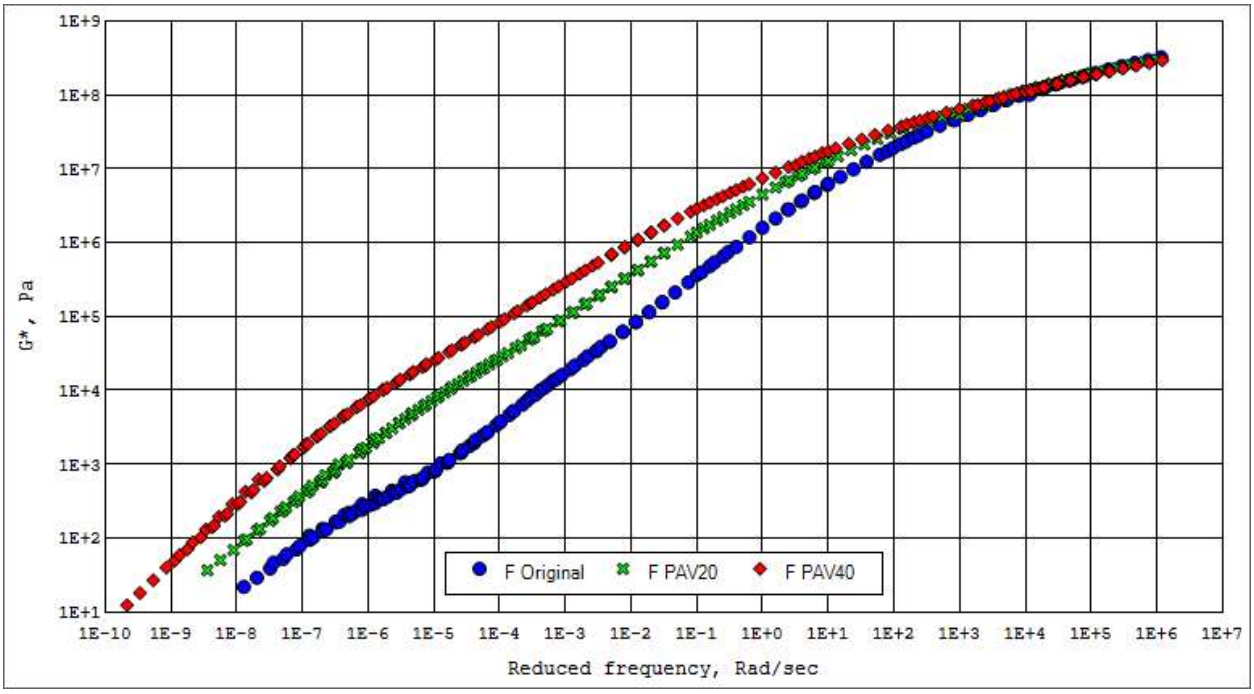

Figure 22. Master curves for Sample F (Original, PAV20 and PAV40 conditioning) - G* versus reduced frequency at a reference temperature (T_{ref}) of 20°C

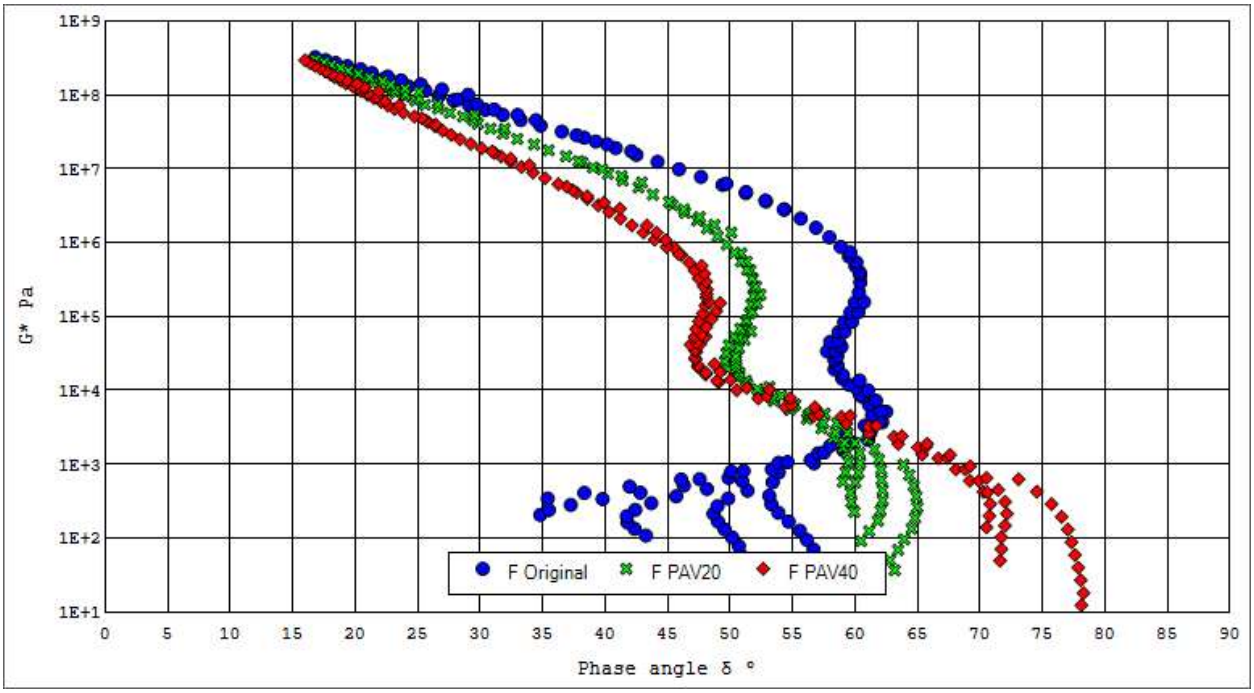

Figure 23. Black Space plot for Sample F, Original, PAV20 and PAV40 conditioning

Linear Viscoelastic Rheological Parameters

The shape of a master curve in the higher stiffness region can typically be defined by one of four parameters. These are:

1) ΔT_c from Bending Beam Rheometer (BBR) analysis;
2) Rheological Index (R-value) from a fit of the data to the Christensen-Anderson model (or via simplifications and closed form solutions);
3) the phase angle at a given modulus value, and/or;
4) the logarithm of the cross-over modulus, G_c (i.e. the modulus where phase angle is 45°)

In this work, the first two methods were not found to be suitable for evaluating the roofing asphalt binder samples. BBR testing was not conducted based on lessons learned from AIF Project 22-03 performed at the Asphalt Institute (Rowe et al., 2023). As in AIF Project 22-03, the use of R-value was not possible since the fit of the data to the Christensen-Anderson model was generally poor, with a root mean square (RMS) error greater than 2.5%. Thus, the two methods used in this work were the logarithm of the cross-over modulus (log G_c) (Farrar et al., 2013) and phase angle at a given modulus value (Kriz, 2020). Each of these methods effectively define the shape of the master curve in the higher stiffness region in a manner similar to the R-value.

The value of G* (modulus) used for the phase angle calculation is 10 MPa. This value was chosen for several reasons:

1. It is a modulus that can be consistently obtained from DSR measurements using 8-mm parallel plate geometry
2. It is similar to the value proposed by Pavel Kriz for paving-grade binders (8.967 MPa) (Kriz et al., 2020)
3. It is the same value of modulus used by the Federal Aviation Administration (FAA) in recent work, in which they use the tangent of phase angle at a G* of 10 MPa (Bennert, et al., 2022)
4. It appears to be a good descriptor of the shape of the master curve in the high stiffness region, related to the relaxation properties
5. It is the same value adopted in AIF Project 22-03

Thus, a reasonable body of work will be available on binders at this value of modulus (G*=10 MPa) which can support the work of this research. Furthermore, if the temperature is obtained (at a fixed frequency) corresponding to this modulus value ($T_{G^*=10\ MPa}$), a measure of the hardness of the binder can be determined. Higher temperatures for $T_{G^*=10\ MPa}$ correspond to stiffer binders.

The shape of the master curves and the modification types reveal that, for certain binders, a relationship exists between two common ways of defining the shape of the master curve in the higher stiffness region (Figure 24). However, with certain modification systems, the retention of stiffness caused by the polymer network occurs in a different region of the master curve, resulting in the atypical behavior as shown by various materials (for example, see Figure 11, Figure 13, Figure 15 and Figure 17). Material F in Figure 23 is closer in behavior to a heavily modified paving-grade binder. For typical paving-grade binders, a good correlation will exist for cross-over modulus and phase angle at

10 MPa (Rowe et al., 2023). However, for roofing materials, such as those noted, the cross-over modulus occurs in a stiffness region much lower than the range typically associated with cracking/toughness properties. This finding was also observed in the work conducted for AIF Project 22-03 (Rowe et al., 2023). This type of result has also recently been reported for highly modified paving-grade binders (Rowe et al., 2025).

An example relevant to this study is shown in Figure 25. Unaged material (B Original) has five locations for which the cross-over modulus can be determined with one of these above a G* stiffness of $1x10^6$Pa. Material B, after 40 hours of aging in the PAV (B PAV40), has one location for which the cross-over modulus can be obtained, which is at approximately $1x10^4$ Pa; this is significantly below the range of stiffness associated with cracking and durability. This clearly demonstrates that the cross-over modulus and any other cross-over property cannot be used as a cracking parameter for these roofing-type materials, which is consistent with the work developed in AIF Project 22-03.

Since the use of properties in the cross-over region is problematic, the modulus and temperature associated with a phase angle of 27 degrees is used instead. This phase angle has been shown to be consistent with BBR m-value of approximately 0.300 (i.e. the critical m-value for paving-grade binders) (Rowe, 2014). In a similar manner to cross-over temperature (denoted as T_{Gc}), the $T_{\delta=27°C}$ can provide an indication of the relative hardness/stiffness of the product being used.

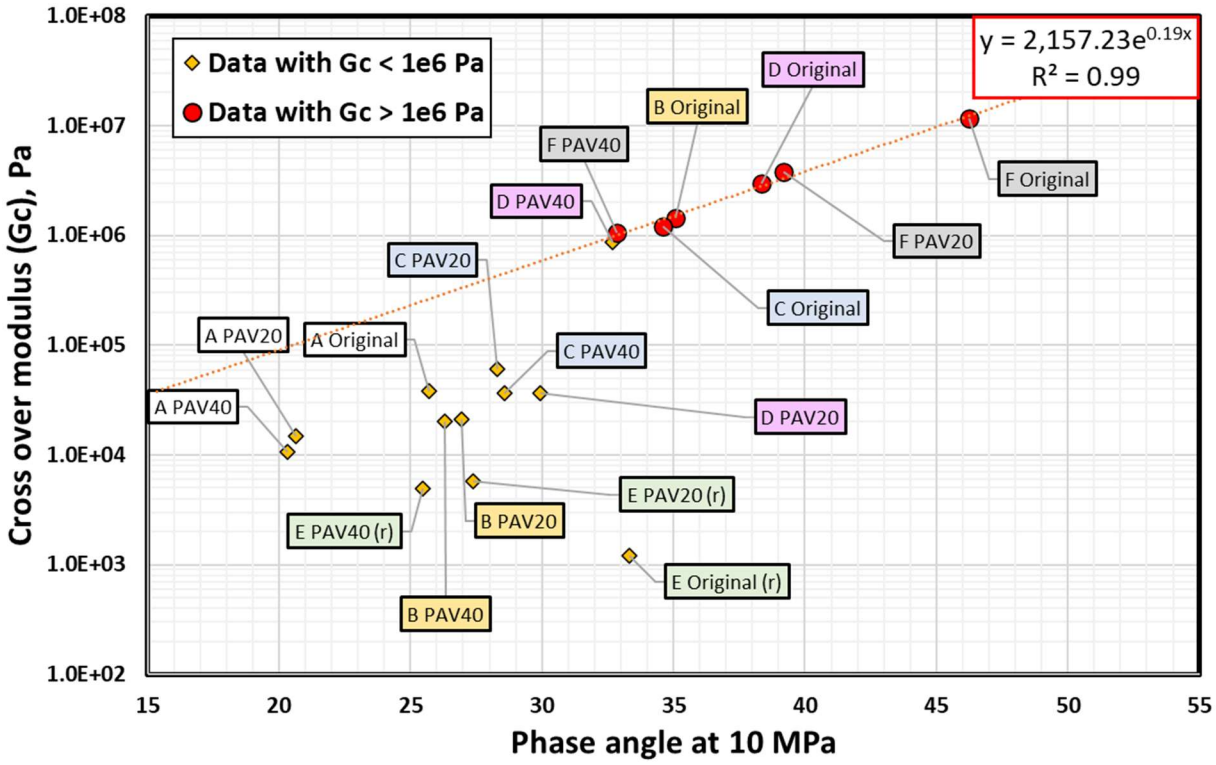

Figure 24. Relationship between two measures of master curve shape – Phase Angle at Constant Modulus of 10 MPa and logarithm of the Cross-over Modulus (Log G_c)

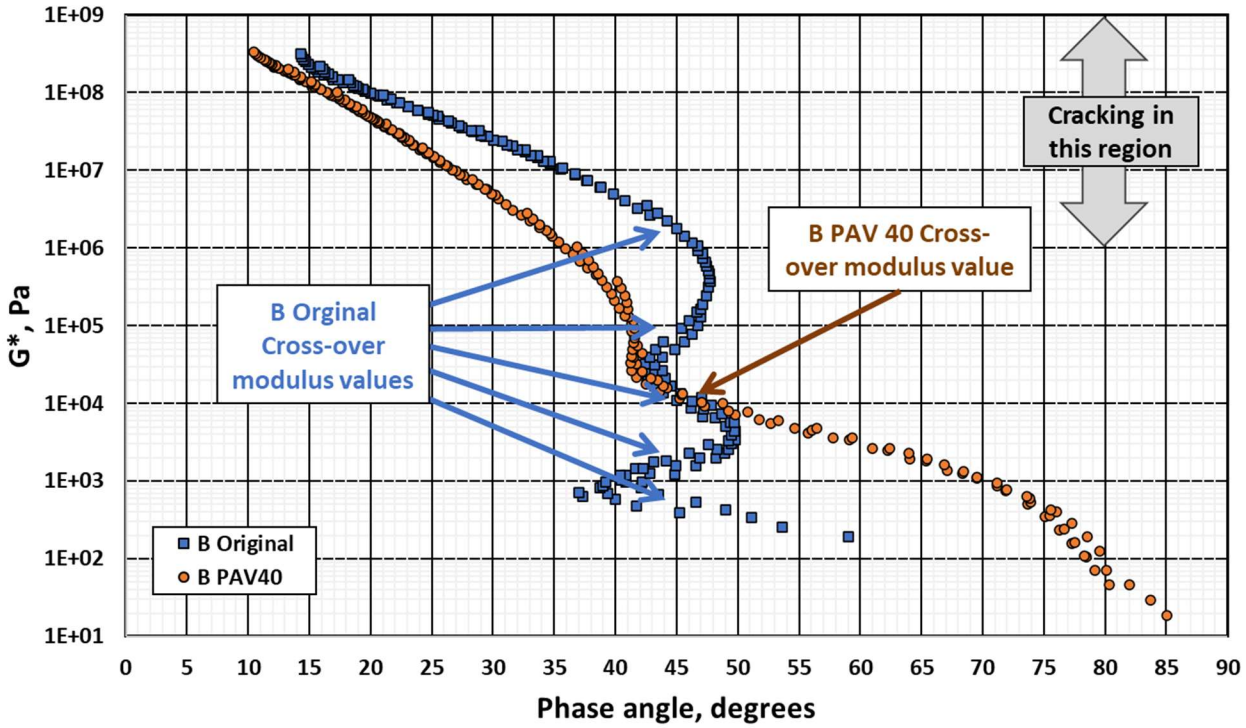

Figure 25. Black Space plot showing location of values representing cross-over modulus for Material B (original and PAV40 conditioning)

As a material ages, a typical response exhibits a decrease in the phase angle and the cross-over modulus, compared to the unaged or less-aged conditions. The data shown in Table 2 indicates that the expected trend is more evident in phase angle results than for log G_c.

The large difference between the temperature corresponding to phase angle of 27 degrees[4] is associated with the change that occurs in aging and the significant change in properties in this range that relate to cracking. A rapid test procedure has been submitted to ASTM for determination of the temperature that corresponds to a phase angle of 27 degrees, which is included in this report as Appendix C.

[4]A similar result applies for a phase angle of 30 degrees but the correlations are marginally better with a phase angle of 27 degrees.

Table 2. Analysis parameters determined from master curves, T_{ref} = 20°C

Test	Error in Fit,rms%			Tref °C	Glover-Rowe Analysis, 0.005 rads/sec, 15°C			Glover-Rowe Analysis, 10 rads/sec, 15°C		
	LVE spectra	Poly Fit	CA model		G*, Pa	δ°	G-R, kPa	G*, Pa	δ°	G-R, kPa
A Original	0.96	0.64	7.22	20	1,853,000	31.35	2,598	1.84E+07	23.97	37,750
A PAV20	1.01	0.56	≥15.0	20	5,823,000	21.89	13,450	3.08E+07	17.99	90,080
A PAV40	1.87	0.83	≥15.0	20	9,315,000	20.34	23,560	4.29E+07	16.37	140,100
B Original	2.67	2.64	2.97	20	41,950	44.65	30	2.04E+06	44.28	1,497
B PAV20	2.58	2.01	1.48	20	344,700	41.27	295	7.58E+06	28.87	12,040
B PAV40	2.96	2.04	0.96	20	848,000	37.84	862	1.21E+07	25.17	23,380
C Original	1.67	0.98	2.43	20	54,960	47.36	34	2.77E+06	42.15	2,265
C PAV20	1.95	1.78	1.89	20	230,300	42.94	181	5.98E+06	31.61	8,280
C PAV40	1.97	1.55	2.86	20	1,488,000	36.78	1,594	1.99E+07	25.22	38,230
D Original	5.91	5.78	6.13	20	165,200	52.71	76	9.03E+06	39.11	8,619
D PAV20	3.12	2.63	2.59	20	759,900	41.33	649	1.45E+07	27.15	25,190
D PAV40	2.86	1.68	2.53	20	2,208,000	41.53	1,866	3.34E+07	23.15	71,910
E Original	4.44	3.79	5.71	20	365,200	43.4	281	1.14E+07	32.44	15,070
E PAV20	2.06	1.91	9.03	20	656,000	33.54	825	8.77E+06	27.71	14,780
E PAV40	1.61	1.21	≥15.0	20	1,057,000	27.35	1,815	1.00E+07	25.45	19,010
F Original	4.29	4.23	2.52	20	158,400	58.7	50	1.55E+07	42.28	12,630
F PAV20	2.54	2.26	3.87	20	652,600	50.18	348	2.46E+07	32.67	32,330
F PAV40	3.22	2.77	2.31	20	1,562,000	43.32	1,205	2.86E+07	27.08	49,810
Test		**Temperature (°C) at defined value, 10 rads/sec**								
	G*=8.967 MPa	G*=10 MPa	G*=100 MPa	G*=111 MPa	G"= 5 MPa	G"= 6 MPa	G-R= 5 MPa	δ°=27	δ°=30	δ°=45
A Original	23.3	22.05	-4.63	-5.86	20.14	17.81	34.77	26.7	36.42	82.86
A PAV20	31.77	30.29	-0.66	-2.2	24.7	21.94	48.58	54.38	62.78	112.79
A PAV40	38.93	37.33	1.79	0.17	30.87	27.55	56.91	67.51	77.36	126.21
B Original	4.28	3.47	-16.51	-17.67	4.75	3.03	8.19	-5.79	-1.85	17.54
B PAV20	13.18	11.99	-13.83	-15.16	10.74	8.64	21.51	12.15	16.18	76.04
B PAV40	18.5	17.27	-11.36	-12.91	15.46	12.84	28.21	18.34	25.06	85.29
C Original	6.37	5.54	-14.84	-16.03	6.64	5.05	10.55	-3.33	0.18	21.04
C PAV20	10.84	9.7	-16.5	-17.89	9.05	6.4	18.91	7.75	12.79	62.94
C PAV40	23.65	22.52	-4.55	-5.97	21.93	19.5	32.17	19.52	25.9	81.6
D Original	15.05	14.23	-6.71	-7.94	16.12	14.54	18.08	3.46	6.22	23.16
D PAV20	19.52	18.55	-5.07	-6.34	18.53	16.15	26.18	14.73	18.63	74.54
D PAV40	29.88	28.75	-0.09	-1.61	29.73	27.43	35.91	20.48	24.85	51.75
E Original	16.99	16.08	-15.94	-18.44	17.07	15.15	21.56	6.5	11.95	140.49
E PAV20	14.76	13.62	-10.85	-11.96	12.53	10.34	25.47	12.83	24.21	115.15
E PAV40	16.31	15.03	-10.96	-12.16	13.15	11	30.4	31.77	98.27	130.9
F Original	18.04	17.45	-1.28	-2.7	19.72	18.6	18.53	-0.32	4.62	16.64
F PAV20	22.56	21.75	-0.39	-2.01	23.79	22.19	25.11	9.35	12.96	28.71
F PAV40	25.82	24.84	0.5	-1.14	25.7	23.73	31.32	14.84	20.17	43.91
Test	**Phase angle, δ°, at constant G* (MPa)**				**G*, Pa at constant phase angle, δ°**			**CA Model Analysis, G* ≥ 1e6Pa**		
	G*=8.967	G*=10	G*=100	G*=111	δ°=27	δ°=30	δ°=45	ω_{cr} , rads/sec	Gc, Pa	R value
A Original	25.97	25.69	19.66	19.41	6,669,000	2,813,000	37,860	2.048E-06	30,990	5.17
A PAV20	20.92	20.66	16.02	15.83	1,673,000	867,400	14,700	N/A	N/A	N/A
A PAV40	20.77	20.34	14.81	14.66	1,186,000	572,600	10,650	N/A	N/A	N/A
B Original	36.03	35.07	19.03	17.98	31,000,000	19,440,000	1,433,000	1.113E+01	1,153,000	3.07
B PAV20	27.5	26.93	16	15.37	9,858,000	6,745,000	21,130	3.619E-03	150,600	3.96
B PAV40	27.1	26.29	15.21	14.7	9,099,000	4,912,000	20,250	1.348E-04	84,490	4.22
C Original	35.07	34.58	17.63	16.72	29,810,000	19,720,000	1,217,000	6.124E+00	1,162,000	2.93
C PAV20	28.73	28.3	15.88	15.2	12,080,000	7,477,000	60,320	1.629E-02	211,500	3.79
C PAV40	29.2	28.58	16.08	15.58	13,200,000	7,216,000	36,790	1.515E-04	153,600	3.96
D Original	39.16	38.36	17.22	16.65	38,000,000	27,640,000	2,972,000	2.230E+00	2,215,000	2.58
D PAV20	30.61	29.93	15.81	15.16	14,930,000	9,913,000	36,560	2.670E-03	264,000	3.64
D PAV40	33.42	32.7	17.13	16.32	21,420,000	14,480,000	869,700	1.825E-03	682,700	3.13
E Original	34.2	33.32	19.5	18.96	26,000,000	15,770,000	1,206	8.943E-02	741,000	3.27
E PAV20	27.68	27.36	20.3	19.75	10,770,000	3,798,000	5,709	2.186E-05	29,700	5.33
E PAV40	25.56	25.46	21.34	20.78	2,555,000	41,550	4,936	N/A	N/A	N/A
F Original	47.08	46.25	26.44	25.76	92,870,000	60,020,000	11,590,000	2.412E+01	9,553,000	2.08
F PAV20	39.91	39.17	22.16	21.51	46,410,000	31,650,000	3,773,000	3.145E-01	2,527,000	2.75
F PAV40	33.44	32.83	20.64	19.89	29,070,000	16,570,000	1,063,000	5.511E-03	720,100	3.42

High temperature rheology

The MSCR test measures the stress dependence of the viscous response of a binder. The test uses a load pulse of 1 second in shear, followed by a recovery period of 9 seconds. Viscous flow that occurs in the test is associated only with load duration that occurs (1 second). If the elastic response is fully recovered at the completion of the recovery time, the non-recoverable strain remaining can be associated with viscosity. Since the time of loading is 1 second, the strain at the end of the recovery period is then effectively the strain rate. Thus, the approximated (or pseudo) viscosity from $J_{nr3.2}$ ($\eta_{Jnr,\ pseudo}$) can be defined as the reciprocal of the test value. The normal value obtained is multiplied by 1,000 to convert the data to Pascal seconds, thus:

$$\eta_{\mathrm{Jnr,pseudo}} = 1000/J_{nr\ .2} \qquad \text{[Equation 1]}$$

where: $\eta_{Jnr,\ pseudo}$ = pseudo-viscosity, Pa·s

$J_{nr3.2}$ = non-recoverable creep compliance at 3200 Pa stress level, kPa^{-1}

If $J_{nr3.2}$ results are compared to the data collected from the temperature-frequency sweep tests and analyzed for an approximation of the zero-shear viscosity[5], it is observed that $\eta_{Jnr,\ pseudo}$ is substantially below the result obtained from the temperature-frequency sweep tests for the modified binders, as shown by the examples in Figure 26. The deviation is significant for the more complex binders, B & C compared to binder A.

[5]The zero-shear viscosity can be estimate using a number of techniques. The viscosity data from the DSR was estimated by fitting a discrete retardation spectrum to the results of the temperature-frequency sweep data. This analysis was accomplished using the method within the RHEA software as discussed by Rowe et al., 2002.

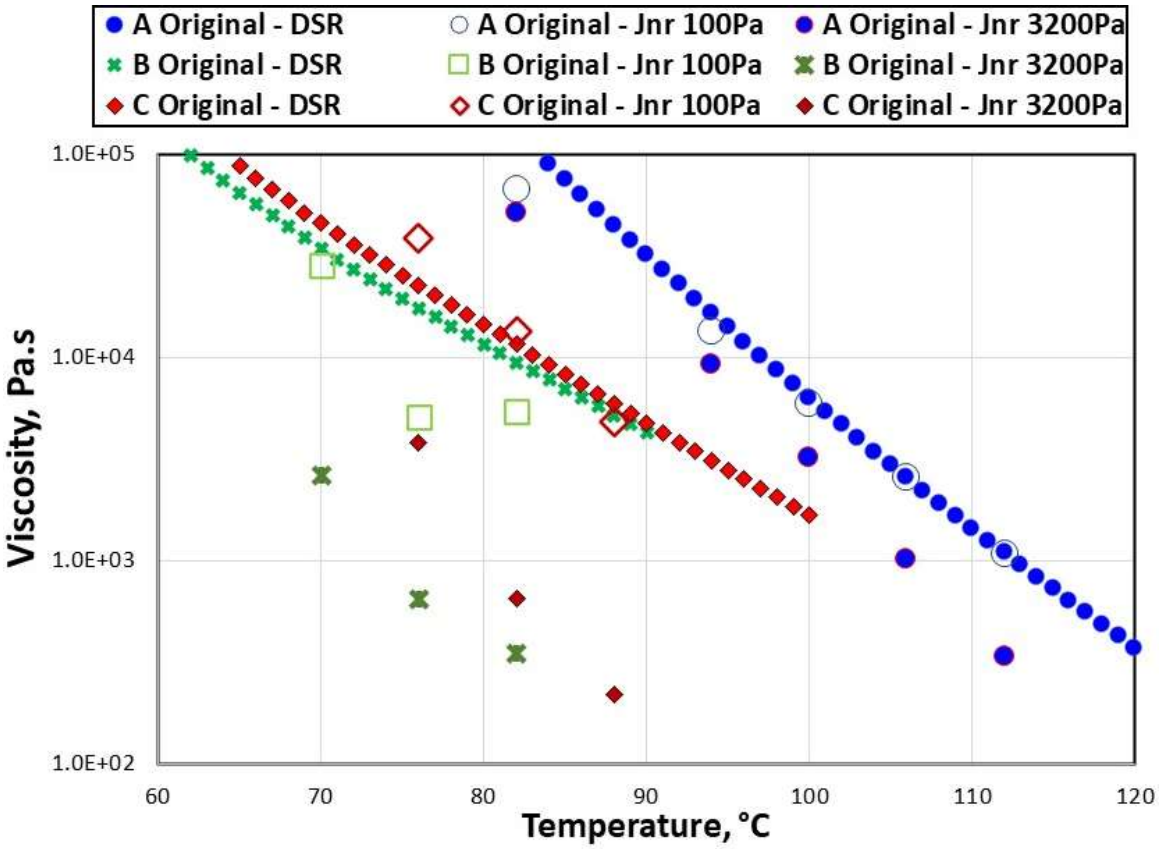

Figure 26. Viscosity computed from the MSCR test ($1/J_{nr3.2}$) versus viscosity from the DSR tests, estimated as zero-shear viscosity for three binders in the original condition

MSCR data was used to compute the temperature that corresponds to a viscosity of 1,000 Pa.s. It has been previously reported that the softening point corresponds to a dynamic viscosity of 1,200 Pa.s measured with the DSR. The temperature at 1,000 Pa.s was selected to round the 1,200 Pa.s and to assess if this temperature would also correlate with softening point (Mirza and Witczak, 1995). The temperature was estimated using an interpolation considering the logarithm of the pseudo-viscosity versus linear temperature for the two data points that bracketed the 1,000 Pa.s value/$J_{nr3.2}$ value of 1.0 1/kPa. The data obtained for the temperatures for each of the three conditions are presented in Figure 27. It can be seen that the conventional oxidized material (A) had a temperature on this basis above 100°C, whereas materials B, C and D had lower values. Temperatures for Materials E and F were similar to material A.

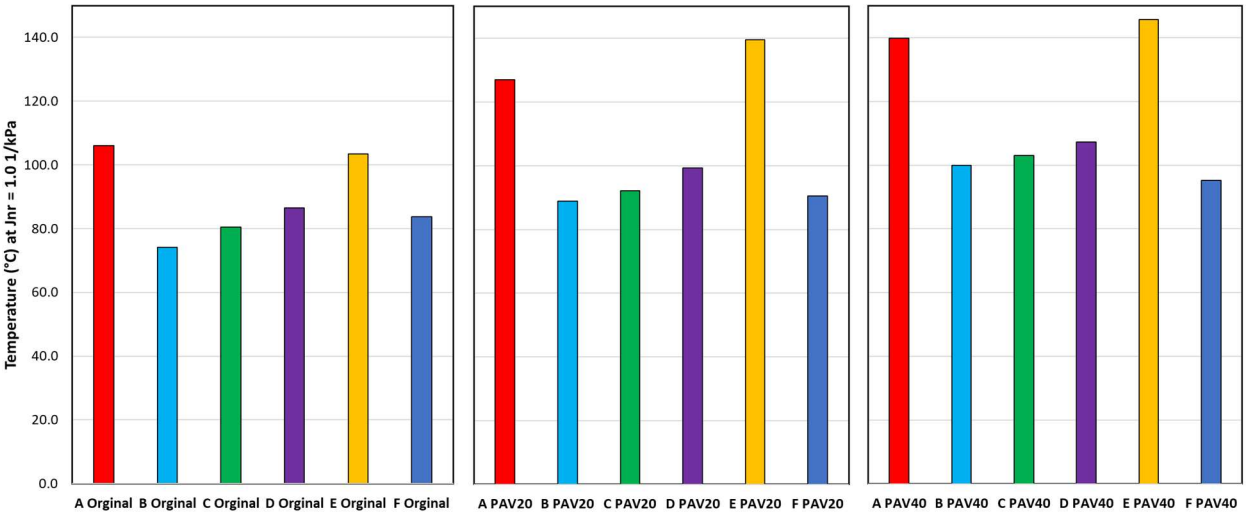

Figure 27. Temperature corresponding to a $J_{nr3.2}$ of 1.0 kPa^{-1} for binders A to F for original, PAV20 and PAV40 condition

If the value of $J_{nr3.2}$ is considered as a viscosity, this can then be analyzed in a stress-dependent characterization using conventional rheological techniques. This was in part the reason for the implementation of this test, in that the level of stress was more consistent with loads imposed on asphalt pavements. The stress sensitivity of materials can be described by the Ostwald-DeWaele power law, as follows:

$$\tau = C\dot{y}^{P} \text{ and } \eta = C\dot{y}^{P-1} \qquad \text{[Equation 2]}$$

where: τ = shear stress
$\dot{y}$ = strain rate
P = exponent that describes sensitivity to shear

The strain rate is assumed to be equivalent to the non-recovered strain after the recovery period has occurred. The percent difference in J_{nr} (J_{nrDiff}) is thus theoretically linked to the P parameter in this description of the viscosity as a direct calculation. The correlation between J_{nrDiff} and P is shown in Figure 28 with a high order polynomial equation describing the interrelationship ($r^2 = 1$). In making this analysis, it is assumed that after the 9-second recovery period in the MSCR test the unrecovered deformation is attributable to the steady state viscosity. With highly modified binders, this assumption will deviate from the true behavior. The level of deviation that is present has not currently been assessed, which may affect the interpretation of the data in subsequent analysis as more information is obtained.

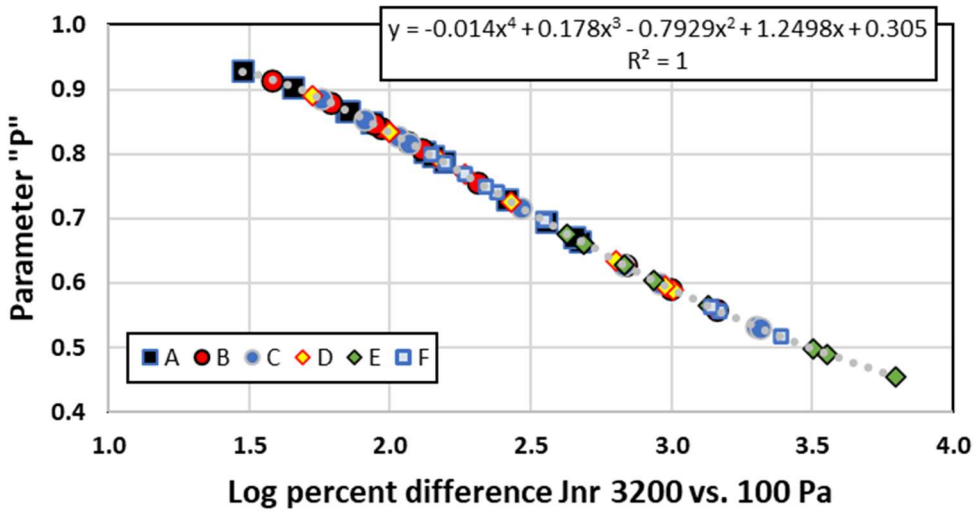

Figure 28. Relationship between $J_{nr,\,Diff}$ and non-linear parameter, *P*

The other parameter measured from the MSCR test is the percent of recovered shear strain at the 3,200 Pa stress level ($R_{3.2}$), or more simply known as "percent recovery". This parameter is linked to viscoelastic solid behavior versus viscoelastic liquid behavior in the non-linear viscoelastic range. A high percentage of strain recovery is generally associated with viscoelastic solid behavior whereas little or no strain recovery is associated with viscoelastic liquid type behavior. However, this is further complicated by the relative hardness of the material. For example, as a linear viscoelastic liquid becomes harder, a higher value of elastic recovery will be obtained.

Figure 29 shows the data from the MSCR test using the traditional approach ($R_{3.2}$ vs. $J_{nr3.2}$). For material A, it can be seen that the $R_{3.2}$ vs. $J_{nr3.2}$ value lies along a line that could be fitted with a r^2 value of 0.961. An oxidized roofing grade binder, regardless of laboratory aging condition, is anticipated to follow a close relationship in this type of plot with $J_{nr3.2}$ being linked to the hardness of the product.

In Figure 30, a plot of $R_{3.2}$ vs. the Ostwald-DeWaele power law parameter *P* is shown. Again, in this plot it is observed that there is a good relationship between the stress sensitivity parameter and the percent recovery for the traditional roofing grade binder. This material becomes more stress sensitive as aging progresses, as indicated by the data labels and the connecting lines.

To allow a better visualization and understanding of the changes that are occurring with aging, each binder has been plotted with respect to these two representations (Figure 31 to Figure 42). A vector is shown on each plot that represents the effect that aging has on the parameters when tests have been conducted at the same temperature. As discussed earlier, testing was not carried out at equal temperatures since the initial goal was to obtain equivalent values of $J_{nr3.2}$. The only exception is Material F tested at PAV20 to PAV40 at 100°C (Figure 41), which may be a result of testing variability (or an outlier).

As a material ages, the $J_{nr3.2}$ decreases (consistent with increasing viscosity) and the recovery percentage increases (consistent with a greater elastic response), while the materials generally

become less stress dependent. Material E (Figure 40) shows an exception when tested at 130°C (PAV20 to PAV40). The slopes of the lines in the figures that show *P* indicate that the PmB blends generally see a greater degree of change in stress sensitivity as aging progresses.

The $R_{3.2}$ vs. $J_{nr3.2}$ plot for the PmB blends presents a more complex understanding. With Materials B, C and D, $R_{3.2}$ drops significantly as the material ages. The opposite behavior is observed for Material E, perhaps due to swelling of particles in the modifier matrix. However, Material F, which is a 50% modifier concentration of Material E, shows behavior closer to Materials B, C and D. This is particularly evident when viewing the representation in Figure 30.

As Material A oxidizes, structures are produced that exhibit different stress dependency. With the PmB blends some changes to the polymer network may be occurring as aging progresses. The relative movement with aging in Figure 29 and Figure 30 provides useful information on the structures in the binders and the changes with aging.

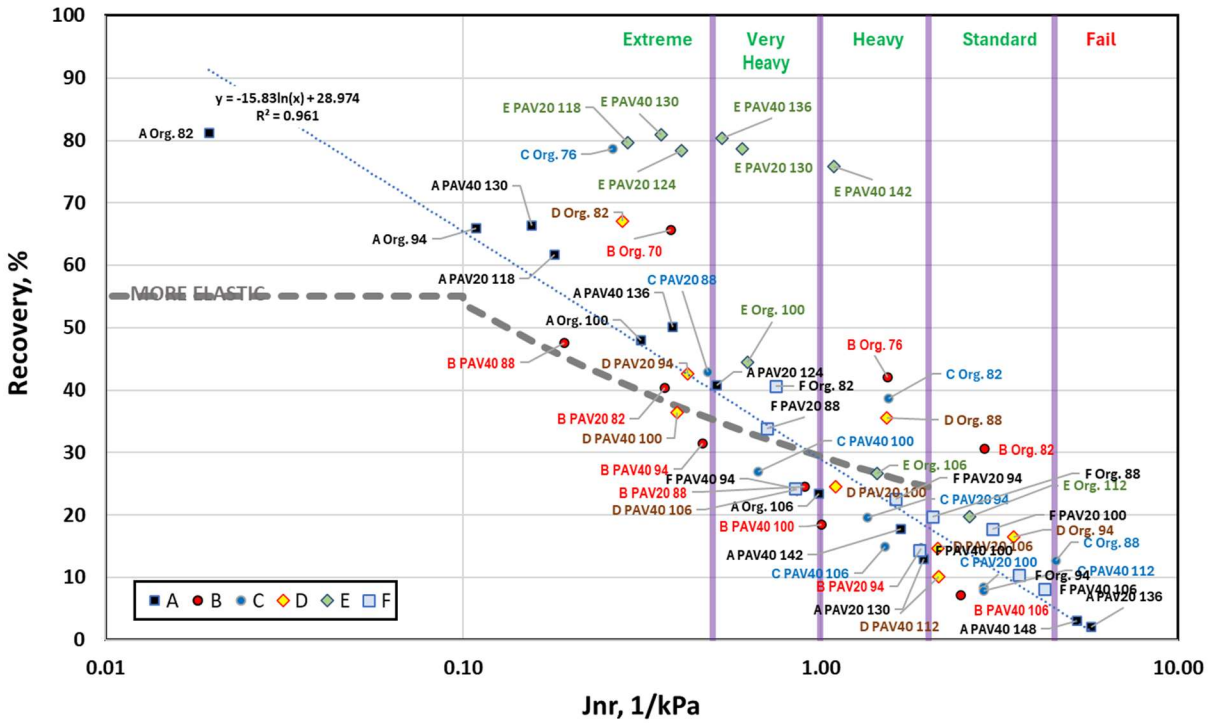

Figure 29. $R_{3.2}$ vs. $J_{nr3.2}$ for materials tested in the MSCR test (data labels indicate material/condition/test temperature in Celsius)

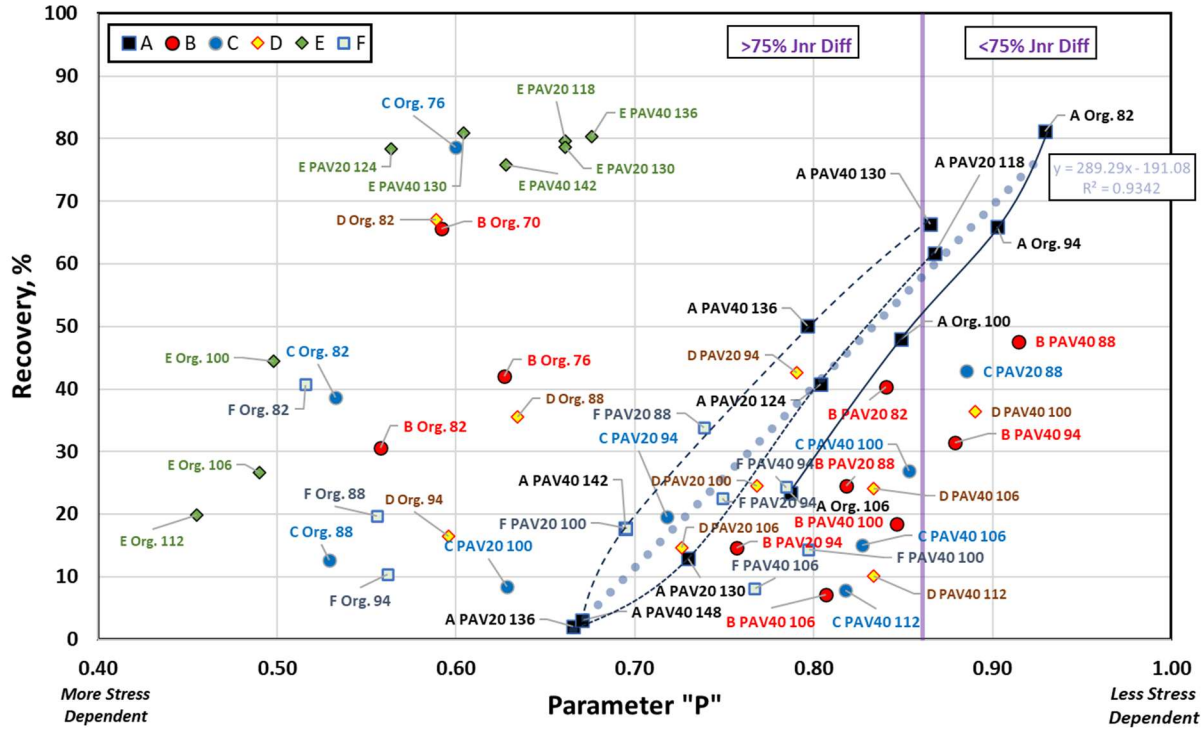

Figure 30. $R_{3.2}$ versus Ostwald-DeWaele power law parameter *P* (data labels indicate material/condition/temperature in Celsius of test) – all materials

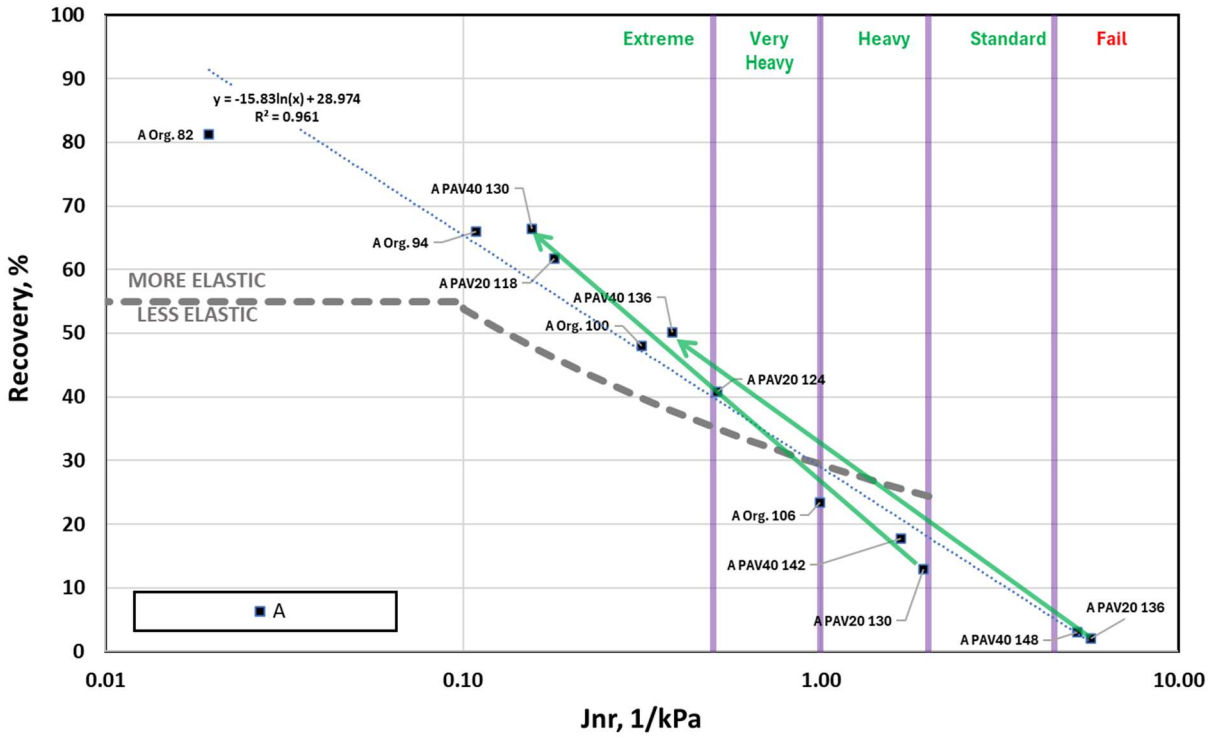

Figure 31. $R_{3.2}$ vs. $J_{nr3.2}$ for Material A tested in the MSCR test

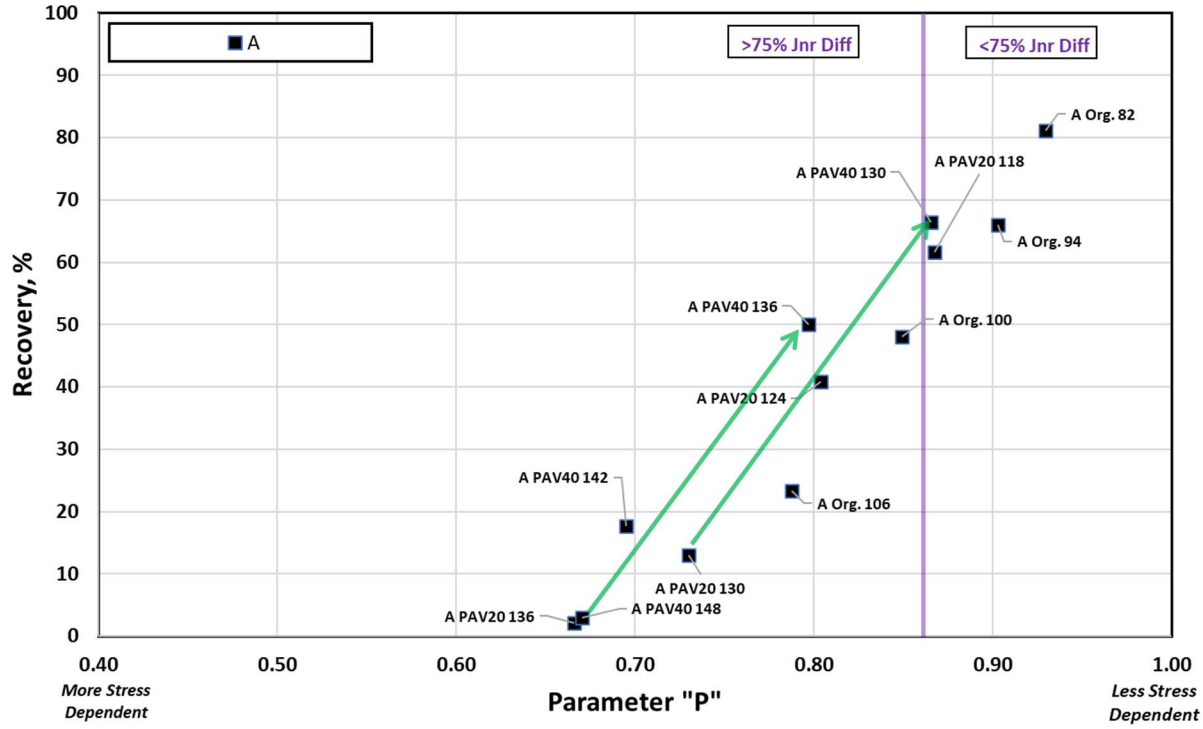

Figure 32. $R_{3.2}$ versus Ostwald-DeWaele power law parameter *P* – Material A

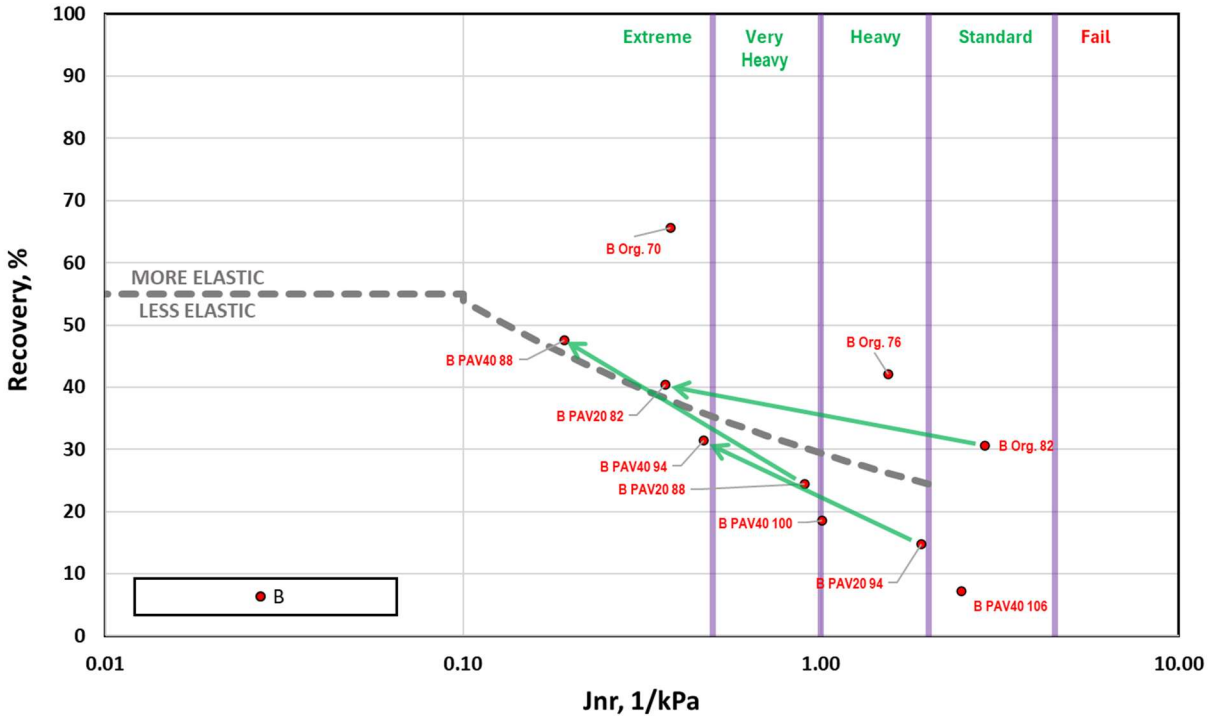

Figure 33. $R_{3.2}$ vs. $J_{nr3.2}$ for Material B tested in the MSCR test

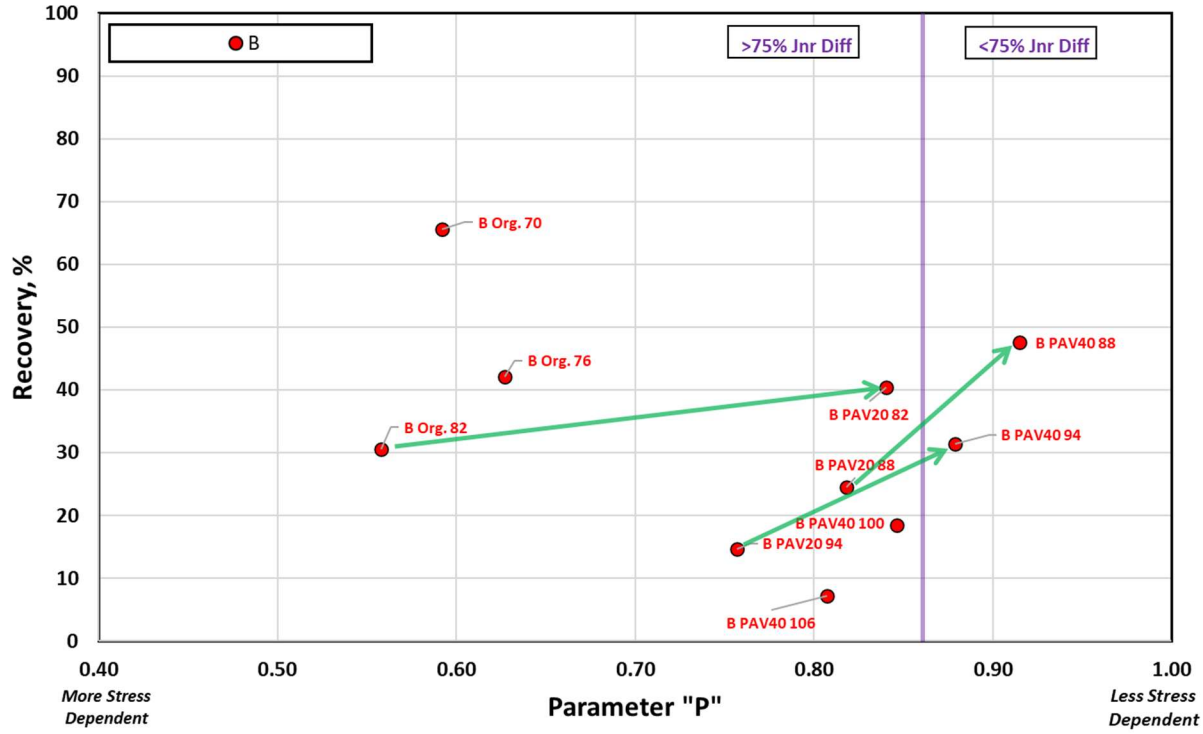

Figure 34. $R_{3.2}$ versus Ostwald-DeWaele power law parameter *P* – Material B

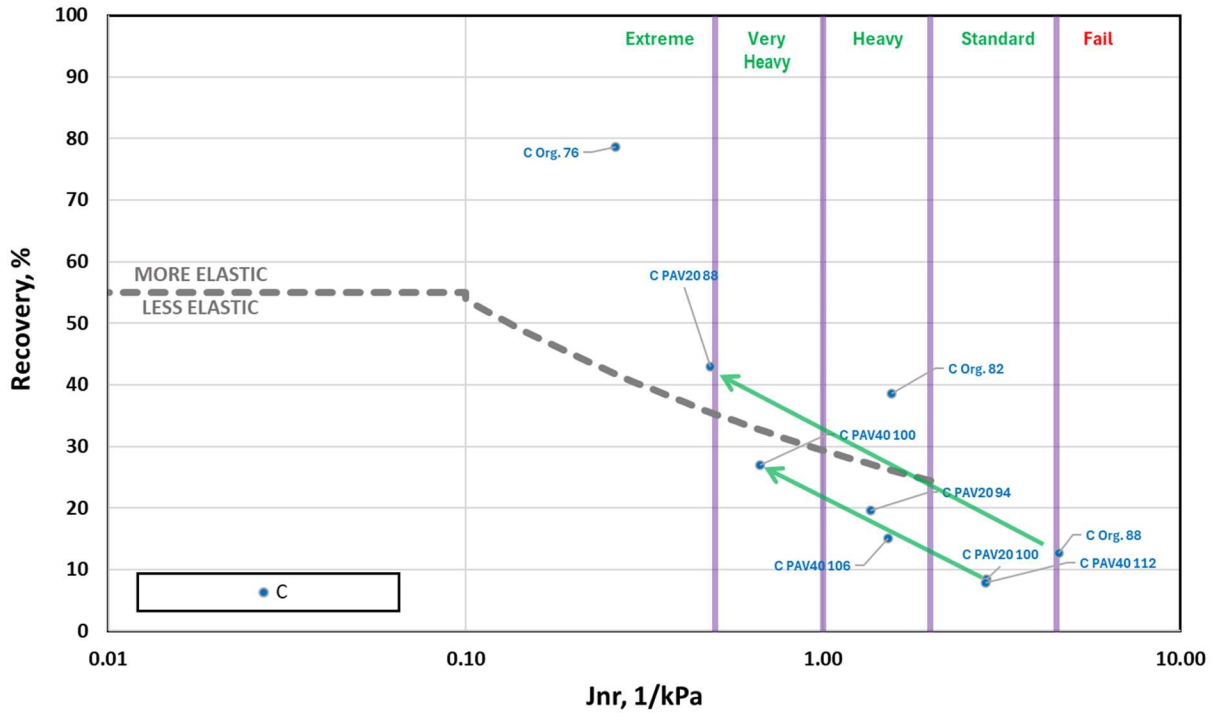

Figure 35. $R_{3.2}$ vs. $J_{nr3.2}$ for Material C tested in the MSCR test

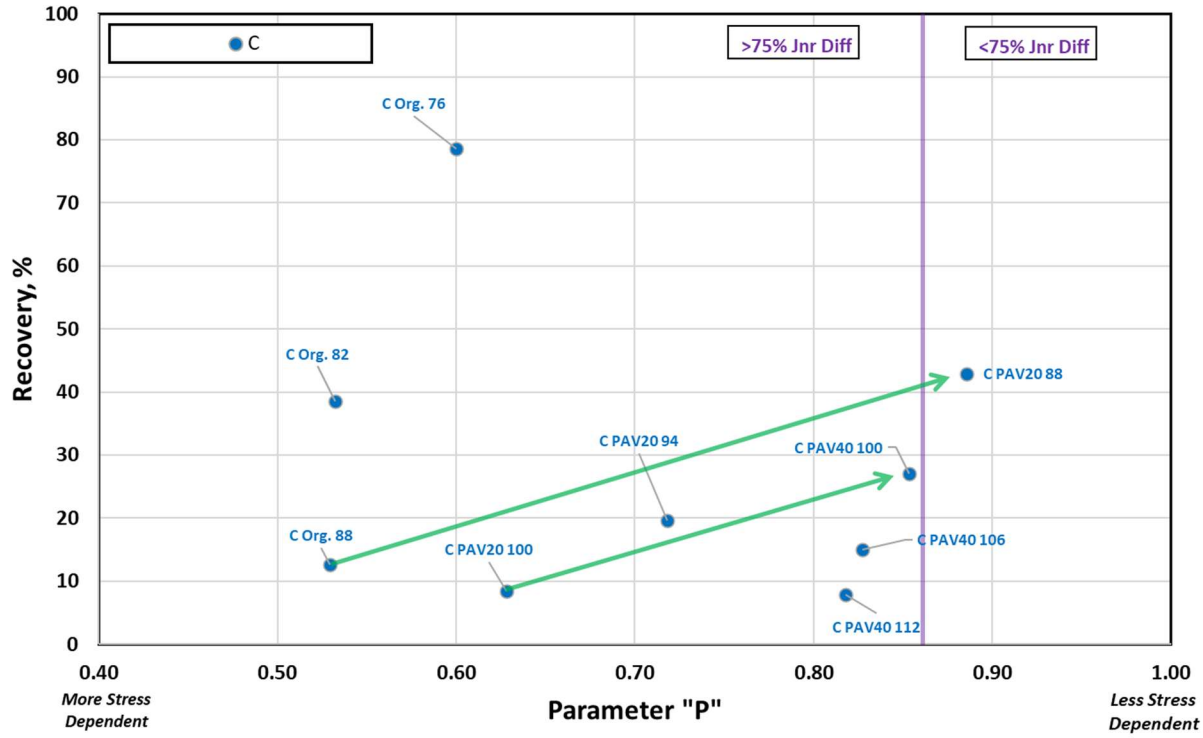

Figure 36. $R_{3.2}$ versus Ostwald-DeWaele power law parameter *P* – Material C

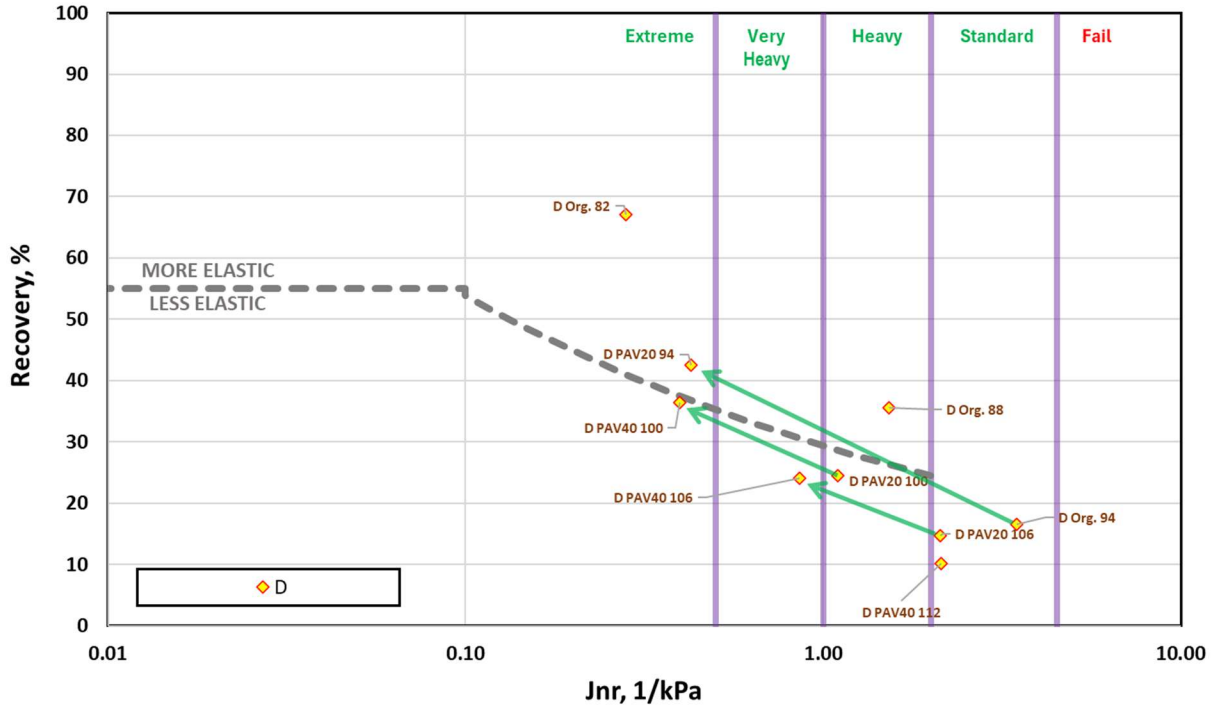

Figure 37. $R_{3.2}$ vs. $J_{nr3.2}$ for Material D tested in the MSCR test

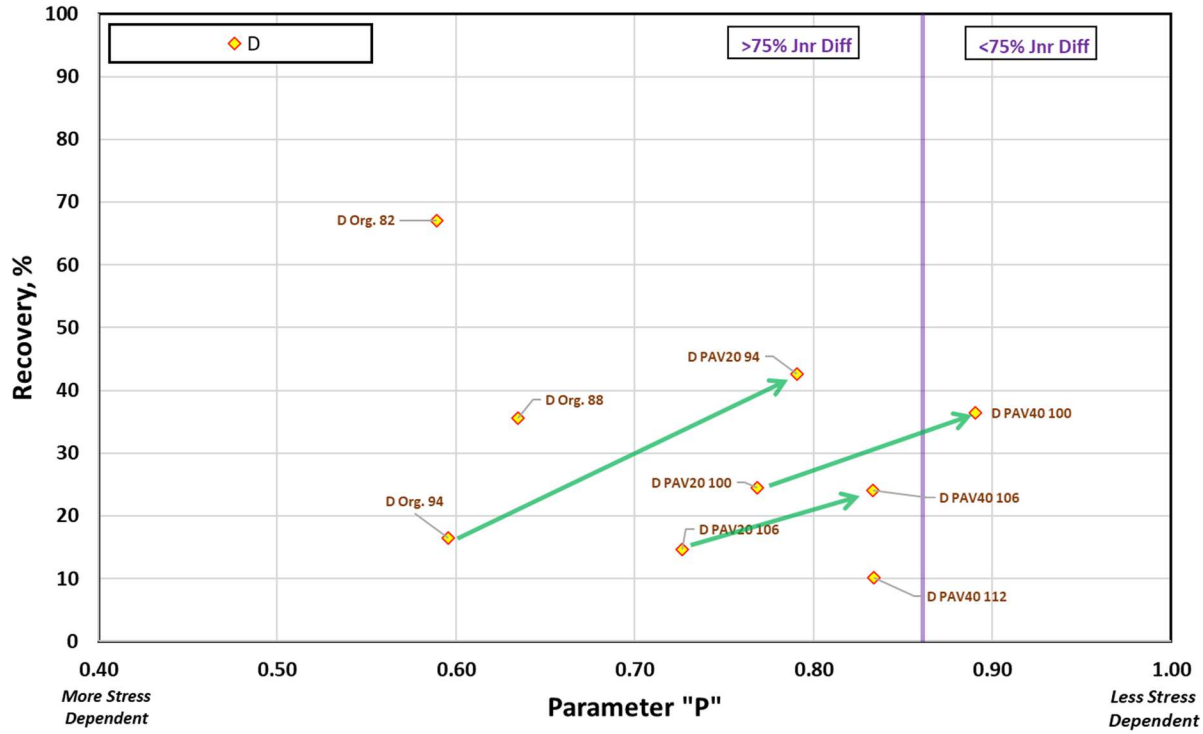

Figure 38. $R_{3.2}$ versus Ostwald-DeWaele power law parameter *P* – Material D

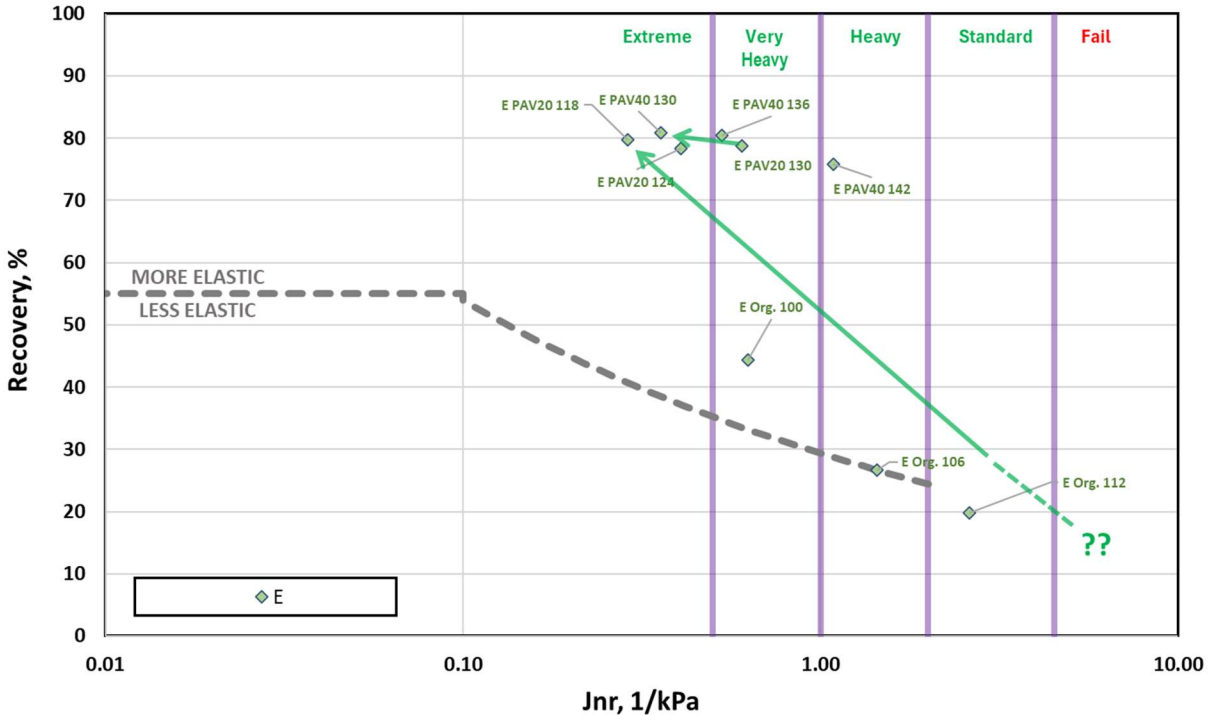

Figure 39. $R_{3.2}$ vs. $J_{nr3.2}$ for Material E tested in the MSCR test

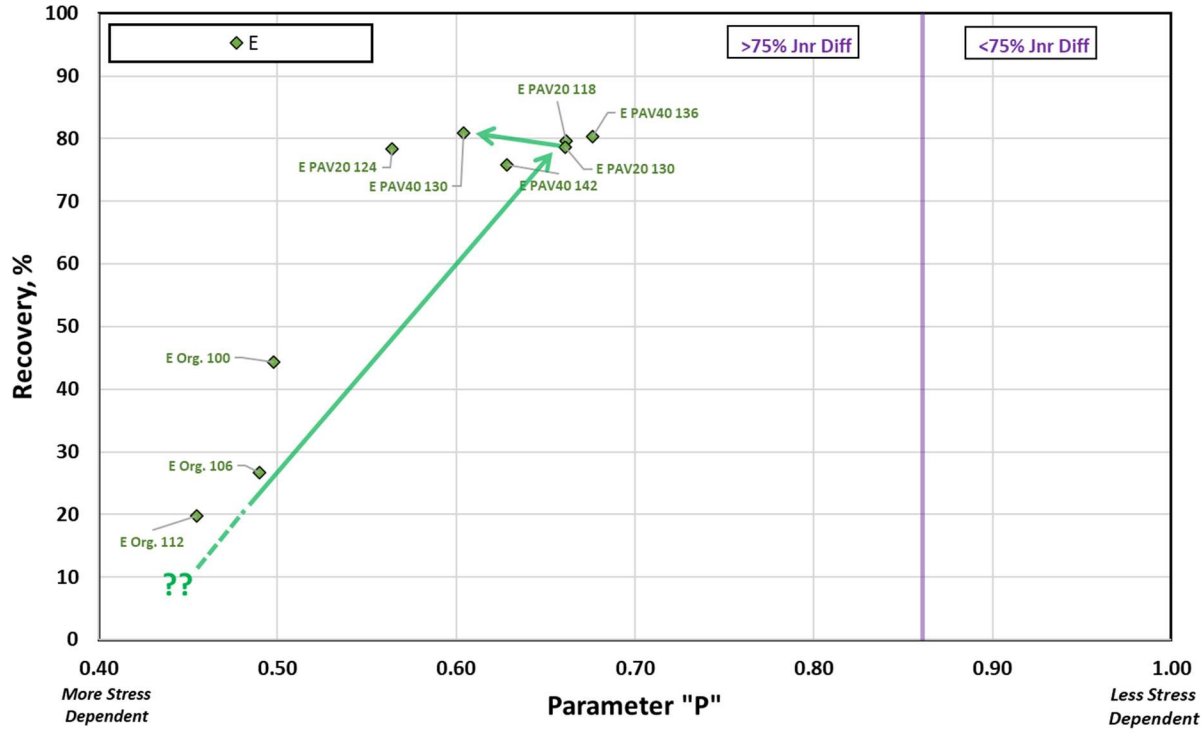

Figure 40. $R_{3.2}$ versus Ostwald-DeWaele power law parameter *P* – Material E

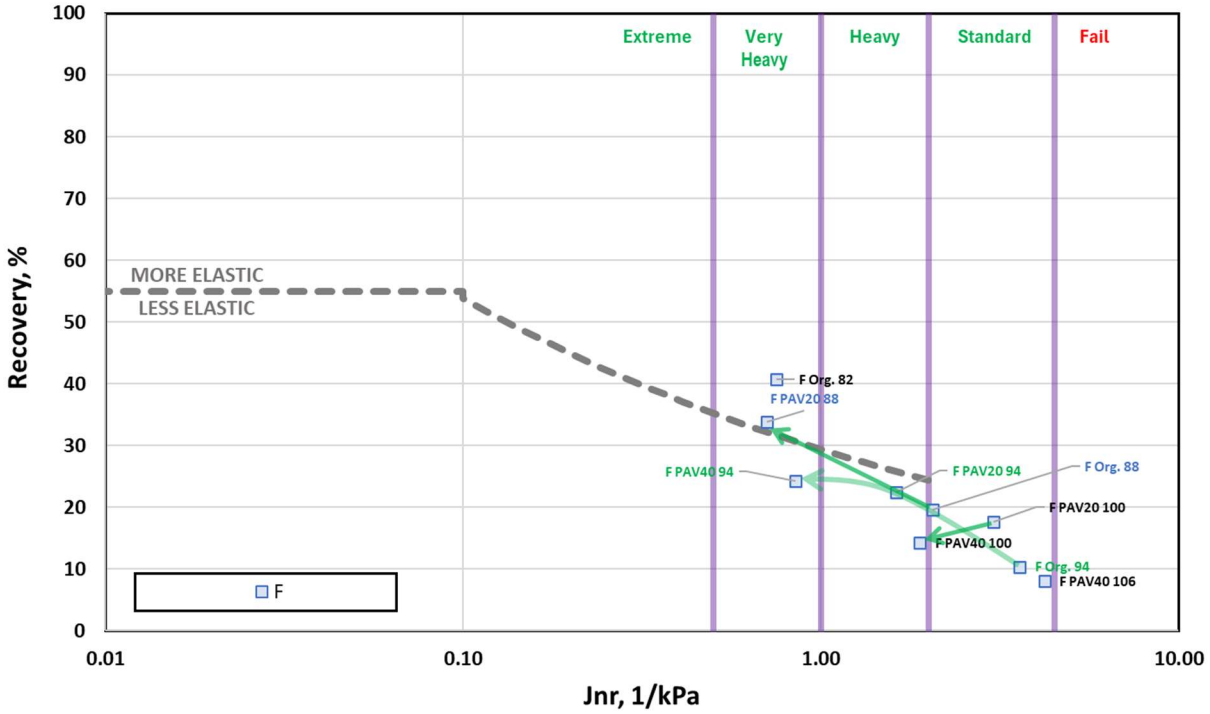

Figure 41. $R_{3.2}$ vs. $J_{nr3.2}$ for Material F tested in the MSCR test

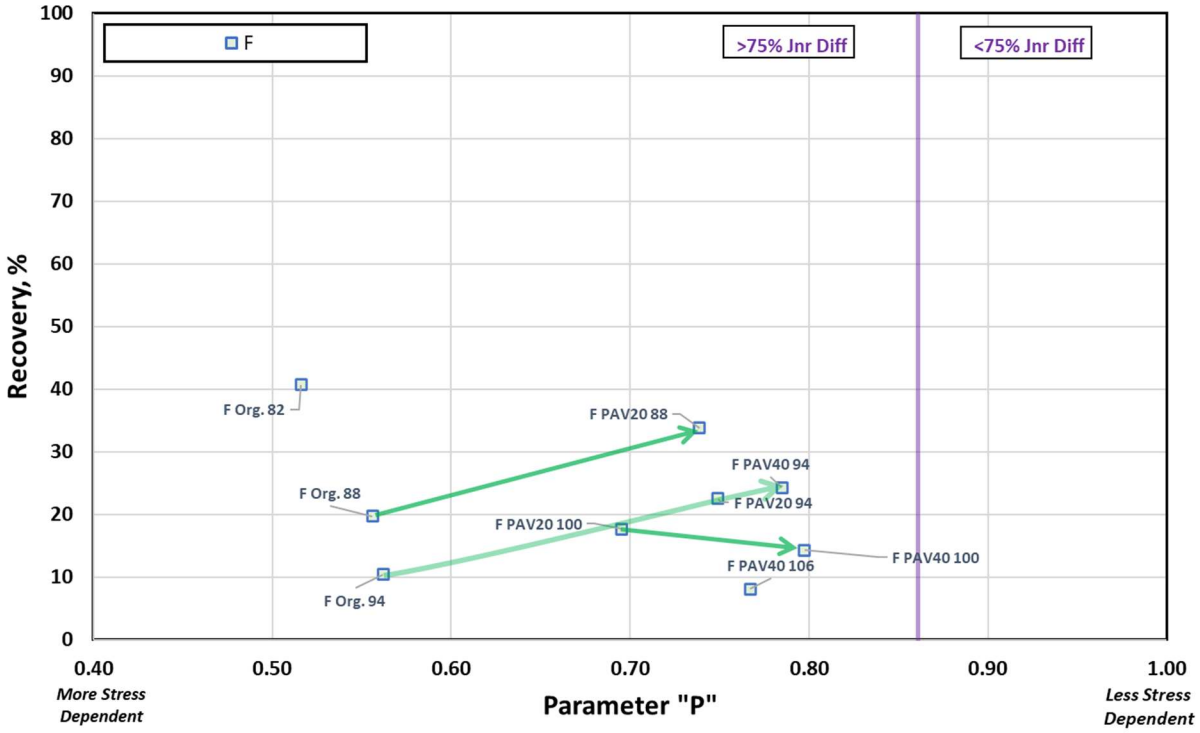

Figure 42. $R_{3.2}$ versus Ostwald-DeWaele power law parameter *P* – Material F

Linear Amplitude Sweep

The Linear Amplitude Sweep (LAS) test uses a DSR to assess the fatigue behavior of asphalt binders by the application of systematically increasing load amplitudes under a cyclic loading pattern. This test was developed by Kim et al., (2006) and further developed by researchers at the Modified Asphalt Research Center (MARC) at the University of Wisconsin (Hintz et al., 2011). The binder test sample is first subjected to a frequency sweep to determine a damage analysis parameter, α. A second test is then conducted in strain-controlled oscillatory shear at a frequency of 10 Hz. Strain is increased linearly from 0.1% to 30% over the course of 3,100 cycles of loading, for a total test time of 310 seconds. Peak shear strain and peak shear stress are recorded every 10 load cycles (1 s), along with phase angle and complex shear modulus. The detailed test method is documented in AASHTO T391-20. Using fatigue model parameters A_{35} and B from the analysis, the binder fatigue performance parameter can be calculated as follows:

$$N_f = A_{35}(\gamma_{max})^{-B} \qquad \text{[Equation 3]}$$

where: N_f = binder fatigue performance parameter
A_{35} *and* B = Fatigue model parameters
γ_{max} = the maximum expected binder strain for a given pavement structure, percent

The results obtained for binders A to C at various test temperatures are presented in Figure 43.

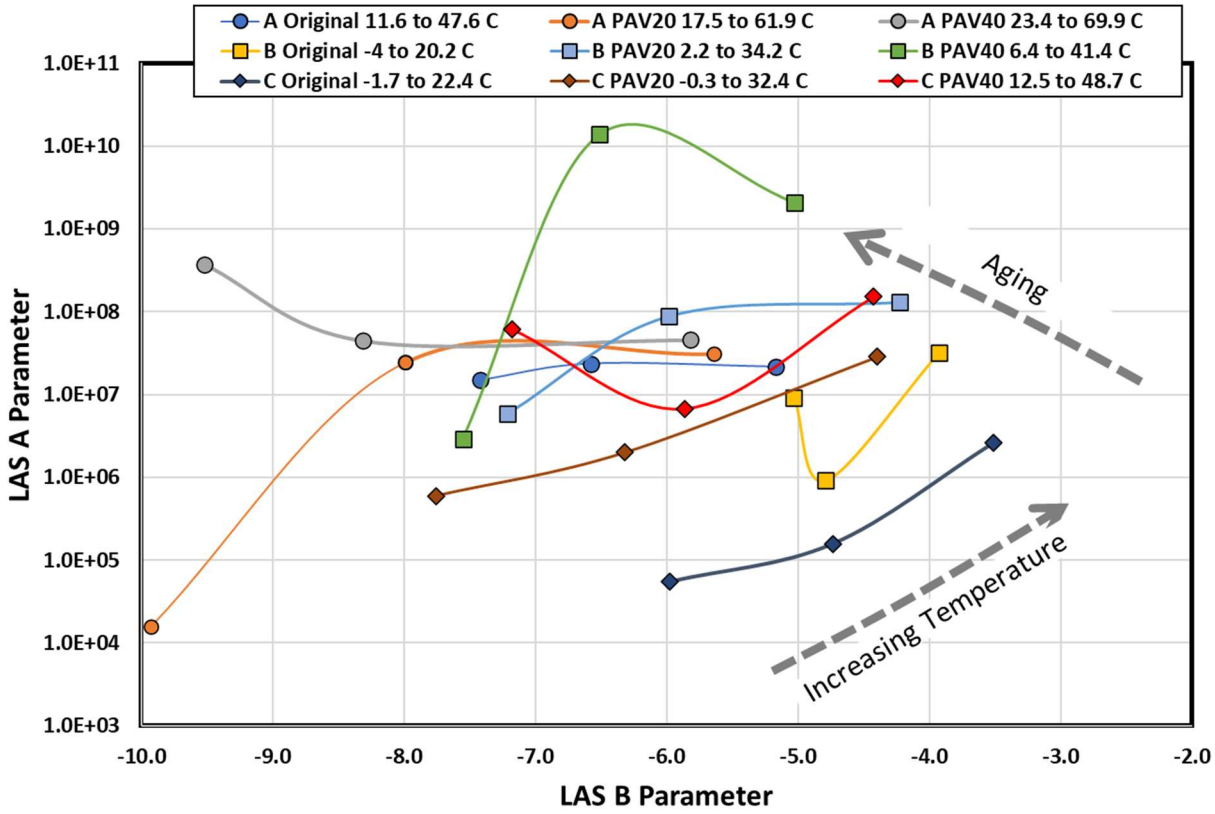

Figure 43. Linear amplitude sweep (LAS) test results, A_{35} & B parameters

Some general trends can be seen in the data. Generally, as aging progressed the value of the A_{35} parameter increased and the B parameter became more negative. However, the results obtained do not present a clear distinction between different materials and how these would be used to classify roofing products would be difficult to assess. Consequently, the use of this testing was curtailed after these three materials were tested.

Ultimate Property Definition with the MOSS Test

The MOSS test procedure was developed by the Asphalt Institute as part of the work conducted for AIF Project 22-03 (Rowe et al., 2023). The use of ultimate tests that consider the stress, strain and/or energy to a defined failure condition is considered important for modified binder systems to classify their performance attributes. This test can be considered as a refinement of the Binder Yield Energy Test (BYET) which was initially developed by researchers at MARC at the University of Wisconsin (Bahia et al., 2010).

The temperatures used to conduct this test were based on earlier work performed by Heukelom (1966) who showed that binder fracture was related to the binder stiffness. In more recent studies, Anderson et al. (2001) presented research showing that "true fatigue" for asphalt binders generally occurred at shear modulus values from 5 to 18 MPa ($5x10^6$ to $1.8x10^6$ Pa), whereas the term "instability flow" was associated with failure that exhibited large deformations below this stiffness level. This principle is consistent with brittle-to-ductile behavior that can be observed with Direct

Tension Test (DTT) data (Rowe and Sharrock, 2004). In the work by Rowe and Sharrock, the peak energy associated with fracture was considered to occur when the relaxation modulus, *E(t)*, was approximately 20 MPa – consistent with the range that the transition from instability flow to true fatigue occurred in the work conducted by Anderson et al. (2001). In the research conducted by Anderson et al., the maximum fatigue life occurred at this transition point, which using Rowe and Sharrock's work, is consistent with the maximum toughness (defined here as the area under a stress-strain curve). Using this analysis as a model, the MOSS test was implemented by the Asphalt Institute to analyze the brittle-to-ductile transition of several oxidized roofing coatings used in a separate study (Cooper, 2024). Results showed that the peak toughness for the oxidized roofing coatings occurred at a G* of 1 to 2 MPa (Figure 44), slightly lower than the values determined by Anderson, Rowe and Sharrock.

Consequently, it was decided that ultimate properties should be evaluated in the stiffness range where the shear modulus is in the range 1 to 10 MPa. Note that extensional modulus (E*) can be approximated to 3G*; thus, for comparison to data sets expressed in an extensional modulus the target range was 3 to 30 MPa. While these tests can involve stress and strain magnitudes that are greater than those associated with master curve development and beyond the linear range of viscoelastic behavior, it has been shown that the stiffness from these linear viscoelastic measurements can be used to normalize the data into ultimate property master curves (Rowe and Sharrock, 2004).

The selection of test temperature made use of the master curve expressed as G* versus temperature using an estimated loading frequency of 0.005 rads (roughly the rate of angular rotation of the MOSS procedure). From this a test temperature was selected such that it would produce a result within the target range of stiffness (1 to 10 MPa, or 6.0 to 7.0 considering the logarithm of the modulus expressed in Pascals). The test temperatures used and associated values of stiffness corresponding to the MOSS test time are indicated in Figure 45. The values of G(t) range from 5.6 to 6.7 (log Pascals) whereas the selected temperatures range from -10°C to 37.3°C. While some of these values fall outside of the 1-10 MPa range, the data is still valuable in that it provides a measure the strength and strain tolerance of the binder as it approaches the brittle region.

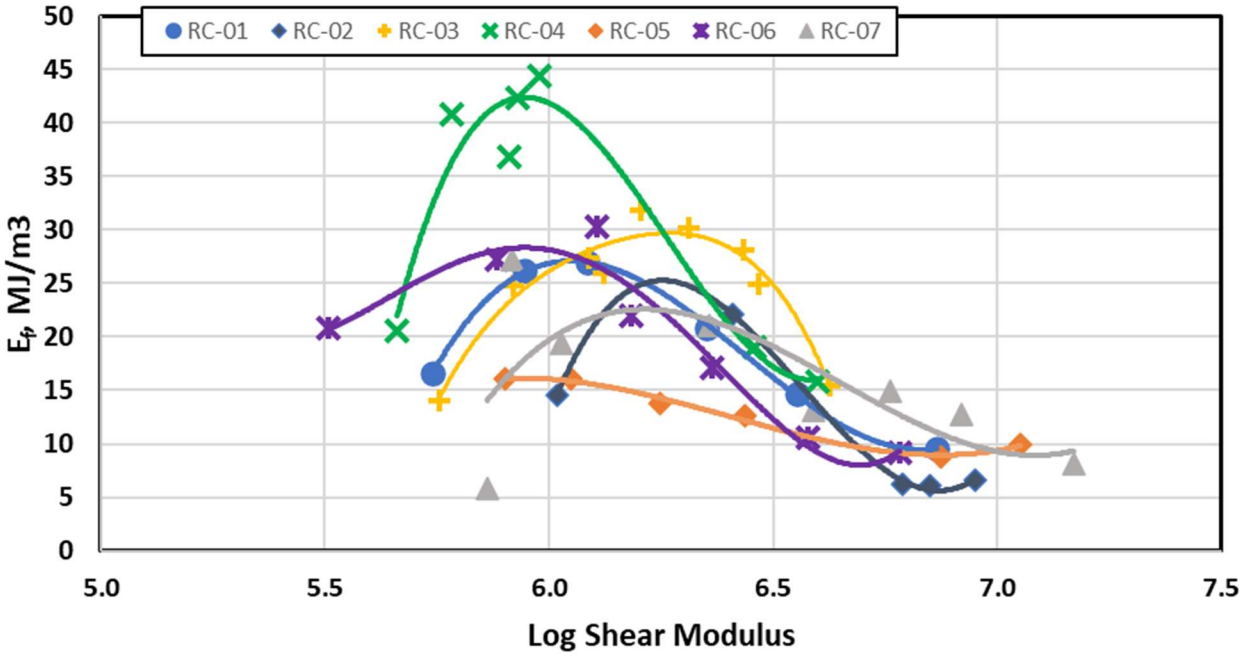

Figure 44. Mapping the brittle-to-ductile transition of oxidized roofing coatings using the MOSS test

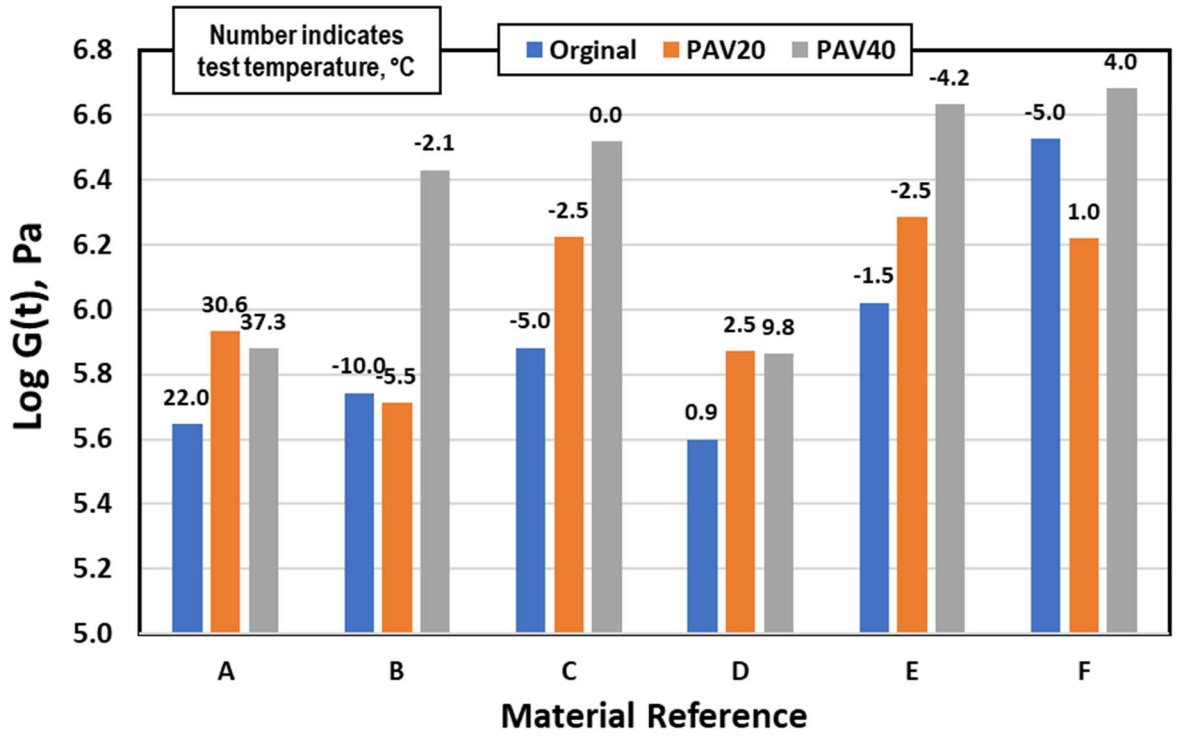

Figure 45. Test temperature selected and G(t) values that corresponded to loading time used in yield strain and peak stress calculations

The materials evaluated as part of this study show a clear distinction between the modified systems (B to F) and the conventional oxidized product (A).

Figure 46 and Figure 47 show the strain and strength of the material versus the log of the shear modulus. The modulus represented here is the secant modulus derived from the yield strain at the maximum shear stress. The shear strength is defined as the value of maximum shear stress, while yield strain is defined as strain at the value of maximum shear stress. These plots combine all data for a material at the three aging levels. It is observed that for each material a strong relationship exists between the yield strain and the value obtained for shear modulus whereas the value obtained for the shear strength remains fairly constant. In Figure 48, the data is represented for each material type at a constant shear modulus value of 1 MPa.

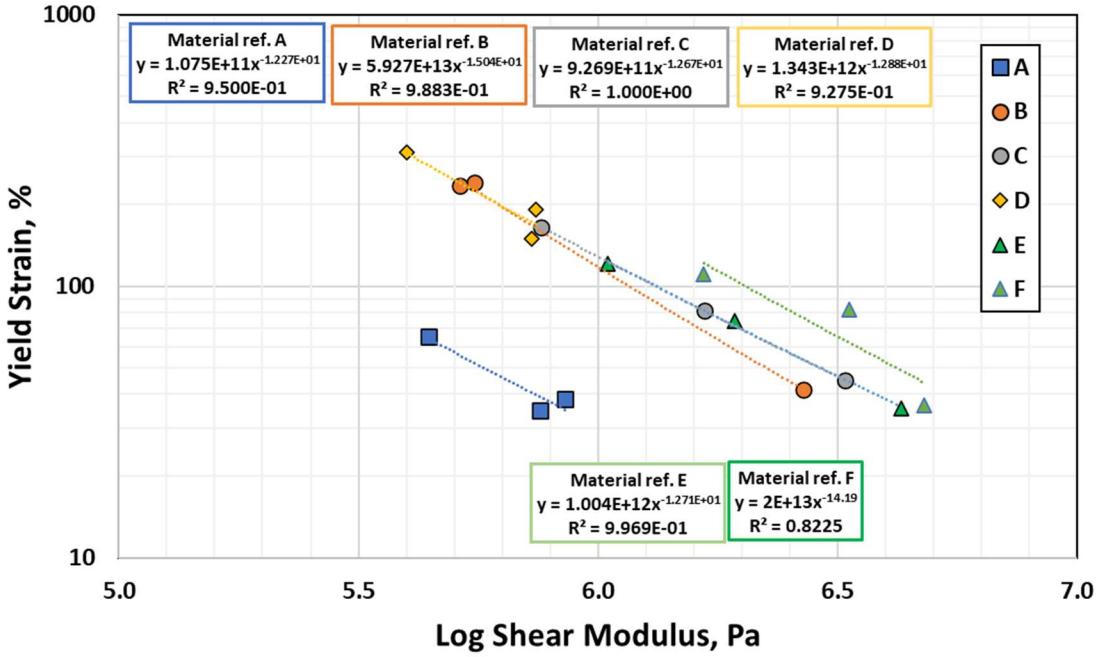

Figure 46. MOSS yield strain versus log shear modulus

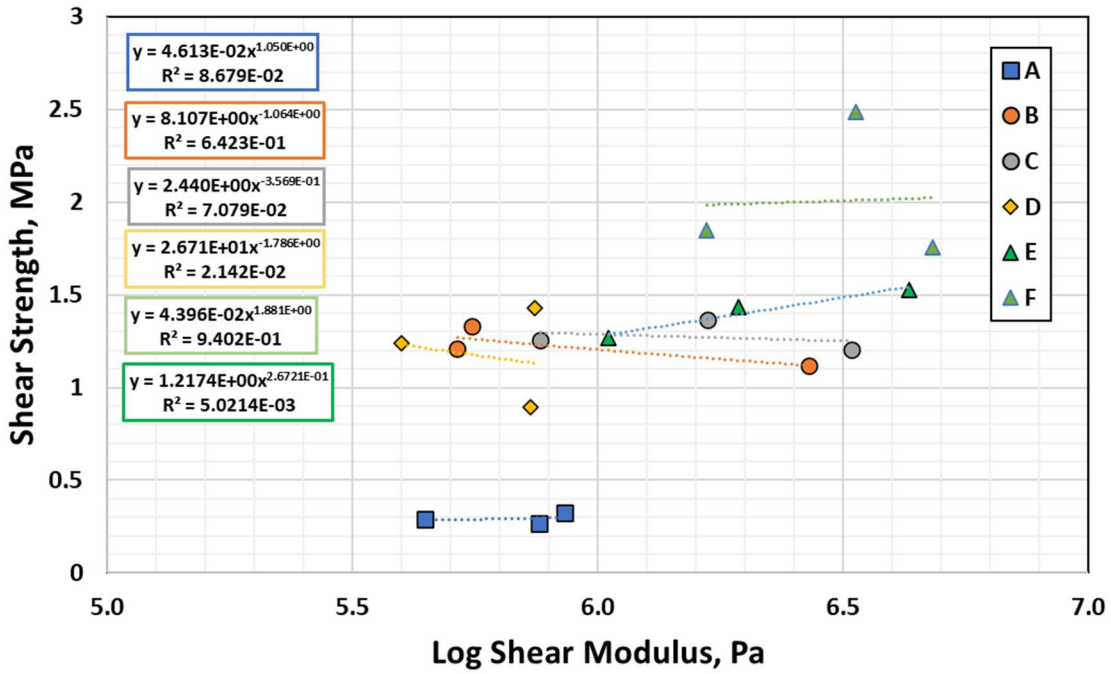

Figure 47. MOSS shear strength versus log shear modulus

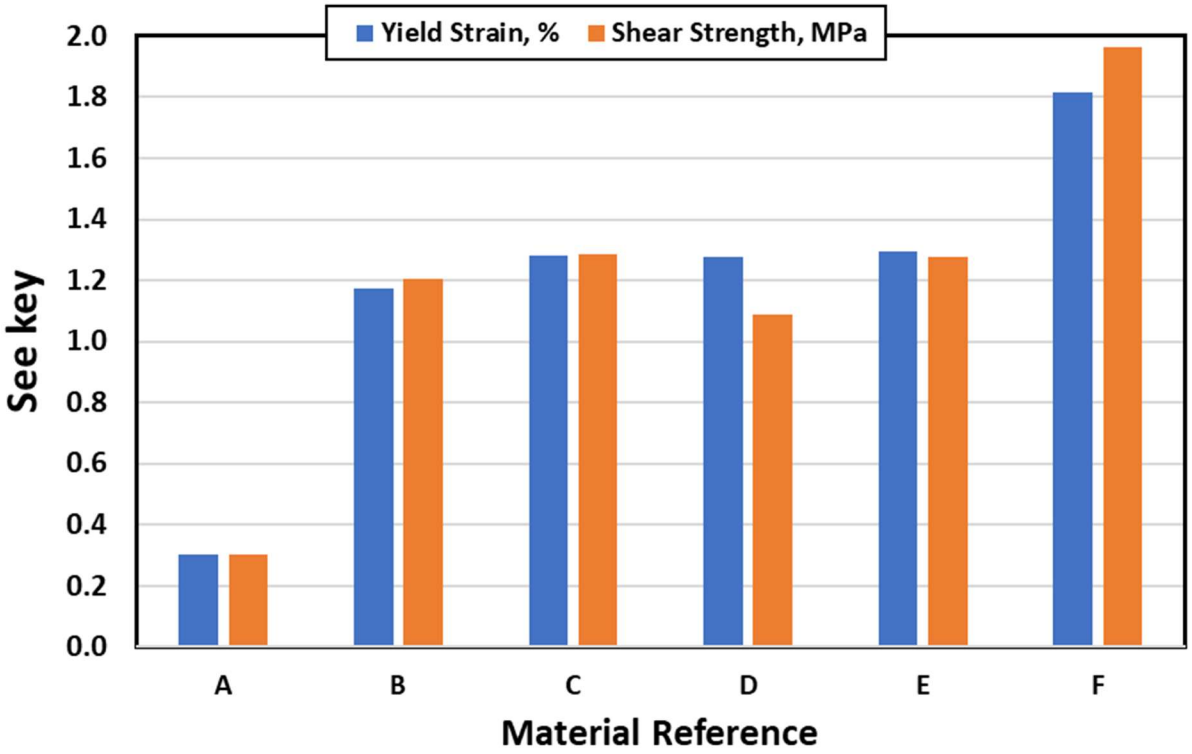

Figure 48. MOSS data, log yield strain and shear strength (MPa) at a shear modulus of 1 MPa

Work presented in NCHRP Report 982 (Christensen and Tran, 2022) considered that the fatigue strain capacity (FSC) of a specific asphalt binder can be compared to the FSC of a generic or conventional binder (FSC*) and expressed as a ratio called Fatigue-Fracture Performance Ratio (FFPR). FFPR is helpful in demonstrating the inherent strain tolerance of an asphalt binder. An FFPR value of 1.0 would mean that the result lies on the same stiffness/fracture performance line that was established for conventional binders. Values above 1.0 would indicate better than average strain tolerance, while values lower than 1.0 would indicate poorer strain tolerance. In AIF Project 22-03, the FSC* was based on work from Heukelom (1966), who established a relationship between binder stiffness and failure strain. The data developed by Heukelom is reproduced here in Figure 49, where the S(t) obtained from Heukelom has been converted to G(t).

If the yield strain results for Materials A-F are superimposed on this graph, then a clear distinction between the two data sets is observed, as shown in Figure 50. In Heukelom's original work, the suggestion was made that the strain could be considered as two regions, represented by differing test types. This break in performance occurs in the region of 3 to 5 MPa represented as a shear stiffness (equivalent to 9 to 15 MPa in bending). This coincidentally is the same region as noted by Anderson et al. (2001), Rowe and Sharrock (2004), and Cooper (2024) which denotes a peak strength and a transition from brittle (true fatigue) to ductile (instability flow) failure. The data points captured by the MOSS measurements lie at a lower stiffness value and thus capture fracture behavior close to the peak value, but within the ductile/ instability flow region.

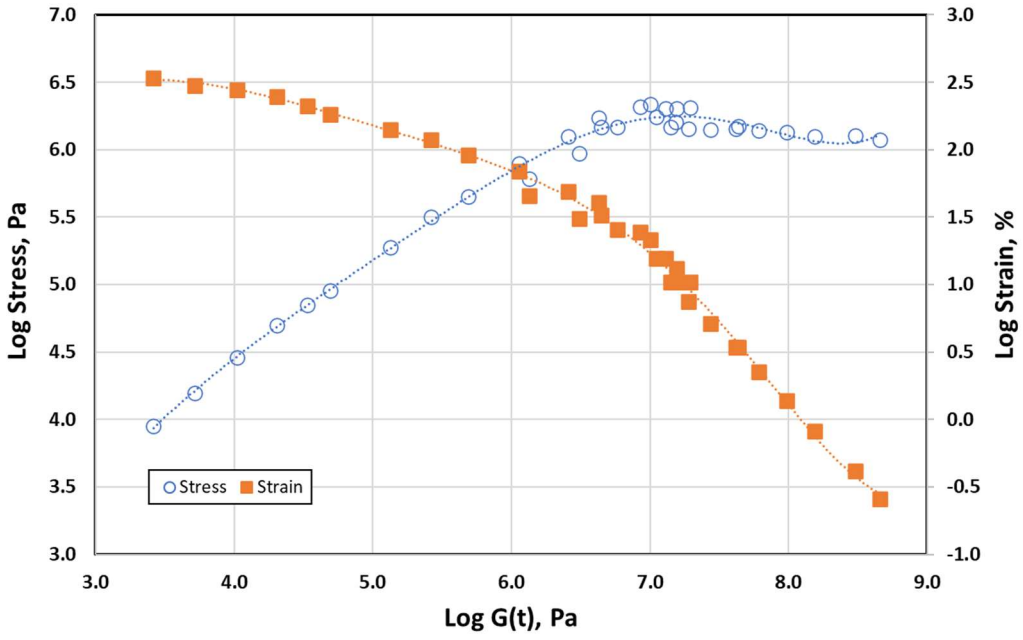

Figure 49. Stress and strain at break, after Heukelom (1966)

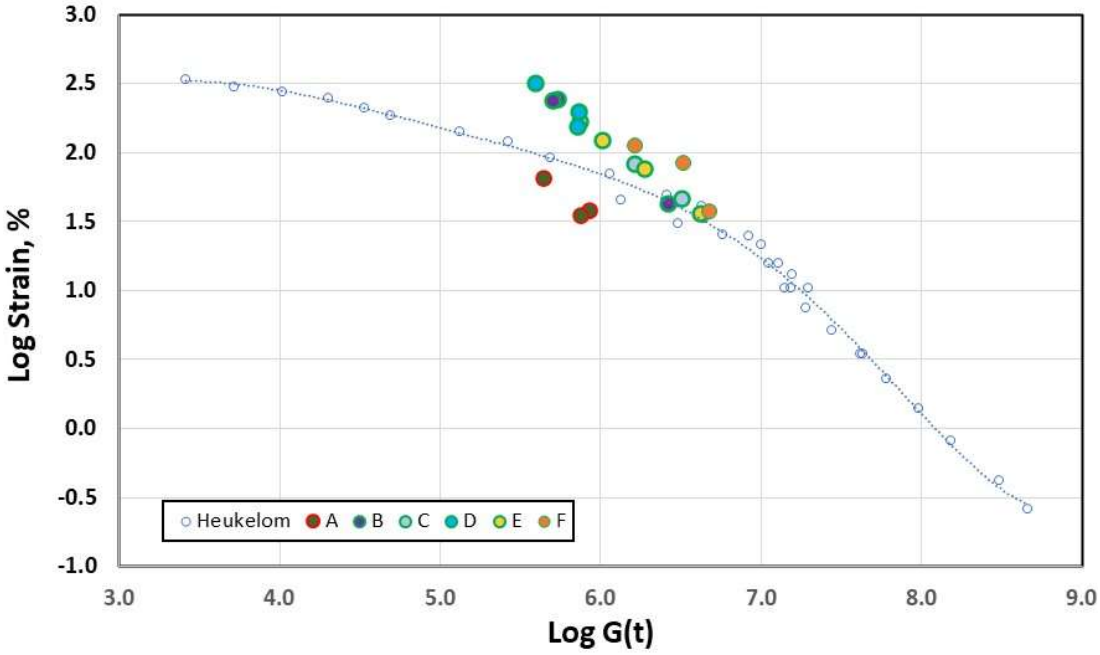

Figure 50. Yield strain versus data produced by Heukelom (1966)

The data in Figure 50, while close to the Heukelom line, does not necessarily follow the same relationship and shape. It should be noted that Heukelom's data is old and measured on equipment that differs from what is used in modern asphalt science. While Heukelom's data can be used as a guide for computing a FFPR, care must be taken in evaluating this parameter since the exact shape of the relationship may not be valid using modern equipment and methods.

A combination plot that includes Materials A-F and the binders evaluated as part of AIF Project 22-03 is shown in Figure 51. In this figure, all modified binders are represented with a circle symbol. It is clear that around a log G(t) value of 1 MPa, the strain at break is significantly different.

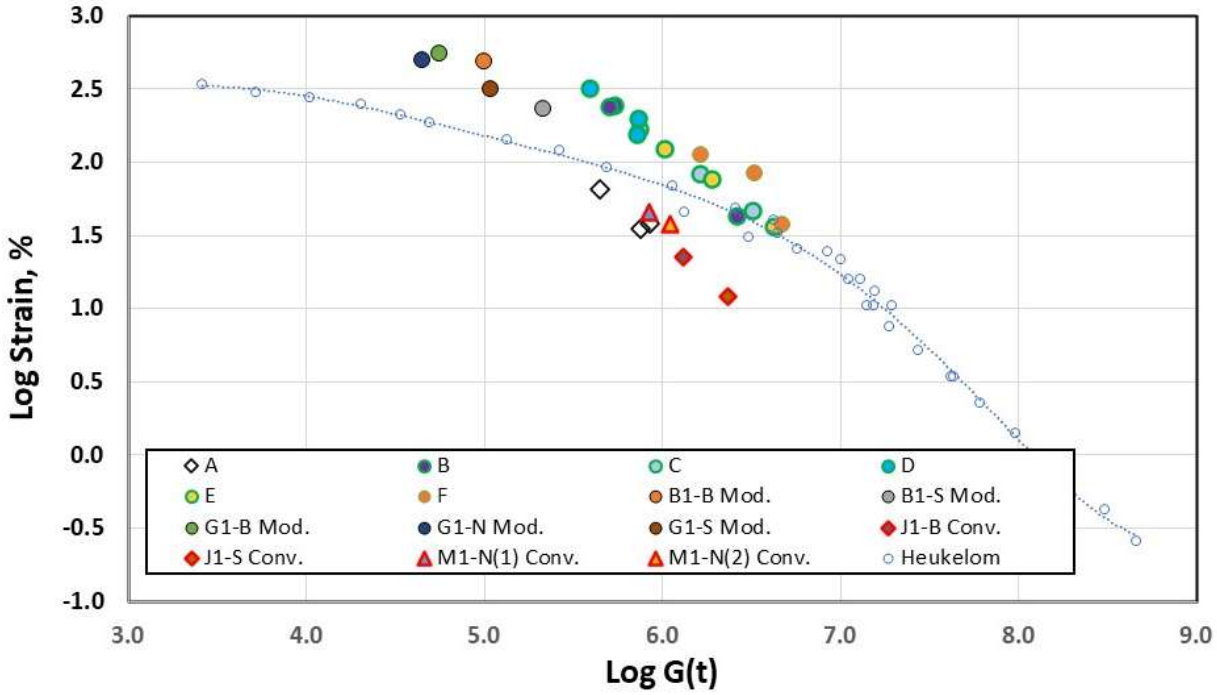

Figure 51. Combined MOSS data for Materials A-F and binders from AIF Project 22-03

Decreasing yield (or failure) energy, E_f, with aging is seen in Figure 52. Yield energy from MOSS testing on unaged, PAV20 and PAV40 coatings. Notably, the inherent strength of the modified binders (B-F) is shown in higher E_f than the oxidized coating (A), again illustrating the strain tolerance gained through polymer modification. Also notable is that, while the polymer blends showed a larger drop in yield energy from an unaged to aged (PAV40) state than the oxidized coating, they still maintained higher yield energy values. This is consistent with findings from AIF Project 22-03 (Rowe et. al, 2023).

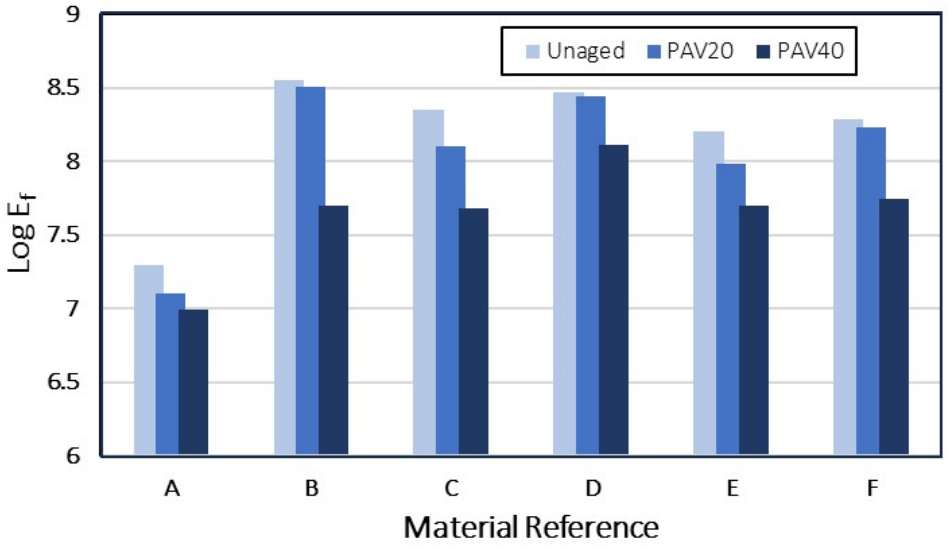

Figure 52. Yield energy from MOSS testing on unaged, PAV20 and PAV40 coatings

Relationships between high-strain MOSS parameters and low-strain rheological parameters are shown in and Figure 53 and Figure 54. Notably, binder hardness (expressed at $T_{\delta=27°}$) and yield energy

show a strong relationship. FFPR, based upon a preliminary analysis of roofing grade binders (Cooper, 2024), shows a correlation with phase angle at a constant modulus, although with a lower coefficient of determination. This looser correlation may owe to the failure of low-strain rheology to fully capture the viscoelastic impacts of the polymer network.

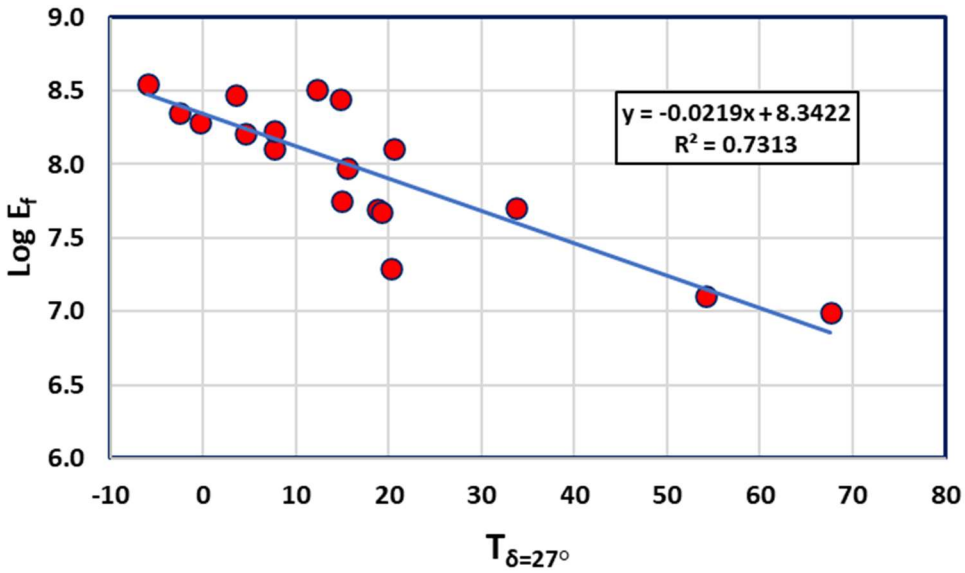

Figure 53. Log E_f vs $T_{\delta=27°}$

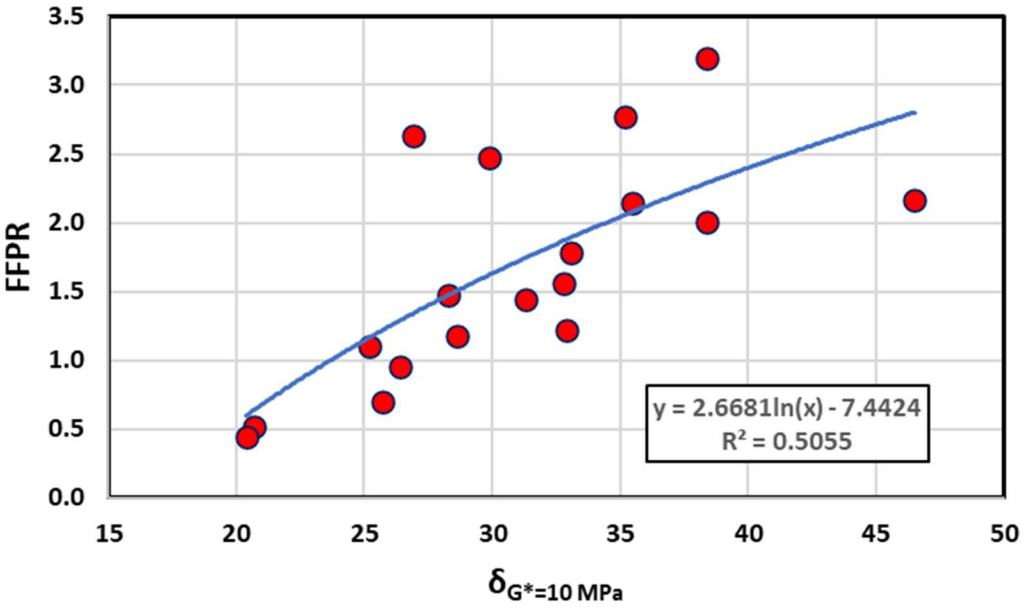

Figure 54. FFPR vs. $\delta_{G^*=10\ MPa}$

Empirical measurements

Performance data was collected for both the rheological measures (Table 2) and empirical tests (Appendix A). Technologists and engineers often like to develop relationships between older parameters and newer rheological parameters to assist with understanding of previous and future material use. For the material set in this study, it has been assessed which rheological parameters correlate best to the traditional parameters.

Penetration and Rheology

An initial assessment reviewed the methods developed by Gershkoff (1995) and Rowe and Baumgardner (2007) that considered G* at 0.4 Hz, a frequency suggested originally by van der Poel's (1954) work. However, after review of the various parameters, it was found that the best correlation with Penetration (PEN) data was with the logarithm of the Glover-Rowe (G-R) parameter measured at 15°C and 10 rad/s. The correlation at other conditions suggested that a reasonable relationship could be obtained with the G-R parameter at 25°C. These correlations are shown in Figure 55.

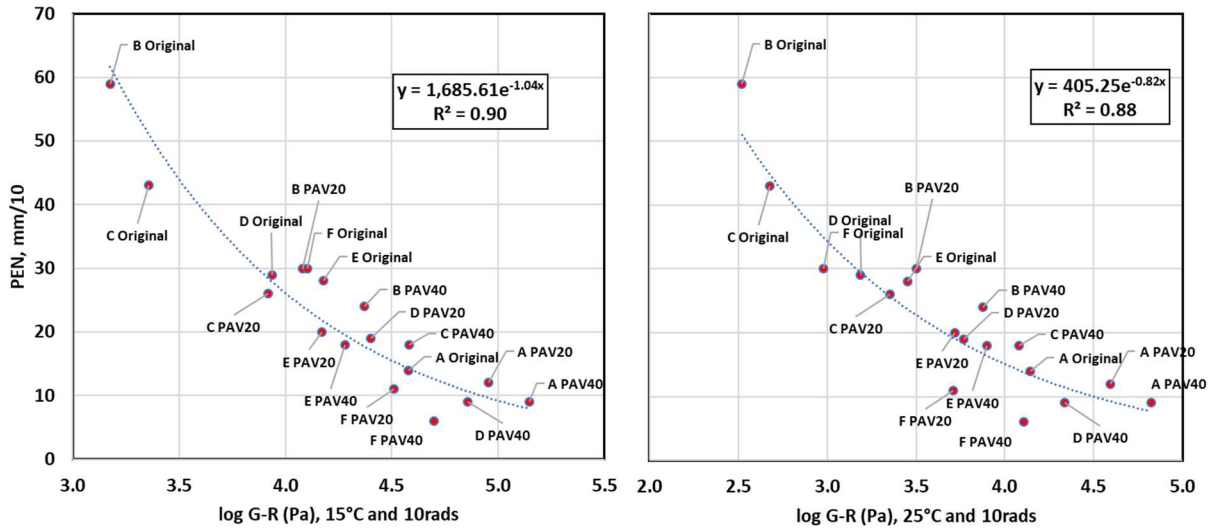

Figure 55. Log G-R (15°C and 25°C, 10 rad/s) versus PEN (dmm)

Softening Point and Rheology

Data presented in Figure 26 showed the difference in viscosity computed from the master curves versus that obtained from simply taking the reciprocal of the $J_{nr3.2}$ value. The viscosity computed from the master curves is a low stress/strain viscosity measured in the linear viscoelastic region. This is contrasted to J_{nr}, which is first measured at a low stress level of 100 Pa and then at a significantly higher stress level of 3,200 Pa. Previous work considering viscosity from master curves (Rowe and Baumgardner, 2007) was unsuccessful in the development of any useful correlations. However, in the current work some useful data was obtained through using the 3,200 Pa stress level from the MSCR test, as shown in Figure 56. It is anticipated that more complex materials will have a greater deviation. This relationship could be extended with other materials, including softer paving grade binders, to assess the robustness of this method.

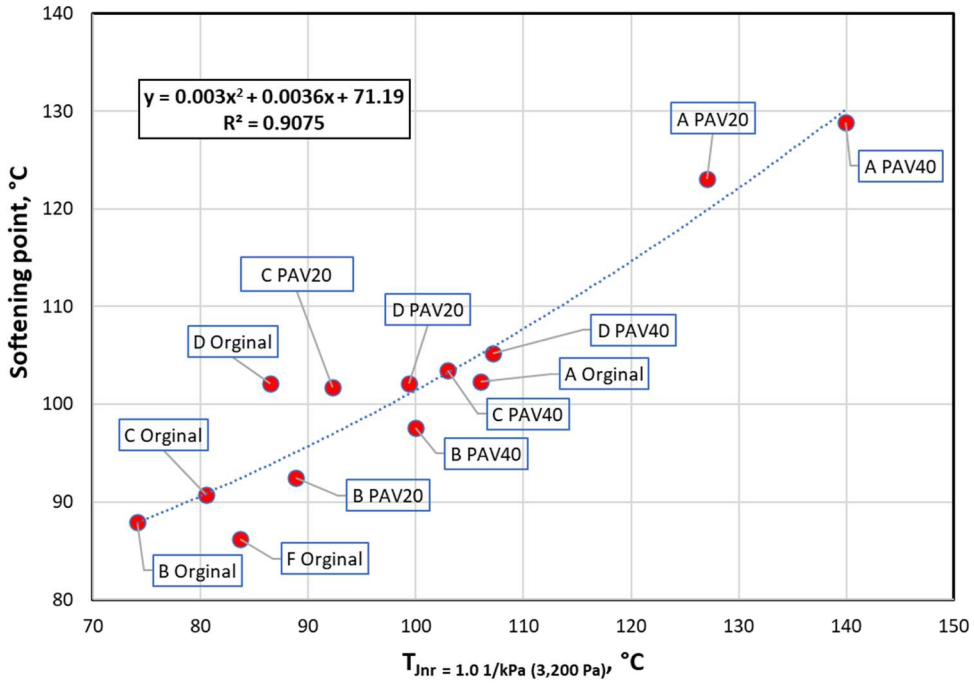

Figure 56. Temperature corresponding to a softening point (°C) versus $J_{nr3.2}$ of 1.0 (kPa^{-1})

Conclusions

Rheology

For each material and aging condition, complex modulus, G^*, and phase angle, δ, data were obtained from temperature-frequency sweeps on the DSR using 4-mm, 8-mm and 25-mm parallel plate geometry across a dynamic stiffness range of 100 Pa to 100 MPa. Master curves were generated using RHEA software and data was analyzed. In the analysis of model and fitting parameters, the following was concluded:

1. The use of the Christensen-Anderson model for roofing grade binders was generally unsuccessful.
2. The determination of a cross-over modulus typically occurred at a stiffness that was too low to be associated with cracking. For some modified materials this proved to be a very unreliable indicator of performance.
3. Better indicators of the shape of the master curve in the high stiffness region were considered to be the phase angle at a constant modulus (10 MPa) and/or the properties associated with a phase angle of 27 degrees. Each of these parameters can be measured with relative ease and were well correlated with observed impact damage in AIF Project 22-03.

With regard to the high temperature performance some testing was conducted using the Multiple Stress Creep and Recovery (MSCR) test. It was observed that percent recovery versus the non-recoverable creep compliance values varied considerably by material and aging condition. Preliminary analysis was conducted by applying the use of stress-dependent viscosity analysis (Ostwald-DeWaele power law relationship) which appears to be applicable for these materials. This power law parameter, P, defines the stress sensitivity and enables an understanding of structures that appear to be associated with different types of modifications. This is particularly evident in Material E which shows unusual behavior when compared to other materials evaluated. The further development of the use of this method is anticipated to be useful in the classification of materials.

Ultimate tests

Several ultimate tests have been recently considered for asphalt roofing materials. Work conducted in AIF Project 22-03 considered the Asphalt Binder Cracking Device (ABCD), Simplifid Double-Edged-Notched Tension Test (S-DENT) and Monotonic Shear Strength (MOSS) tests, whereas this work concentrated on two DSR-based methods:

1. Linear Amplitude Sweep (LAS) Test
   a. The data from this test was analyzed to determine the A_{35} & B parameters associated with the LAS fatigue law.
   b. The data showed some general trends but interpreting the data in its applicability to roofing projects and lack of data consistency resulted in this test being problematic. Further LAS testing was curtailed after the initial three results.

2. MOSS Test
    a. The testing temperatures selected resulted in stiffness at the failure condition which were significantly lower than initially targeted value (1-10 MPa) for some of the materials.
    b. The yield energy, *Ef*, and Fatigue-Fracture Performance Ratio (FFPR) showed correlation with rheology. These parameters were also shown to correlate with hail damage in AIF Project 22-03.
    c. A draft test procedure for the MOSS test is included in Appendix B.

Correlations with empirical measures

Useful correlations have been established with empirical measures for Penetration (25°C at standard loading conditions) and Ring-and-Ball Softening Point. The best correlations were obtained with the G-R parameter measured at 10 rad/s and with the temperature that corresponded to a $J_{nr3.2}$ of 1.0 kPa^{-1}.

Acknowledgments

The authors gratefully acknowledge the financial support and project management offered by RTAC member companies.

Disclaimer

The research described in this report was conducted for the Asphalt Institute RTAC.

References

Anderson, D.A, Le Hir., Y.M., Marasteanu, M.O., Planche, J-P., Martin, D. and Gautherier, G., "*Evaluation of Fatigue Criteria for Asphalt Binders*," Research Record, 1766(1), 48-56. https://doi.org/10.3141/1766-07, 2001.

ARMA, "*A Simple Guide to Understanding Your Shingle Roofing System*," Asphalt Roofing Manufacturers Association, https://www.asphaltroofing.org/a-simple-guide-to-understanding-your-asphalt-shingle-roofing-system/. Accessed 2023/06/11.

Bahia, H., Wen, H. and Johanson C., "*Developments in intermediate temperature binder fatigue specifications*," Transportation Research Circular Number E-C147 pp 25-3. 2010.

Bennert, T., Garg, N., Ericson, C., and Cytowicz, N., "*Evaluation of Test Methods to Identify Asphalt Binders Prone to Surface-initiated Cracking*," Transportation Research Record, 2677(3), 897-910. 2022. https://doi.org/10.1177/03611981221119191.

Christensen, D.W. and Tran, N., "*Relationships Between the Fatigue Properties of Asphalt Binders and the Fatigue Performance of Asphalt Mixtures," NCHRP Report 982*, Washington, D.C.: Transportation Research Board, 2022.

Cooper, W., *"A Visit from the Ghosts of Binders Past: A Fresh Look at Roofing Coatings from Previous Rheological Task Force Work,"* Presentation to the Roofing Technical Advisory Committee at the 2024 Asphalt Institute Annual Meeting in Orlando, FL. December 2024.

Farrar, M.J., Turner, T.F., Planche, J-P., Schabron, J.F. and Harnsberger, P.M., "*Evolution of the Crossover Modulus with Oxidative Aging, Method to Estimate Change in Viscoelastic Properties of Asphalt Binder with Time and Depth on the Road*," Transportation Research Record: Journal of the Transportation Research Board, No. 2370, Transportation Research Board of the National Academies, Washington, D.C., 2013, pp. 76–83. DOI: 10.3141/2370-10.

Gershkoff, D., "*Polymer Modified Bitumen—Performance in Empirical and Rheological Tests*," Proceedings of the 1st European Workshop on the Rheology of Bitumen Binders, 5–7 April, 1995, Brussels, Paper #34.

Gordon, G.V. and Shaw, M.T., "*Computer Programs for Rheologists*," Hanser/Gardner Pubs, 1994.

Heukelom, W., "*Observations on the Rheology and Fracture of Bitumens and Asphalt Mixes*," Proceedings, The Association of Asphalt Paving Technologists, Volume 35, 1966.

Hintz, C., Velasquez, R., Johnson, C., and H. Bahia, "*Modification and Validation of the Linear Amplitude Sweep Test for Binder Fatigue Specification*," Transportation Research Record:

Journal of the Transportation Research Board, Transportation Research Board of the National Academies, Washington, D.C., 2011, pp. 99-106

IBHS, "*Impact Resistance Test Protocol for Asphalt Shingles*," Insurance Institute for Business & Home Safety, June 2019.

IBHS "*Roof Shingle Hail Impact Ratings*," Insurance Institute for Business & Home Safety, Web site - https://ibhs.org/hail/shingle-performance-ratings/, accessed on December 4th, 2024.

Kim, Y., Lee, H. J., Little, D. N., and Kim, Y. R., "*A simple testing method to evaluate fatigue fracture and damage performance of asphalt mixtures*," Journal, Association of Asphalt Paving Technologists, Vol. 75, 2006, pp. 755-788.

Kriz, P., Campbell, C.M., Kucharek, A.S. and Varamini, "*A Simple Binder Specification Tweak to Promote Best Performers*," Proceedings of the Sixty-Fifth Annual Conference of the Canadian Technical Asphalt Technical Asphalt Association (CTAA), November 2020.

Meynard, J.Y., "*Thermal Aging - Influence of Binder Type, Evaluation Methods- Correlation with Aging Resistance to Natural Exposure*," Siplast, Paris, 1983.

Mirza, M.W. and Witczak, M.W. "*Development of a Global Aging System for Short and Long Term Aging of Asphalt Cements*," Journal of the Association of Asphalt Paving Technologists, 64, 393–418. 1995.

Rowe, G.M., "*Interrelationships in Rheology for Asphalt Binder Specifications*," 59th Annual Conference of Canadian Technical Asphalt Association, Winnipeg, Manitoba, November 16 to 19, 2014.

Rowe, G.M., and Baumgardner, G., "*Evaluation of the Rheological Properties and Master Curve Development for Bituminous Binders Used in Roofing*," Journal of ASTM International, Vol. 4, No. 9, 2007.

Rowe, G.M., Bredenhann, S. and Raposo, R., "*Defining the Rheological Type of Asphalt Binders for Use in Performance Related Specifications*," Proceedings, 13th Conference on Asphalt Pavements for Southern Africa, 2023.

Rowe, G.M., Cooper, W.G. and Anderson, R.M., "*Understanding and Improving the Durability of Asphalt Shingles, Phase 1 – Investigation of the Rheological Properties of Binders Recovered from Asphalt Shingles and their Relation to Performance*," Report prepared for the Asphalt Institute Foundation and State Farm Mutual Automobile Insurance Company, AIF Research Project 22-03, Final Report (version 2024-05-10) December 2023.

Rowe, G.M., D'Angelo, J.A. and Sharrock, M.J., "*Use of the Zero Shear Viscosity as a Parameter for the High Temperature Binder Specification Parameter*," Paper presented at the 2nd International Symposium on Binder Rheology and Pavement Performance, San Antonio, Texas, September 23 and 24, 2002.

Rowe, G.M., Mogawer, W.S. and Abdalfattah, I.M., "*Defining Asphalt Binder Performance and Rheological Type via Point and Shape Parameters*," Proceedings, Airfield and Highway Pavements, ASCE, 2025.

Rowe, G.M., and Raposo, S.F., "*RHEA – Rheology Analysis – Software for the Rheological Analysis of Asphalt and Bituminous Binders, Mixtures and Other Visco-Elastic Materials*," Abatech Inc., RHEA User Manual, Version 2.1, November 8th, 2021.

Rowe, G.M. and Sharrock, M.J., "*The Direct Tension Test and The Behavior of Asphalt Binders at Low and Intermediate Temperatures*," 3rd Eurasphalt & Eurobitume Congress, Vienna, 2004.

Singhvi, P. and Yousfi, S., "*Rheology of Coating Asphalt with Dark Oven Aging and PAV aging*," Crafco, Inc., 2023.

van der Poel, C. J., "*A General System Describing the Visco-Elastic Properties of Bitumens and Its Relation to Routine Test Data*," J. Appl. Chem., Vol. 4, 1954, pp. 221–236.

APPENDIX A: Summary of Data for Materials A to F

Description	Test Temperature, °C			Condition		
	Original	PAV20	PAV40	Original	PAV20	PAV40
Penetration	25			x	x	x
R&B SP	-			x	x	x
RV	176.7			x	x	x
MSCR $Jnr_{3.2}$ range of 0.25-4.5 kPa^{-1}	100	124	136	x	x	x
	106	130	142	x	x	x
	112C	136	148	x	x	x
LAS T, G*=1 MPa, 10 MPa, 25 MPa	47.6	61.9	69.9	x	x	x
	22	30.6	37.3	x	x	x
	11.6	17.5	23.4	x	x	x
LVE Strain Sweep 0.1%-10%	-20			x	x	x
	0			x	x	x
	20			x	x	x
	40			x	x	x
	60			x	x	x
	80			x	x	x
	100			x	x	x
	120			x	x	x
Temperature-Frequency Sweep 0.1-10 rad/s, 5 pts/decade	-20C-120			x	x	x

Data Summary

Description	Test Temperature, °C			Result		
	Original	PAV20	PAV40	Original	PAV20	PAV40
$Jnr_{0.1}$, kPa^{-1}	82	118	130	0.015	0.106	0.091
	94	124	136	0.075	0.220	0.159
	100	130	142	0.170	0.538	0.366
	106	136	148	0.389	1.000	0.950
	112			0.933		
$Jnr_{3.2}$, kPa^{-1}	82	118	130	0.020	0.180	0.156
	94	124	136	0.109	0.513	0.385
	100	130	142	0.315	1.938	1.678
	106	136	148	0.992	5.695	5.225
	112			3.001		
$R_{0.1}$, %	82	118	130	86.1	79.6	83.0
	94	124	136	78.5	74.7	80.1
	100	130	142	73.2	67.4	74.7
	106	136	148	66.0	63.6	64.0
	112			57.2		
$R_{3.2}$, %	82	118	130	81.2	61.7	66.4
	94	124	136	66.0	40.8	50.1
	100	130	142	48.0	13.0	17.7
	106	136	148	23.4	2.1	3.0
	112			6.4		
N_f, 2.5% strain	47.6	61.9	69.9	190025	175518	220066
	22	30.6	37.3	56981	16296	21881
	11.6	17.5	23.4	16575	2	60823
N_f, 5% Strain	47.6	61.9	69.9	5292	3518	3902
	22	30.6	37.3	597	64	69
	11.6	17.5	23.4	97	0	82
FFPR	22	30.6	37.3	0.70	0.52	0.45
E_f, Pa				1.97E+07	1.27E+07	9.77E+06
Yield Strain (γ_f), %				65.4	38.3	35.0
Log $G(t)_f$, Pa				5.646	5.932	5.880
Shear Strength (τ_f), Pa				2.90E+05	3.27E+05	2.66E+05
Penetration, dmm	25			14	12	9
Rotational Viscosity, Pa·s	176.7			1.553	12.75	36.75
R&B Softening Point, °C	-			102.3	123.1	128.9
ωc, rad/s	T_{ref}= 20C			2.19E-06	1.21E-09	4.12E-11
G_c - DS Fit				3.60E+04	1.09E+04	7.10E+03
Log G_c - DS Fit				4.55591	4.03918	3.85118
R (assumed Gg of 1e9 Pa) - DS Fit				4.44	4.96	5.15
$T_{VET\ (10\ rad/s)}$				81.25	111.4	124.9
$\delta_{G^*=10\ MPa\ (10\ rad/s)}$, °				25.7	20.7	20.4
$T_{\delta=27°\ (10\ rad/s)}$, °C				20.2	54.2	67.6
Log G*, 25°C, 2.5 rad/s				6.746	7.035	7.231
$T_{Jnr\ =\ 1\ 1/kPa\ (at\ 3200\ Pa)}$				106.0	127.0	139.9

Material A

Description	Test Temperature, °C			Condition		
	Original	PAV20	PAV40	Original	PAV20	PAV40
Penetration	25			x	x	x
R&B SP	-			x	x	x
RV	176.7			x	x	x
MSCR $Jnr_{3.2}$ range of 0.25-4.5 kPa^{-1}	70	82	88	x	x	x
	76	88	94	x	x	x
	82	94	100	x	x	x
LAS T, G*=1 MPa, 10 MPa, 25 MPa	20.2	34.2	41.4	x	x	x
	3.5	12.0	17.4	x	x	x
	-4.0	2.2	6.4	x	x	x
LVE Strain Sweep 0.1%-10%	-20			x	x	x
	0			x	x	x
	20			x	x	x
	40			x	x	x
	60			x	x	x
	80			x	x	x
	100			x	x	x
	120			x	x	x
Temperature-Frequency Sweep 0.1-10 rad/s, 5 pts/decade	-20C-120			x	x	x

Data Summary

Description	Test Temperature, °C			Result		
	Original	PAV20	PAV40	Original	PAV20	PAV40
$Jnr_{0.1}$, kPa^{-1}	70	82	88	0.035	0.190	0.139
	76	88	94	0.196	0.417	0.291
	82	94	100	0.184	0.628	0.537
			106			1.077
$Jnr_{3.2}$, kPa^{-1}	70	82	88	0.381	0.367	0.192
	76	88	94	1.540	0.901	0.469
	82	94	100	2.866	1.911	1.007
			106			2.466
$R_{0.1}$, %	70	82	88	95.8	66.0	60.0
	76	88	94	88.8	58.4	52.3
	82	94	100	90.6	60.2	46.2
			106			40.5
$R_{3.2}$, %	70	82	88	65.6	40.4	47.6
	76	88	94	42.1	24.5	31.4
	82	94	100	30.6	14.7	18.5
			106			7.2
N_f, 2.5% strain	20.2	34.2	41.4	884069	2683868	20796527
	3.5	12.0	17.4	11384	362217	35378683
	-4.0	2.2	6.4	91861	7835	2897
N_f, 5% Strain	20.2	34.2	41.4	58147	143559	638301
	3.5	12.0	17.4	411	5711	387679
	-4.0	2.2	6.4	2806	53	15
FFPR	-10.0	-5.5	-2.1	2.77	2.63	0.96
E_f, Pa				3.53E+08	3.23E+08	4.97E+07
Yield Strain (γ_f), %				240.0	234.0	41.5
Log $G(t)_f$, Pa				5.743	5.713	6.430
Shear Strength (τ_f), Pa				1.33E+06	1.21E+06	1.12E+06
Penetration, dmm	25			59	30	24
Rotational Viscosity, Pa·s	176.7			1.138	1.633	2.173
R&B Softening Point, °C	-			87.9	92.5	97.6
ωc, rad/s - CAM	T_{ref}= 20C			2.07E+01	3.62E-03	1.35E-04
G_c - CAM				1.51E+06	1.51E+05	8.45E+04
Log G_c - CAM				6.18004	5.17773	4.92681
R - CAM				2.85	3.96	4.22
$T_{VET\ (10\ rad/s)}$				15.41	74.39	84.7
$\delta_{G^*=10\ MPa\ (10\ rad/s)}$, °				35.2	26.9	26.4
$T_{\delta=27°\ (10\ rad/s)}$, °C				-6.0	12.3	18.7
Log G*, 25°C, 2.5 rad/s				5.400	6.188	6.488
$T_{Jnr\ =\ 1\ 1/kPa\ (at\ 3200\ Pa)}$				74.1	88.8	99.9

Material B

Description	Test Temperature, °C			Condition		
	Original	PAV20	PAV40	Original	PAV20	PAV40
Penetration	25			x	x	x
R&B SP	-			x	x	x
RV	176.7			x	x	x
MSCR $Jnr_{3.2}$ range of 0.25-4.5 kPa^{-1}	76	88	100	x	x	x
	82	94	106	x	x	x
	88	100	112	x	x	x
LAS T, G*=1 MPa, 10 MPa, 25 MPa	22.4	32.4	45.7	x	x	x
	5.6	9.7	22.5	x	x	x
	-1.7	-0.3	12.5	x	x	x
LVE Strain Sweep 0.1%-10%	-20			x	x	x
	0			x	x	x
	20			x	x	x
	40			x	x	x
	60			x	x	x
	80			x	x	x
	100			x	x	x
	120			x	x	x
Temperature-Frequency Sweep 0.1-10 rad/s, 5 pts/decade	-20C-120			x	x	x

Data Summary						
Description	Test Temperature, °C			Result		
	Original	PAV20	PAV40	Original	PAV20	PAV40
$Jnr_{0.1}$, kPa^{-1}	76	88	100	0.026	0.309	0.368
	82	94	106	0.074	0.347	0.736
	88	100	112	0.209	0.368	1.318
$Jnr_{3.2}$, kPa^{-1}	76	88	100	0.262	0.484	0.667
	82	94	106	1.551	1.355	1.518
	88	100	112	4.552	2.859	2.855
$R_{0.1}$, %	76	88	100	97.2	83.8	53.6
	82	94	106	94.7	74.5	47.8
	88	100	112	89.5	79.4	41.0
$R_{3.2}$, %	76	88	100	78.6	42.9	27.0
	82	94	106	38.6	19.6	15.0
	88	100	112	12.7	8.4	7.9
N_f, 2.5% strain	22.4	32.4	45.7	103857	511095	2616231
	5.6	9.7	22.5	2045	6068	31134
	-1.7	-0.3	12.5	228	486	85777
N_f, 5% Strain	22.4	32.4	45.7	9087	24260	121720
	5.6	9.7	22.5	77	76	534
	-1.7	-0.3	12.5	4	2	591
FFPR	-5.0	-2.5	0.0	2.14	1.48	1.18
E_f, Pa				2.23E+08	1.27E+08	4.77E+07
Yield Strain (γ_f), %				165.0	81.5	45.0
Log $G(t)_f$, Pa				5.882	6.223	6.517
Shear Strength (τ_f), Pa				1.26E+06	1.36E+06	1.20E+06
Penetration, dmm	25			43	26	18
Rotational Viscosity, Pa·s	176.7			1.405	3.060	4.430
R&B Softening Point, °C	-			90.7	101.7	103.5
ωc, rad/s - CAM	T_{ref}= 20C			5.31E+00	5.48E-02	1.29E-03
G_c - CAM				1.08E+06	3.44E+05	3.58E+05
Log G_c - CAM				6.03513	5.53689	5.55333
R - CAM				3.01	3.44	3.37
$T_{VET\ (10\ rad/s)}$				22.2	61.9	80.0
$\delta_{G^*=10\ MPa\ (10\ rad/s)}$, °				35.5	28.3	28.6
$T_{\delta=27°\ (10\ rad/s)}$, °C				-2.6	7.7	19.2
Log G*, 25°C, 2.5 rad/s				5.552	6.077	6.691
$T_{Jnr\ =\ 1\ 1/kPa\ (at\ 3200\ Pa)}$				80.5	92.2	103.0

Material C

Description	Test Temperature, °C			Condition		
	Original	PAV20	PAV40	Original	PAV20	PAV40
Penetration	25			x	x	x
R&B SP	-			x	x	x
RV	176.7			x	x	x
MSCR $Jnr_{3.2}$ range of 0.25-4.5 kPa^{-1}	82	94	100	x	x	x
	88	100	106	x	x	x
	94	106	112	x	x	x
MBYET T, G*=50 MPa (10 rad/s)	0.9	2.5	9.8	x	x	x
LVE Strain Sweep 0.1%-10%	-20			x	x	x
	0			x	x	x
	20			x	x	x
	40			x	x	x
	60			x	x	x
	80			x	x	x
	100			x	x	x
	120			x	x	x
Temperature-Frequency Sweep 0.1-10 rad/s, 5 pts/decade	-20C-120			x	x	x

Data Summary

Description	Test Temperature, °C			Result		
	Original	PAV20	PAV40	Original	PAV20	PAV40
$Jnr_{0.1}$, kPa^{-1}	82	94	100	**0.025**	**0.170**	**0.259**
	88	100	106	**0.208**	**0.387**	**0.430**
	94	106	112	**0.330**	**0.578**	**1.069**
$Jnr_{3.2}$, kPa^{-1}	82	94	100	**0.280**	**0.426**	**0.397**
	88	100	106	**1.531**	**1.100**	**0.860**
	94	106	112	**3.467**	**2.130**	**2.137**
$R_{0.1}$, %	82	94	100	**96.2**	**74.3**	**54.5**
	88	100	106	**86.5**	**67.0**	**54.1**
	94	106	112	**84.1**	**66.6**	**39.9**
$R_{3.2}$, %	82	94	100	**67.1**	**42.6**	**36.4**
	88	100	106	**35.6**	**24.5**	**24.1**
	94	106	112	**16.5**	**14.7**	**10.1**
FFPR	0.9	2.5	9.8	**3.20**	**2.47**	**1.56**
E_f, Pa				**2.96E+08**	**2.77E+08**	**1.28E+08**
Yield Strain (γ_f), %				**311.0**	**192.0**	**150.0**
Log $G(t)_f$, Pa				**5.600**	**5.871**	**5.863**
Shear Strength (τ_f), Pa				**1.24E+06**	**1.43E+06**	**8.94E+05**
Penetration, dmm	25			**29**	**19**	**9**
Rotational Viscosity, Pa·s	176.7			**1.915**	**6.750**	**7.350**
R&B Softening Point, °C	-			**102.1**	**109.0**	**105.2**
ωc, rad/s - CAM	T_{ref}= 20C			**3.09E+00**	**4.86E-03**	**1.45E-03**
G_c - CAM				**2.66E+06**	**3.31E+05**	**6.30E+05**
Log G_c - CAM				**6.42473**	**5.51932**	**5.79956**
R - CAM				**2.42**	**3.50**	**3.18**
$T_{VET\ (10\ rad/s)}$				**23.2**	**74.4**	**51.8**
$\delta_{G^*=10\ MPa\ (10\ rad/s)}$, °				**38.4**	**29.9**	**32.8**
$T_{\delta=27°\ (10\ rad/s)}$, °C				**3.5**	**14.8**	**20.5**
Log G*, 25°C, 2.5 rad/s				**6.044**	**6.445**	**6.943**
$T_{Jnr\ =\ 1\ 1/kPa\ (at\ 3200\ Pa)}$				**86.5**	**99.4**	**107.2**

Material D

Description	Test Temperature, °C			Condition		
	Original	PAV20	PAV40	Original	PAV20	PAV40
Penetration	25			x	x	x
R&B SP	-				n/a	n/a
RV	176.7			x	n/a	n/a
MSCR $Jnr_{3.2}$ range of 0.25-4.5 kPa^{-1}	100			x	x	x
	106			x	x	x
	112			x	x	x
MOSS T, G*=50 MPa (10 rad/s)	-1.5	4.4	-4.2			x
LVE Strain Sweep 0.1%-10%	-20			x	x	x
	0			x	x	x
	20			x	x	x
	40			x	x	x
	60			x	x	x
	80			x	x	x
	100			x	x	x
	120			x	x	x
Temperature-Frequency Sweep 0.1-10 rad/s, 5 pts/decade	-20C-120			x	x	x

Data Summary

Description	Test Temperature, °C			Result		
	Original	PAV20	PAV40	Original	PAV20	PAV40
$Jnr_{0.1}$, kPa^{-1}	100	118	130	**0.019**	**0.049**	**0.037**
	106	124	136	**0.039**	**0.028**	**0.101**
	112	130	142	**0.041**	**0.102**	**0.140**
$Jnr_{3.2}$, kPa^{-1}	100	118	130	**0.626**	**0.289**	**0.358**
	106	124	136	**1.437**	**0.408**	**0.531**
	112	130	142	**2.604**	**0.603**	**1.089**
$R_{0.1}$, %	100	118	130	**95.6**	**94.6**	**97.0**
	106	124	136	**93.1**	**97.3**	**94.0**
	112	130	142	**93.8**	**92.6**	**95.0**
$R_{3.2}$, %	100	118	130	**44.4**	**79.7**	**80.9**
	106	124	136	**26.7**	**78.4**	**80.4**
	112	130	142	**19.8**	**78.7**	**75.8**
FFPR	-1.5	-2.5	-4.2	**1.78**	**1.44**	**1.10**
E_f, Pa				**1.61E+08**	**9.55E+07**	**5.03E+07**
Yield Strain (γ_f), %				**121.0**	**74.2**	**35.5**
Log $G(t)_f$, Pa				**6.021**	**6.286**	**6.633**
Shear Strength (τ_f), Pa				**1.27E+06**	**1.43E+06**	**1.53E+06**
Penetration, dmm	25			**28**	**20**	**18**
Rotational Viscosity, Pa·s	204			**3.875**	-	-
R&B Softening Point, °C	-				-	-
ωc, rad/s - CAM	T_{ref}= 20C			**1.08E-01**	**1.00E-02**	-
G_c - CAM				**6.33E+05**	**2.82E+05**	-
Log G_c - CAM				**5.80156**	**5.44971**	-
R - CAM				**3.45**	**3.86**	-
$T_{VET\ (10\ rad/s)}$				**136.1**	**115.8**	**128.5**
$\delta_{G^*=10\ MPa\ (10\ rad/s)}$, °				**33.1**	**31.3**	**25.2**
$T_{\delta=27°\ (10\ rad/s)}$, °C				**4.5**	**15.5**	**33.7**
Log G*, 25°C, 2.5 rad/s				**6.157**	**6.649**	**6.452**
$T_{Jnr\ =\ 1\ 1/kPa\ (at\ 3200\ Pa)}$				**103.4**	**139.6**	**145.6**

Material E

Description	Test Temperature, °C			Condition		
	Original	PAV20	PAV40	Original	PAV20	PAV40
Penetration	25			x	x	x
R&B SP	-			x	n/a	n/a
RV	176.7			x	n/a	n/a
MSCR $Jnr_{3.2}$ range of 0.25-4.5 kPa^{-1}	82	88	94	x	x	x
	88	94	100	x	x	x
	94	100	106	x	x	x
MOSS T, G*=50 MPa (10 rad/s)	-5	1				
LVE Strain Sweep 0.1%-10%	-20			x	x	x
	0			x	x	x
	20			x	x	x
	40			x	x	x
	60			x	x	x
	80			x	x	x
	100			x	x	x
	120			x	x	x
Temperature-Frequency Sweep 0.1-10 rad/s, 5 pts/decade	-20C-120			x	x	x

Data Summary

Description	Test Temperature, °C			Result		
	Original	PAV20	PAV40	Original	PAV20	PAV40
$Jnr_{0.1}$, kPa^{-1}	82	88	94	**0.029**	**0.208**	**0.328**
	88	94	100	**0.129**	**0.509**	**0.785**
	94	100	106	**0.241**	**0.664**	**1.474**
$Jnr_{3.2}$, kPa^{-1}	82	88	94	**0.749**	**0.708**	**0.848**
	88	94	100	**2.051**	**1.625**	**1.893**
	94	100	106	**3.588**	**3.028**	**4.221**
$R_{0.1}$, %	82	88	94	**95.3**	**74.9**	**62.7**
	88	94	100	**87.5**	**65.9**	**50.8**
	94	100	106	**81.4**	**69.1**	**48.2**
$R_{3.2}$, %	82	88	94	**40.7**	**33.8**	**24.3**
	88	94	100	**19.7**	**22.5**	**14.3**
	94	100	106	**10.4**	**17.7**	**8.1**
FFPR	-5	1	4	**1.20**	**1.09**	**1.07**
E_f, Pa				**1.94E+08**	**1.70E+08**	**5.60E+07**
Yield Strain (γ_f), %				**82.1**	**111.0**	**36.6**
Log $G(t)_f$, Pa				**6.526**	**6.221**	**6.681**
Shear Strength (τ_f), Pa				**2.48E+06**	**1.85E+06**	**1.75E+06**
Penetration, dmm	25			**30**	**11**	**6**
Rotational Viscosity, Pa·s	176.7			**1.673**	-	-
R&B Softening Point, °C	-			**86.2**	-	-
ωc, rad/s - CAM	T_{ref}= 20C			**2.31E+01**	**2.82E-01**	-
G_c - CAM				**9.36E+06**	**2.42E+06**	-
Log G_c - CAM				**6.97128**	**6.38396**	-
R - CAM				**2.11**	**2.79**	-
$T_{VET\ (10\ rad/s)}$				**16.6**	**28.9**	**43.6**
$\delta_{G^*=10\ MPa\ (10\ rad/s)}$, °				**46.5**	**38.4**	**32.9**
$T_{\delta=27°\ (10\ rad/s)}$, °C				**-0.3**	**7.7**	**14.9**
Log G*, 25°C, 2.5 rad/s				**5.945**	**6.514**	**6.762**
$T_{Jnr\ =\ 1\ 1/kPa\ (at\ 3200\ Pa)}$				**83.7**	**90.5**	**95.2**

Material F

APPENDIX B: Draft Test Method for Monotonic Shear Strength (MOSS) Test

Standard Method of Test for

Determining the Peak Stress Energy and Shear Fatigue Resistance of Asphalt Binder Using a Dynamic Shear Rheometer (DSR)

Monotonic Shear Strength (MOSS) Test

ASTM Designation: DXXXX-XX

1. Scope

1.1. This test method covers the determination of asphalt binder peak stress (τ_f), peak stress energy (E_f) and peak strain (γ_f) using the Monotonic Shear Strength (MOSS) Test. τ_f, E_f and γ_f can be used to measure the strength, toughness and strain tolerance of an asphalt binder under constant shear loading. The MOSS test is conducted using the Dynamic Shear Rheometer (DSR) utilizing monotonic shear loading, and can performed on unaged or aged material, including materials conditioned in the Rolling Thin-Film Oven (RTFO) and Pressure Aging Vessel (PAV).

1.2. The values stated in SI units are to be regarded as the standard.

1.3. A precision and bias statement for this test method has not been completed at this time. Therefore, this test method should not be used for acceptance or rejection of a material for purchasing purposes.

1.4. *This standard does not purport to address all of the safety concerns, if any, associated with its use. It is the responsibility of the user of this standard to establish appropriate safety and health practices and determine the applicability of regulatory limitations prior to use.*

2. Reference Documents

2.1. ASTM Standards

D8 Standard Terminology Relating to Materials for Roads and Pavements
D2872 Standard Test Method for Effect of Heat and Air on a Moving Film of Asphalt Binder (Rolling Thin-Film Oven Test)
D6373 Standard Specification for Performance-Graded Asphalt Binder
D6521 Standard Practice for Accelerated Aging of Asphalt Binder Using a Pressurized Aging Vessel (PAV)
D7175 Standard Test Method for Determining the Rheological Properties of Asphalt Binder Using a Dynamic Shear Rheometer

3. Terminology

3.1. *Definitions of terms used in this practice may be found in ASTM D8, ASTM D7175, determined from common English usage, or combinations of both.*

3.1.1. *Monotonic shear, n* – refers to a mode of loading where constant shear is applied in a single direction for a given period of time

3.1.2. *Peak Stress (τ_f), n* – the maximum level of shear stress experienced during a period of shear loading. Defined as the point at which shear stress begins to decrease after constant loading

3.1.3. *Shear Modulus (G_γ), n* – ratio of shear stress to shear strain at a given point of monotonic loading time

3.1.4. *Peak Stress Energy (E_f), n* – the amount of energy required to reach peak stress during monotonic shear loading. Calculated as the area under the stress-strain curve from the start of loading to peak stress

3.1.5. *Peak Strain (γ_f), n* – the value of shear strain at which peak stress occurs during monotonic shear loading

4. Summary of Test Method

4.1. A sample of asphalt binder is tested in the DSR using the 8-mm plate geometry with a 1.7-mm gap setting or the 4-mm geometry with a 1.5-mm gap setting. The sample is tested in monotonic shear mode over a maximum time interval of 20 minutes (1200 seconds).

4.2. After testing is completed, the shear stress values are plotted as a function of shear strain. From the plots, peak stress and strain points are determined, and peak stress energy can be calculated.

5. Significance and Use

5.1. This test method is designed to evaluate the shear strength, toughness and strain tolerance of an asphalt binder under constant shear loading.

5.2. The peak stress is an indicator of the shear strength of an asphalt binder under constant loading at a given temperature or stiffness

5.3. The peak stress energy is an indicator of the toughness of an asphalt binder under constant loading at a given temperature or stiffness

5.4. The peak strain is an indication of the strain tolerance of the binder at a given temperature or stiffness

6. Interferences

6.1. Refer to ASTM D7175 Section 6 for common interference in rheological measurement.

6.2. Testing should be performed in the temperature region such that G_γ at peak stress occurs in an approximate stiffness range of 1 MPa to 10 MPa. Tests at temperatures which are too high will result in lower stiffness and instability flow, inconsistent stress-strain curves and indiscernible stress peaks. Test temperatures that are too low may result in adhesive failure or indiscernible stress peaks.

6.2.1. Adhesive failure can be observed in stress-strain curves that are erratic or inconsistent, or a in sudden drop in normal force during the course of the test. This type of failure typically occurs at the beginning of the test and should be monitored to ensure data quality. If adhesive failure is observed or suspected, the operator should test a new specimen.

7. Apparatus

7.1. Refer to ASTM D7175 Section 7 for information regarding the DSR apparatus.

8. Materials

8.1. Refer to ASTM D7175 Section 8 for information regarding materials needed for the procedure.

9. Verification

9.1. Refer to ASTM D7175 Section 8 for information regarding verification of the apparatus

10. Preparation of the Apparatus

10.1. Refer to ASTM D7175 Section 8 for information regarding preparation of the apparatus

11. Preparing Test Specimens

11.1. Specimen preparation, transfer, and trimming for the MOSS test is equivalent to the procedure outlined in D7175 using the 8-mm plates, with the exception as outlined in 11.1.1.

11.1.1. Elevated loading temperatures (higher than 46°C) should be used for stiffer materials. Use a loading temperature high enough to promote good sample adhesion, but not so hot as to cause the sample to flow from the plates. Table 1 shows recommended loading temperature ranges for common material types. For extremely stiff materials, the specimen may be briefly "buttered" with a hot spatula prior to transfer and before squeezing the specimen.

Table 1 – Recommended Specimen Loading Temperatures

Material Type	Loading Temperature, °C Range
Paving-Grade Binder (Unaged/RTFO-conditioned)	30-40
Paving-Grade Binder (Aged)	50-70
Oxidized Roofing Coating (Unaged)	80-100
Oxidized Roofing Coating (Aged)	80-120
Modified Roofing Coating (Unaged)	60-80
Modified Roofing Coating (Aged)	70-90

12. Preparation of the Apparatus

12.1. Program the DSR software to perform a 10-minute soak time at the selected loading temperature to allow the specimen to sufficiently adhere to the plates.

12.2. Program the DSR software to lower the temperature controller to the designated test temperature at a rate of 5-7°C/minute. Program the DSR to reduce the test gap at a linear rate over the course of the cooling period.

12.2.1. When using the 8-mm geometry, program the DSR to reduce the test gap at a linear rate from 2.00 mm to 1.75 mm over the course of the cooling period.

12.2.2. When using the 4-mm geometry, program the DSR to reduce the test gap at a linear rate from 2.00 mm to 1.55 mm over the course of the cooling period.

12.2.3. The length of the cooling period will vary based on loading temperature and cooling rate. Ensure that the gap closes at an even (linear) rate over the period of decreasing temperature.

12.3. Once the test temperature and gap are reached, allow the specimen to equilibrate at the test temperature for 5-10 minutes. Program the gap to close at a linear rate to the final test gap over the course of the equilibration period.

12.4. At the end of the equilibration period, perform the monotonic shear test at the test gap by setting the DSR to rotate the upper plate at 0.05 RPM. Record data points at 1-second intervals.

12.4.1. The following data should be collected during the course of the test:

12.4.1.1. Loading time, t, seconds;

12.4.1.2. Shear strain, γ, %;

12.4.1.3. Shear stress, τ, Pa;

12.4.1.4. Modulus, G_γ, Pa;

12.4.1.5. G_γ at peak stress, $G_{\gamma f}$, Pa;

13. Calculations

13.1. Using the results obtained in Section 7, create a plot of shear stress (τ) versus shear strain (γ).

13.2. Fit a 4th order polynomial line to the stress curve from the beginning of the test to peak strain, γ_f.

13.3. From the polynomial fit, calculate E_f (Equation 1):

$$E_f = \int_0^{\gamma_f} ax^4 + bx^3 + cx^2 + dx + e \qquad (1)$$

where:

E_f = *peak stress energy,* J^3

γ_f = *peak strain, %*

a, b, c, d, and e = constants from 4th order polynomial fit

14. Report

14.1. Report the following information:

14.1.1. Sample identification;

14.1.2. Test Temperatures, nearest 1.0 °C;

14.1.3. Peak strain; %;

14.1.4. Peak stress, Pa;

14.1.5. Peak stress energy, J

15. Precision and Bias

15.1. *Precision* - The research required to develop precision estimates has not been conducted.

15.2. *Bias* – The research required to establish the bias has not been conducted.

16. Keywords

16.1. *Peak stress energy; peak stress; peak strain; strain tolerance; Dynamic Shear Rheometer (DSR); asphalt binder; modified asphalt binder.*

Appendix

X.1. Sample Test Results

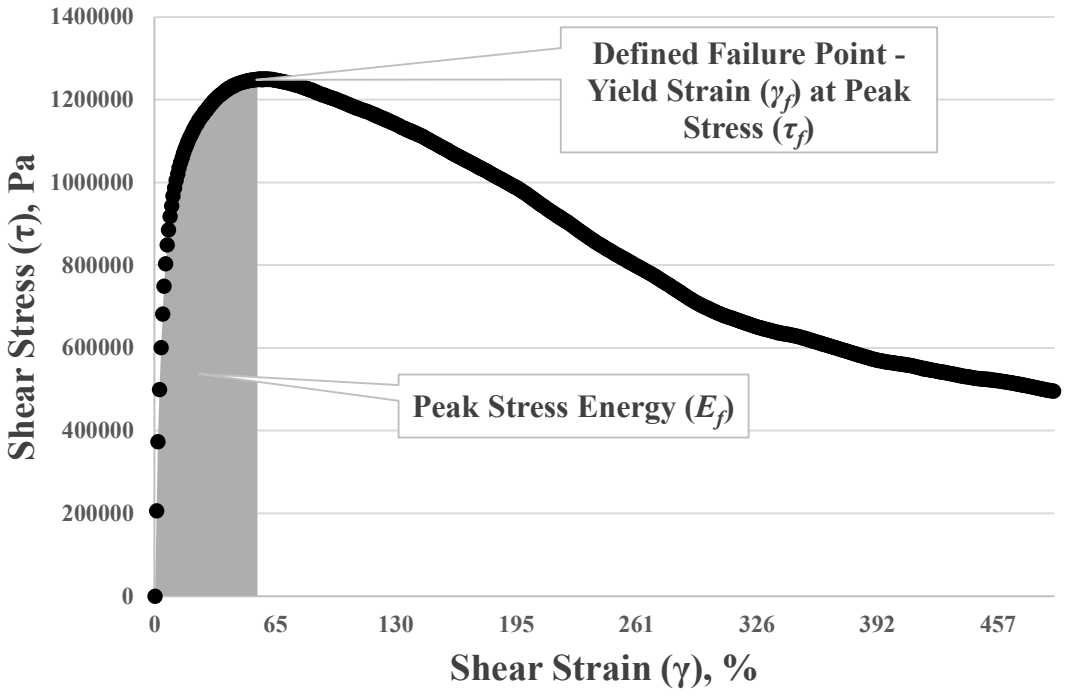

Figure X.1. Example of a shear stress-shear strain plot from MOSS test data

X.2. Determining Critical Strain Value

1.1. Appendix X.2 demonstrates a potential method of analysis for using data collected from the MOSS test method to determine a critical strain value (γ_{cr}) at a given modulus. Critical strain is a method of measuring the strain tolerance of an asphalt binder by normalizing stiffness. In the example shown below, two binders (one unmodified, one modified) are tested at two temperatures within the 1-10 MPa modulus range. Values for peak strain (γ_f) and the corresponding moduli at the peak strain (G_{yf}) are shown in Table X.2. These values are plotted in Figure X.2, along with a vertical dashed line at a modulus value of approximately 3 MPa. Table X.2.1 shows how critical strain is calculated using linear fits of the plotted data points in the form $y=ax+b$. The value for critical strain is represented in logarithmic form.

Table X.2 – Example Dataset for an Unmodified and Modified Binder

Binder Type	*Log* γ_{f1}	*Log* γ_{f2}	*Log* G_{yf1}	*Log* G_{yf2}
Unmodified	6.239	6.891	1.908	1.757
Modified	6.112	6.440	2.292	2.152

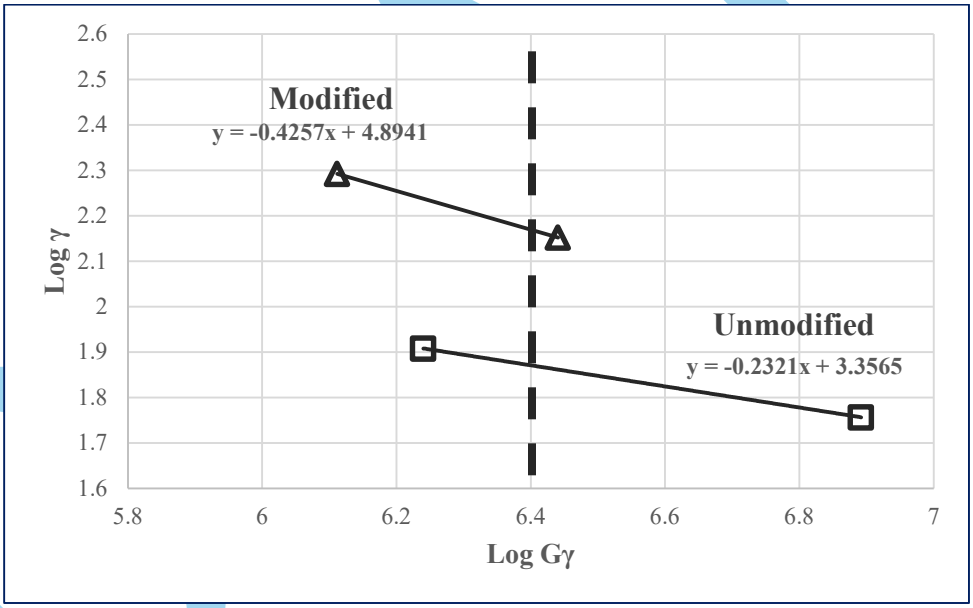

Figure X.2. Plot of data from Table X.2.

Binder Type	*a*	*b*	*x*	γ_{cr}
Unmodified	-0.2321	3.3565	6.4	**1.871**
Modified	-0.4257	4.8941	6.4	**2.170**

Table X.2.1 – Calculating Critical Strain from MOSS Data

APPENDIX C: Draft Test Method for Determining Intermediate & Low-Temperature Rheological Properties of Asphalt Binders Using a DSR

Standard Method of Test for

Determining Intermediate- and Low-Temperature Rheological Properties of Asphalt Binders Using a Dynamic Shear Rheometer (DSR)

ASTM Designation: DXXXX-XX

1. Scope

1.1. This test method covers the determination of parameters calculated from the measurement of modulus (G*) and phase angle (δ) of asphalt binders when tested in dynamic (oscillatory) shear using parallel plate geometry in accordance with ASTM D7175. These parameters are considered important to the design of roofing binders, but will also be applicable to other paving and industrial applications that require a greater knowledge of rheological parameters relating to performance.

1.2. The values stated in SI units are to be regarded as the standard.

1.3. A precision and bias statement for this test method has not been completed at this time. Therefore, this test method should not be used for acceptance or rejection of a material for purchasing purposes.

1.4. *This standard does not purport to address all of the safety concerns, if any, associated with its use. It is the responsibility of the user of this standard to establish appropriate safety and health practices and determine the applicability of regulatory limitations prior to use.*

2. Referenced Documents

2.1. *ASTM Standards*

D8 Standard Terminology Relating to Materials for Roads and Pavements

D2872 Standard Test Method for Effect of Heat and Air on a Moving Film of Asphalt Binder (Rolling Thin-Film Oven Test)

D6373 Standard Specification for Performance-Graded Asphalt Binder

D6521 Standard Practice for Accelerated Aging of Asphalt Binder Using a Pressurized Aging Vessel (PAV)

D7175 Standard Test Method for Determining the Rheological Properties of Asphalt Binder Using a Dynamic Shear Rheometer

D7643 Grading or Verifying the Performance Grade (PG) of an Asphalt Binder

3. Terminology

3.1 *Definitions of terms used in this practice may be found in ASTM D8, ASTM D7175, determined from common English usage, or combinations of both.*

4. Summary of Test Method

4.1 This standard includes the procedure to obtain complex shear modulus (G*) and phase angle (δ) of asphalt binders using the dynamic shear rheometer (DSR) with parallel-plate geometry.

4.2 Test specimens, nominally 8-mm in diameter by 2 mm thick, are formed between parallel metal plates.

4.3 During testing, one of the parallel plates is oscillated with respect to the other at a pre-selected frequency and shear strain. The designated shear strain is such that the testing is expected to be within the linear viscoelastic region of the asphalt binder.

4.4 The procedure uses a multi-point measurement to determine G* and δ at multiple temperatures (T) and a fixed frequency (ω).

4.4.1 The values of T, G* and δ from multi-point measurements can be used to interpolate various rheological parameters or make single-point determinations, such as those shown in Table 1.

4.4.2 Parameters are designated in the form R_s, where R is the dependent rheological property, Y, at a specified critical value, s, for an independent property, X

4.4.3 Interpolation is performed using a form equation similar to **Equation 3** in Section 6.2.3 of D7643.

Table 1. Rheological Parameters

Rheological Parameter	Description[A]
$\delta_{G^*=10\ MPa}$	δ where G* =10 MPa
Log $G^*_{\delta=27°}$	Logarithm of G* where δ=27°
G_c (or G_{VET})	G* where δ=45°
$T_{G^*=10\ MPa}$	T where G*=10 MPa
$T_{\delta=27°}$	T where δ=27°
$T_{\delta=45°}$ (or T_c or T_{VET})	T where δ=45°
Glover-Rowe	$G^*(\cos\delta)^2/\sin\delta$ at a given T

[A]Tested at a constant angular frequency of 10 rad/s. This analysis method can be applied to work conducted at other frequencies.

5. Significance and Use

5.1 This test method provides a means of using rheological measurements for characterizing the hardness and relaxation properties of an asphalt binder in the high-stiffness region.

6. Interferences

6.1 Refer to ASTM D7175 Section 6 for common interference in rheological measurement.

7. Apparatus

7.1 Refer to ASTM D7175 Section 7 for information regarding the DSR apparatus.

8. Materials

8.1 Refer to ASTM D7175 Section 7 for information regarding materials needed for the procedure.

9. Verification

9.1 Refer to ASTM D7175 Section 7 for information regarding verification of the apparatus.

10. Preparation of Apparatus

10.1 Refer to ASTM D7175 Section 10 for information regarding preparation of the DSR apparatus, with the following exceptions:

10.1.1 Use 8-mm parallel plate geometry with a 2-mm gap.

10.1.2 Zero the gap at 25°C.

10.1.3 Preheat the 8-mm plates from 45°C-75°C prior to loading samples.

Note 1 – Loading temperatures may vary based on coating type and aging condition. Oxidized and aged coatings require higher loading temperatures to achieve proper adhesion. Loading temperatures above 75°C may be used for extremely stiff binders, so long as the binder is able to be loaded and trimmed without compromising specimen integrity.

11. Preparing Test Specimens

11.1.1 *Annealing Asphalt Binder* – Anneal the asphalt binder sample by heating in a container in an oven until it is sufficiently fluid to pour. Cover the sample and stir it as needed during the heating process to ensure homogeneity and to remove air bubbles. Annealing prior to testing removes reversible molecular associations (steric hardening) that occur during normal storage at ambient temperature. Cold samples must be annealed prior to testing. Structure developed during storage can result in overestimating the modulus by as much as 50%. Annealing temperature will depend on the grade and type of asphalt binder. Always minimize the heating temperature and time to avoid hardening the sample. Hot plates shall not be used to heat the asphalt binder

11.2 *Transferring Asphalt Binder to Test Plate* – Transfer the asphalt binder to one of the test plates through pouring, direct transfer, or use of a silicone mold.

11.2.1 Refer to ASTM D7175, Sections 11.3.1-11.3.3 for information on transferring the binder to the test plates.

11.3 *Trimming Test Specimen*

11.3.1 Refer to ASTM D7175, Section 11.4 for information on trimming the test specimen.

11.4 *Creating Bulge*

11.4.1 Refer to ASTM D7175, Section 11.5 for information on creating the bulge.

12. Test Procedure

12.1 Perform a temperature sweep in oscillatory mode using 0.1% shear strain and a loading frequency of 10 rad/s.

12.1.1 Perform the temperature sweep on the same specimen in decreasing temperature steps at intervals of no greater than 6°C, allowing 10 minutes for thermal equilibration at each test temperature. Test temperatures should be selected such that the desired critical G* and δ values will be bracketed.

12.1.2 Perform the measurement at each test temperature for sixteen loading cycles. Determine G* in Pa and δ in degrees as the average of the last eight loading cycles.

12.2 Unload the sample and clean the DSR.

13. Calculations

13.1 Determine the logarithm of the measured G* values

13.2 Use Equation 1 to calculate rheological parameter R_s at a specified critical property value X_s

$$R_s = Y_1 + \{X_s - X_1\}\{Y_2 - Y_1\}/\{X_2 - X_1\} \quad (1)$$

Where:

R_s = Rheological parameter
Y_1, Y_2 = Test result for dependent rheological property
X_s = Specified critical dependent property value
X_1, X_2 = Test results for independent rheological property

14. Report

14.1 Report the following information:

14.1.1 Sample and Operator information;

14.1.2 Rheological parameter to the appropriate decimal place as notated in D7175

15. Precision and Bias

15.1 *Precision* – The research required to develop precision estimates has not been conducted.

15.2 *Bias* – The research required to establish the bias has not been conducted.

16. Keywords

16.1 *Rheology; relaxation; Dynamic Shear Rheometer (DSR); asphalt binder; modified asphalt binder, parameters*

APPENDIX

X1. Example Dataset and Calculations

TABLE X1.1 Example Data Table

T, °C[A]	G*, Pa	Log G*	δ, 10 rad/s
40	1.51E+06	6.179	56.0
34	3.81E+06	6.581	50.1
28	9.52E+06	6.979	43.9
22	2.02E+07	7.305	37.9
16	4.61E+07	7.664	31.5
10	8.84E+07	7.946	26.2
4	2.40E+08	8.380	20.5

[A]It is recommended, but not required, to test at temperatures consistent with performance grading per ASTM D6373

TABLE X1.2 Example Calculations

Parameter	X_s	X_1	X_2	Y_1	Y_2	R_s
$\delta_{G^*=10\ MPa}$	7.0	***6.979***	***7.305***	43.9	37.9	43.5°
Log $G^*_{\delta=27°}$	27.0	***31.5***	***26.2***	7.664	7.946	7.903
Log G_c (or G_{VET})	45.0	***50.1***	***43.9***	6.581	6.979	6.908
$T_{G^*=10\ MPa}$	7.0	***6.979***	***7.305***	28	22	27.6 °C
$T_{\delta=27°}$	27.0	***31.5***	***26.2***	16	10	10.9 °C
T_{Gc} (or T_{VET})	45.0	***50.1***	***43.9***	28	22	23.1 °C
Log Glover-Rowe, 22°C	-	-	-	-	-	6.819

Note: Bold and italicized results show values bracketing X_s